UNIVERSITY OF OKLAHOMA

GRADUATE COLLEGE

# MOLECULAR DYNAMICS SIMULATIONS OF AQUEOUS SYSTEMS AT THE SOLID-LIQUID INTERFACE

A DISSERTATION

SUBMITTED TO THE GRADUATE FACULTY

in partial fulfillment of the requirements for the

Degree of

DOCTOR OF PHILOSOPHY

By

DIMITRIOS ARGYRIS
Norman, Oklahoma
2010

Downloaded from SHAREOK. Persistent Handle URL: https://hdl.handle.net/11244/318900

MOLECULAR DYNAMICS SIMULATIONS OF AQUEOUS SYSTEMS
AT THE SOLID-LIQUID INTERFACE

A DISSERTATION APPROVED FOR THE
SCHOOL OF CHEMICAL, BIOLOGICAL AND MATERIALS ENGINEERING

BY

Dr. Alberto Striolo, Chair

Dr. Jana Shen

Dr. Brian P. Grady

Dr. Dimitrios V. Papavassiliou

Dr. Daniel E. Resasco

© Copyright by DIMITRIOS ARGYRIS 2010
All Rights Reserved.

*To my parents*
*Spyridoula and Christos*

*Στους γονείς μου*
*Σπυριδούλα και Χρίστο*

## Acknowledgements

It was indeed a unique experience and great pleasure to conduct scholarly research as a doctoral candidate under the guidance of Dr. Alberto Striolo at the University of Oklahoma. This work would not have been possible without his help, guidance, encouragement, and support. His mentorship, innovative way of thinking, and expertise in my field of research significantly helped me to not only complete my research goals but also grow as an independent thinker. I would like to express my sincere gratitude to my advisor, Dr. Striolo for his understanding, patience, and friendship all these years.

I would like to acknowledge Dr. Paul D. Ashby from Lawrence Berkeley National Laboratory and Dr. David R. Cole from Oak Ridge National Laboratory for the fruitful collaborations that resulted in several publications. Their mentorship, guidance, expertise, and primarily their support were essential for the successful completion of this work and are much appreciated. I would also like to thank my committee members Dr. Jana Shen, Dr. Brian P. Grady, Dr. Dimitrios V. Papavassiliou, and Dr. Daniel Resasco for their help and support during my graduate studies at the University of Oklahoma.

The completion of this work would have not been possible without the generous allocations of computing time provided by the OU Supercomputing Center for Education and Research (OSCER) in Norman, Oklahoma and the National Energy Research Scientific Computing Center (NERSC) in Berkeley, California. I would also like to acknowledge Dr. Henry Neeman for introducing me to high-performance

computing and for his tireless effort to make OSCER computing resources available to users like myself.

This research work would not have been feasible without the financial support of the Office of Basic Energy Sciences, U.S. Department of Energy. I am also grateful to the Scientific User Program at the Molecular Foundry in Lawrence Berkeley National Laboratory and specifically to Dr. Miquel Salmeron and his group members for the help and feedback they provided while I was working in Berkeley.

I would like to thank all my colleagues from Dr. Striolo's research group, primarily Dr. Naga Rajesh Tummala and Dr. Brian H. Morrow for the fruitful collaboration and help especially during my first years as a graduate student at the University of Oklahoma. I truly enjoyed working closely with them over the years, have tremendous respect for them, and do greatly appreciate their friendship. I would like to take this opportunity to thank all of my friends and family who have directly and indirectly supported me during my graduate studies and made these past four years a very memorable time of my life.

I would like thank my parents, Spyridoula and Christos, and my brother Nikos for their unconditional love, encouragement, and support throughout my life. Most importantly, I would like to thank my wife Arlette for her constant source of love, understanding, and patience. Her unending encouragement and support have given me the drive and strength to overcome all challenges and without her this accomplishment would not have been possible.

## Table of Contents

**1 Introduction ..... 1**

**2 Molecular Structure and Dynamics in Thin Water Films at the Silica and Graphite Surfaces ..... 6**

2.1 Abstract ..... 6

2.2 Introduction ..... 7

2.3 Simulation Methodology and Details ..... 9

2.4 Results and Discussion ..... 14

2.4.1 Atom Density Profiles ..... 14

2.4.2 Planar Radial Distribution Functions ..... 17

2.4.3 Surface Density Distributions ..... 20

2.4.4 Water Orientation ..... 27

2.4.5 Hydrogen Bonding ..... 32

2.4.6 Residence Correlation Functions ..... 33

2.4.7 Reorientation Correlation Functions ..... 36

2.5 Conclusions ..... 39

**3 Hydration Structure on Crystalline Silica Substrates ..... 41**

3.1 Abstract ..... 41

3.2 Introduction ..... 42

3.3 Simulation Methodology ..... 44

3.4 Results and Discussion ..... 47

3.4.1 Density Profiles ..... 47

3.4.2 Planar Radial Distribution Functions ..... 52

3.4.3 Planar Density Distributions ..... 56

3.4.4 Hydrogen Bond Density Profiles ..... 66

3.5 Conclusions ..... 69

**4 Dynamic Behavior of Interfacial Water at the Silica Surface ..... 71**

4.1 Abstract ..... 71

4.2 Introduction ..... 72

4.3 Simulation Methodology ..... 74

4.4 Results and Discussion ..... 77

4.4.1 Equilibrium Properties ....77
4.4.2 Residence Probability....83
4.4.3 Translational Dynamics....86
4.4.4 Rotational Dynamics....91
4.4.5 Hydrogen Bond Dynamics....96
4.5 Conclusions....99

**5 Molecular Dynamics Studies of Interfacial Water at the Alumina Surface..101**
5.1 Abstract....101
5.2 Introduction....101
5.3 Simulation Details....103
5.4 Results and Discussion....106
5.4.1 Density Profiles....106
5.4.2 Planar Density Distributions....109
5.4.3 Molecular Orientation....113
5.4.4 Hydrogen Bond Network....114
5.4.5 Residence Time....117
5.4.6 Surface Wettability....119
5.5 Conclusions....122

**6 Structure and Orientation of Interfacial Water Determine Atomic Force Microscopy Results: Insights from Molecular Dynamics Simulations....124**
6.1 Abstract....124
6.2 Introduction....125
6.3 Simulation Details....128
6.4 Results and Discussion....130
6.4.1 Force Profiles....130
6.4.2 Density Profiles....133
6.4.3 Charge Density Profiles....140
6.4.4 Planar Density Distributions....142
6.5 Conclusions....145

**7 Ion-Specific Effects under Confinement: The Role of Interfacial Water....147**
7.1 Abstract....147
7.2 Introduction....148

7.3 Simulation Details ..... 151
7.4 Results and Discussion ..... 153
7.4.1 Cation-Anion Distributions ..... 153
7.4.2 Relation between Water Structure and Ion Distributions ..... 157
7.4.3 Mixed Solute Behavior ..... 160
7.4.4 Dynamics of Confined Water and Ions ..... 162
7.5 Conclusions ..... 164

**8 Advantages and Limitations of Molecular Dynamics Simulations ..... 166**

**9 Conclusions and Future Work ..... 169**

**10 References ..... 172**

## List of Tables

Table 2.1: Parameters used within the force fields implemented in our simulations. In the case of silica, bO and nbO stand for bridging and non-bridging oxygen atoms, respectively. .....12

Table 2.2: Location (expressed at distance $z$ from the surface) of the atomic density peaks of oxygen and hydrogen atoms on the various surfaces considered in Figure 2.4. On the fourth column we provide the labels used in our discussion to refer to the peaks. The first and second letters of the labels indicate the substrate and the atomic species, respectively. The number in the label corresponds to the layer, with layer 1 being the one closer to the substrate.....17

Table 2.3: Time required for the autocorrelation function to decay from 1 to $1/e$ for all layers on the different surfaces considered. Results are obtained from the ACFs shown in Figure 2.17. .....36

Table 3.1: Location (expressed as distance $z$ from the surface) of the atomic density peaks of oxygen and hydrogen atoms on the various surfaces considered in Figure 3.2. On the forth column we provide the labels used in our discussion to refer to the peaks. First and second letters of the label indicate the substrate and the atomic species, respectively. The number in the label corresponds to the layer, number 1 being the one closest to the substrate. .....49

Table 4.1: Vertical distance of the atomic density peaks for oxygen atoms of water molecules (Figure 4.2a) from the plane of the non-bridging oxygen atoms of the fully, partially, and non-hydroxylated surfaces considered. .....80

Table 4.2: Dipole moment and hydrogen-hydrogen autocorrelation functions calculated at time $t$ = 5 ps for interfacial water molecules (data shown in Figure 4.9 and Figure 4.10). The layer position is reported in Table 4.1. Properties for "bulk" water are estimated at 14 Å from the surface, and are independent on the surface considered herein. .....96

Table 4.3: Location (expressed as distance $z$ from the surface) of the hydrogen bond density peaks on the fully, partially, and non-hydroxylated surfaces as shown in Figure 4.11a. .....98

Table 7.1: Positions of the first two atomic layers for the cations, anions and water considered in this study.[a] The data reported is for the mixture with 32 pairs of NaCl and CsCl. The same layer positions are observed for the simulated systems with 64 pairs of NaCl or CsCl. .....159

## List of Figures

Figure 2.1: Side and top views of LD $SiO_2$ (a) and HD $SiO_2$ (b) surfaces. Blue, red and tan spheres represent the hydrogen atoms of the surface hydroxyl groups; oxygen and silicon atoms, respectively. .....10

Figure 2.2: Snapshots of the graphite substrates used in our simulations. (a) Side view of the entire simulation box with water molecules in contact with the lower graphite surface. (b) Top and (c) side view of the graphite surface. In the top view only one of the graphene sheets is shown for clarity. .....13

Figure 2.3: Oxygen atomic density as a function of distance $z$ from the graphite surface. The oxygen atoms are those of water molecules. Three cases are shown in which 2592 (solid line), 1296 (dotted line), and 1008 (dashed line) water molecules were simulated. In all cases $T$ = 300 K. .....15

Figure 2.4: (a) Oxygen and (b) hydrogen atom density profiles as a function of distance $z$ from the solid surfaces. The reference $z$ = 0 is the top plane of carbon atoms in the case of the graphite surface and the plane of non-bridging oxygen atoms in the case of both LD and HD silica surfaces. .....16

Figure 2.5: In-plane oxygen-oxygen radial distribution functions $g_{oo}(r)$ of graphite (a), LD $SiO_2$ (b), and HD $SiO_2$ (c). The dashed line of figure (a) corresponds to an in-plane RDF far from the surfaces ($z$ > 14 Å) and is identical in all cases. .....19

Figure 2.6: In-plane hydrogen-hydrogen radial distribution functions $g_{HH}(r)$ of graphite (a), LD $SiO_2$ (b), and HD LD $SiO_2$ (c). The dashed line of figure (a) corresponds to an in-plane RDF far from the surfaces ($z$ > 14 Å) and is identical in all cases. .....20

Figure 2.7: In-plane oxygen-hydrogen radial distribution functions $g_{OH}(r)$ of graphite (a), LD $SiO_2$ (b), and HD LD $SiO_2$ (c). The dashed line of figure (a) corresponds to an in-plane RDF far from the surfaces ($z$ > 14 Å) and is identical in all cases. .....20

Figure 2.8: (a) Surface density distribution of oxygen atoms on graphite for the layer AO-1 that corresponds to the first peak of the density profile as shown schematically in panel (b). The surface density distribution is calculated on a slab of thickness 1 Å. See Table 2.2 for details on peak position. The units of the atomic density distribution (panel a) are given in $Å^{-3}$. .....22

Figure 2.9: Surface density distribution of oxygen atoms on LD $SiO_2$ for the BO-1 (a) and BO-2 (b) layers. See Table 2.2 for details on peak position. The units of the atomic density distribution are given in $Å^{-3}$. .....23

Figure 2.10: Surface density distribution of hydrogen atoms on BH-1 layer on LD $SiO_2$. See Table 2.2 for details on peak position. The units of the atomic density distribution are given in $Å^{-3}$.....24

Figure 2.11: Surface density distribution of oxygen atoms on HD $SiO_2$ for the CO-1 (a) and CO-2 (b) layers. See Table 2.2 for details on peak position. The units of the atomic density distribution are given in $Å^{-3}$.....25

Figure 2.12: Surface density distribution of hydrogen atoms for the CH-1 (a), CH-2 (b), CH-3 (c), and CH-4 (d) layers on HD $SiO_2$. See Table 2.2 for details on peak position. The units of the atomic density distribution are given in $Å^{-3}$. .....27

Figure 2.13: Order parameter $cos(\theta)$ for water molecules as a function of their distance from the surface. The angle $\theta$ is that between the opposite to the dipole moment vector of water and the normal to the surface vector.....29

Figure 2.14: Contour plots showing the water orientation for water layers BO-1 (a) and BO-2 (b) on the LD $SiO_2$ surface. The average values of the angle $\theta$ between the vector opposite to the dipole moment of water and that normal to the surface are plotted in respect to the $x$ and $y$ direction. See Table 2.2 for details on peak position. The angle $\theta$ is in degrees. .....30

Figure 2.15: Same as Figure 2.14.The angle $\theta$ is calculated for water molecules on the HD $SiO_2$ surface for the oxygen layer CO-1 (a) and CO-2 (b). See Table 2.2 for details on peak position. The angle $\theta$ is in degrees.....31

Figure 2.16: (a) Density profiles of the hydrogen bonds formed between water molecules as a function of distance from the solid surface. (b) Hydrogen bond surface density distribution correspondent to the first peak found for water on HD $SiO_2$, as shown in Figure 2.16a. .....33

Figure 2.17: Residence correlation functions for oxygen atoms in the various layers at the graphite (a), LD $SiO_2$ (b), and HD $SiO_2$ (c) surfaces. See Table 2.2 for details on peak position. .....36

Figure 2.18: Reorientation autocorrelation function for the vector opposite to the molecular dipole moment of water. Results are shown in correspondence to various layers at the graphite (a), LD $SiO_2$ (b), and HD $SiO_2$ (c) surfaces. See Table 2.2 for details on peak position. .....37

Figure 2.19: Reorientation autocorrelation function for the hydrogen-hydrogen vector of water. Results are shown in correspondence to various layers at the graphite (a), LD $SiO_2$ (b), and HD $SiO_2$ (c) surfaces. See Table 2.2 for details on peak position. .....38

Figure 3.1: Top view of the fully hydroxylated (a), 50 % hydroxylated (b), and non-hydroxylated (c) $SiO_2$ surfaces. Only hydroxyl groups and non-bridging oxygen atoms are shown for clarity. White and red spheres represent hydrogen and oxygen atoms of the surface hydroxyl groups, respectively. .....46

Figure 3.2: Oxygen (a) and hydrogen (b) atom density profiles as a function of distance $z$ from the solid surfaces. The reference $z$ = 0 is the plane of non-bridging oxygen atoms. Black solid, blue dotted, and red dash lines correspond to the fully hydroxylated, partially hydroxylated, and non-hydroxylated surfaces, respectively. Only oxygen and hydrogen atoms belonging to water molecules are considered here. .....48

Figure 3.3: In-plane oxygen-oxygen (a), hydrogen-hydrogen (b), and oxygen-hydrogen (c) radial distribution functions. The RDFs shown in this figure were calculated along planes located 14 Å above the surface. The data are identical for all three surfaces considered here. .....53

Figure 3.4: In-plane oxygen-oxygen radial distribution functions $g_{OO}(r)$ of the fully hydroxylated (a), partially hydroxylated (b), and non-hydroxylated (c) silica surface. Black solid, blue dotted, and red dash lines correspond to first, second, and third oxygen layer respectively. The location of each oxygen layers is given in Table 3.1. .....54

Figure 3.5: In-plane hydrogen-hydrogen radial distribution functions $g_{HH}(r)$ of the fully hydroxylated (a), partially hydroxylated (b), and non-hydroxylated (c) silica surface. Black solid, blue dotted, red dash, and green dash-dotted lines correspond to first, second, third, and fourth hydrogen layer respectively. The location of the hydrogen layers is given in Table 3.1. .....55

Figure 3.6: In-plane oxygen-hydrogen radial distribution functions $g_{OH}(r)$ of the fully hydroxylated (a), partially hydroxylated (b), and non-hydroxylated (c) silica surface. Black solid, blue dotted, and red dash lines correspond to first, second, and third oxygen layer respectively. The location of the oxygen layers is given in Table 3.1. .....55

Figure 3.7: Surface density distribution of oxygen atoms for the FO-1 (a) and FO-2 (b) layers on the fully hydroxylated surface. Refer to Table 3.1 for location of the layers. The units of the atomic density distribution are given in $Å^{-3}$. .....57

Figure 3.8: Surface density distribution of hydrogen atoms for the FH-1 (a) and FH-2 (b) layers on the fully hydroxylated surface. Refer to Table 3.1 for location of the layers. The units of the atomic density distribution are given in $Å^{-3}$. .....57

Figure 3.9: Simulation snapshot of four interfacial water molecules at the fully hydroxylated surface. The purple oxygen atom identifies the water molecule in layer FO-1, which is in contact with the surface. The water molecules with red oxygen atoms belong to layer FO-2. The blue dashed lines illustrate hydrogen bonds. The surface is

not shown for clarity, but we point out that the hydrogen atom pointing towards the surface is at the center of the hexagons formed by the surface hydroxyl groups. .....59

Figure 3.10: Surface density distribution of oxygen atoms for the PO-1 (a) and PO-2 (b) layers on the partially hydroxylated surface. The layers location is given in Table 3.1. The units of the atomic density distribution are given in $Å^{-3}$. .....60

Figure 3.11: Surface density distribution of hydrogen atoms for the PH-1 (a) and PH-2 (b) layers on the partially hydroxylated surface. The layers location is given in Table 3.1. The units of the atomic density distribution are given in $Å^{-3}$.....60

Figure 3.12: Simulation snapshot of three interfacial water molecules on the partially hydroxylated surface. The purple oxygen atom identifies the "anchoring" water molecule in layer PO-1 that is in contact with the surface. The far right water molecule belongs to layer PO-1 as well. The blue dashed lines illustrate the atomic species that are hydrogen bonded. The surface is not shown for clarity.....62

Figure 3.13: Surface density distribution of oxygen atoms for the NO-1 (a) and NO-2 (b) layers on the non-hydroxylated surface. The layers location is given in Table 3.1. The units of the atomic density distribution are given in $Å^{-3}$. .....63

Figure 3.14: Surface density distribution of hydrogen atoms for the NH-1 (a) and NH-2 (b) layers on the non-hydroxylated surface. The layers location is given in Table 3.1. The units of the atomic density distribution are given in $Å^{-3}$. .....64

Figure 3.15: Simulation snapshot of four interfacial water molecules at the non-hydroxylated surface. The purple oxygen atom identifies the water molecule in layer NO-1 that is in contact with the surface. The remaining water molecules (red oxygen atom) belong to layer NO-2 and illustrate three different orientations. The blue dashed lines represent hydrogen bonds. The surface is not shown for clarity. .....65

Figure 3.16: Density profiles of hydrogen bonds formed between water molecules as a function of distance from the fully hydroxylated (black solid line), partially hydroxylated (blue dotted line), and non-hydroxylated (red dashed line) solid substrates. .....68

Figure 3.17: Surface density distribution of hydrogen atoms (a) for the layer PH-1 and in-plane hydrogen bond density distribution (b) in a layer of thickness 1 Å centered at 2.95 Å from the partially hydroxylated surface. The units of the density distributions are given in $Å^{-3}$. .....68

Figure 4.1: Schematic representation of top view of the fully hydroxylated (a), 50 % hydroxylated (b), and non-hydroxylated (c) $SiO_2$ surfaces. Only hydroxyl groups and

non-bridging oxygen atoms are shown for clarity. White and red spheres represent hydrogen and oxygen atoms of the surface hydroxyl groups, respectively.....76

Figure 4.2: Atomic density profiles of water oxygen (panel a) as a function of distance $z$ from the solid surfaces. The cumulative density profile of oxygen atoms as a function of distance is shown in panel b. The reference $z = 0$ is the plane of non-bridging oxygen atoms. Black solid, blue dotted, and red dash lines correspond to the fully hydroxylated, partially hydroxylated, and non-hydroxylated surfaces, respectively.....79

Figure 4.3: Charge density profiles of water as a function of the vertical distance $z$ from the three solid substrates considered. The reference $z = 0$ is the plane of non-bridging oxygen atoms. Continuous, dotted, and dashed lines represent results obtained on the fully hydroxylated, partially hydroxylated, and non-hydroxylated surfaces, respectively. .....81

Figure 4.4: $z$-component of total dipole moment normalized by the surface area as a function of distance from the three surfaces types. Continuous, dotted and dashed lines represent water on the fully hydroxylated, partially hydroxylated, and non-hydroxylated surfaces, respectively.....83

Figure 4.5: Residence probability for water molecules on distinct layers formed on the fully hydroxylated (a), partially hydroxylated (b), and non-hydroxylated (c) surfaces. Results are shown for the first layers formed on each surface. Black continuous, blue dotted, and red dashed lines represent water on the first, second, and third layer, respectively. The results for water molecules on the third layer are only shown on the fully hydroxylated surface. The position of each layer is shown in Table 4.1. The green dot-dash line represents the residence probability for water molecules located 14 Å above the surface, and corresponds to water with bulk properties. .....84

Figure 4.6: (a) Residence probability for the first interfacial oxygen atomic layers at the fully hydroxylated, partially hydroxylated, and non-hydroxylated surfaces. (b) Residence probability of the hydrogen-down (solid line), hydrogen-up water molecules (dashed line), and for all water molecules in the contact layer with the partially hydroxylated surface. .....86

Figure 4.7: Layer-by-layer in-plane mean square displacement parallel to the solid surfaces for water molecules on the fully hydroxylated (a), partially hydroxylated (b), and non-hydroxylated surface (c). Solid, dotted, and dashed lines represent water on the first, second, and third layer (when considered), respectively. The position of each layer is shown in Table 4.1.....88

Figure 4.8: Average distance from the surface (bottom panels) and mean square displacement parallel to the solid surface (top panels) for one selected water molecule on each of the three surfaces considered. Data are shown for water molecules on the

fully hydroxylated (left), partially hydroxylated (center), and non-hydroxylated surfaces (right). The dashed lines indicate the position of interfacial water layers reported in Table 4.1. .....91

Figure 4.9: Dipole moment (a) and hydrogen-hydrogen vector (b) autocorrelation functions for interfacial water molecules on the fully hydroxylated (black), partially hydroxylated (blue), and non hydroxylated surface (red). Continuous and dashed black lines represent water in the first and second layers at the fully hydroxylated surface, respectively. The green line represents water molecules located 14 Å above the surface and have the bulk properties of water. In all cases $C(0) = 1$ (not shown for clarity). The position of each layer is shown in Table 4.1. .....94

Figure 4.10: Dipole moment (a) and hydrogen-hydrogen vector (b) autocorrelation functions for water molecules in the first layer on the partially hydroxylated surface. Data for H-down water molecules (black solid line), H-up water molecules (dashed line), and all water molecules (blue solid line) in the first layer are provided in the figures. In all cases $C(0) = 1$ (not shown for clarity).....95

Figure 4.11: Hydrogen bond density profile (a) and number of hydrogen bonds per water molecule (b) as a function of the distance $z$ from the three surfaces considered. The probability of finding hydrogen-bonded water molecules at a given distance from the three surfaces is given in panel b. Solid, dashed, and dotted lines represent water molecules on the fully hydroxylated, partially hydroxylated, and non-hydroxylated surfaces, respectively.....97

Figure 4.12: Hydrogen bond – hydrogen bond autocorrelation functions on the three surfaces considered. Solid, dashed, and dotted lines represent hydrogen bonds on the fully hydroxylated, partially hydroxylated, and non-hydroxylated surfaces, respectively. The layer position is reported in Table 4.3. The green dash-dot line corresponds to hydrogen bonds formed between water molecules 14 Å above the surface, where the results are identical on all three surfaces and resemble those obtained for bulk water...99

Figure 5.1: Top view of the Al-terminated (left panel) and OH-terminated (right panel) alumina surfaces. Tan and red spheres represent aluminum and oxygen atoms, respectively. Top layer aluminum atoms at the Al-terminated alumina surface are shown in grey. Surface hydroxyl groups are shown with purple for oxygen and white for hydrogen atoms. Only the upper five atomic layers are shown for clarity. The thickness of the alumina surface along the $z$-axis (perpendicular to the planes shown herein) is approximately 12.75 and 12.10 Å for the Al-terminated and OH-terminated surfaces, respectively. .....105

Figure 5.2: (a) Atomic density profile of oxygen and hydrogen atoms on Al-terminated alumina surface. (b) Atomic density profile of oxygen and hydrogen atoms on OH-terminated alumina surface. (c) Atomic charge density profile of water molecule on Al-

terminated and OH-terminated alumina surfaces in solid black and dashed blue lines, respectively. .....108

Figure 5.3: Surface density distributions along the $x-y$ plane (parallel to the surface) for water oxygen in the first layer (b) and water hydrogen in the first layer (a) and second layer (c) at Al-terminated alumina surface. The positions of the atomic layers are shown in Figure 5.2a. Densities are expressed in $Å^{-3}$. .....110

Figure 5.4: Surface density distributions along the $x-y$ plane (parallel to the surface) for water oxygen in the first layer (b) and water hydrogen in the first layer (a) and second layer (c) at OH-terminated alumina surface. The positions of the atomic layers are shown in Figure 5.2b. Densities are expressed in $Å^{-3}$. .....111

Figure 5.5: Simulation snapshots of selected interfacial water molecules at the Al-terminated (left panel) and OH-terminated (right panel) alumina surfaces. Only the first few atomic layers of the alumina surface are shown for clarity. Tan, red, and white spheres represent aluminum, oxygen, and hydrogen atoms, respectively. Water molecules with no OH bonds pointing toward to the surface are shown with purple oxygen atoms. The blue dashed lines represent hydrogen bonds. .....112

Figure 5.6: Order parameter $\cos\theta$ for water molecules as a function of distance from the Al-terminated (black solid) and OH-terminated (blue dashed line) surfaces. The angle $\theta$ is the one formed between the water dipole moment vector and the vector normal to the surface.....114

Figure 5.7: Hydrogen bond density profiles as a function of distance $z$ from the alumina surface. Solid black and dashed blue lines represent hydrogen bonding between water molecules at the Al-terminated and OH-terminated surfaces, respectively. .....117

Figure 5.8: Residence probability for water molecules in the first (solid black line) and second (blue dashed line) interfacial layers at the Al-terminated (a) and OH-terminated (b) alumina surfaces. Data in red dotted line corresponds to water molecules located at 14 Å above the surface and are identical for both surface terminations. As detailed in our prior work,[116] water molecules within a layer formed at 14 Å above the surface essentially reproduce bulk-like behavior.....119

Figure 5.9: Close-up side views of the Al-terminated (top panel) and OH-terminated (bottom panel) alumina surfaces with 1000 water molecules. Red and white spheres represent oxygen and hydrogen atoms of water molecules, respectively. Color scheme for alumina substrates is the same as in Figure 5.1.....120

Figure 5.10: Side views of the Al-terminated (top left) and OH-terminated (bottom left) alumina surfaces with 2000 water molecules. Top views of interfacial water are shown

in the right and the alumina surfaces are not shown for clarity. Color scheme for alumina substrates is the same as in Figure 5.1. .....121

Figure 6.1: Cross-sectional view of one flat alumina substrate, the CNT, and water molecules considered in our simulations. Aluminum, oxygen, hydrogen atoms of the fully hydroxylated alumina surface are shown as green, red, and white spheres, respectively. Carbon atoms are shown in dark grey. Water molecules are represented by red (oxygen) and white (hydrogen) spheres. Carbon atoms considered for the force calculation of Figure 6.2 are those below the blue dashed line. The snapshot also provides a side view of the cylindrical volume considered for the calculation of atomic and charge densities (blue box below the CNT tip). .....129

Figure 6.2: The $z$-component of the total force experienced by one (28, 0) CNT, used as AFM tip, as a function of the tip-surface distance in the presence of water is shown as black curve (filled circles). The contributions due to interfacial water molecules and to the alumina surfaces are shown as blue dashed (open triangles) and red dash-dotted (filled squares) curves, respectively. .....132

Figure 6.3: (a) Atomic density profiles of water oxygen as a function of the distance $z$ perpendicular to the OH-terminated alumina surface for tip-surface distances at 12.0, 8.5, 8.0 and 5.5 Å are shown in solid black, dashed blue, dash-dotted red, and dash-double-dotted green curves respectively. The two vertical black lines highlight the second hydration layer, whose position changes as the CNT tip approaches the surface. (b-e) The $x - y$ planar density distributions of the second interfacial water layer at 5.25 Å for the four tip-surface distances. .....136

Figure 6.4: (a) Peak density of hydration layers located at 1.90 (solid circles) and 4.55 Å (empty triangles) at the Al-terminated alumina shown as a function of tip-surface distance. (b) Peak density of hydration layers at 2.60 and 5.25 Å at the OH-terminated alumina. .....138

Figure 6.5: Atomic density profiles for water oxygen as a function of the distance $z$ perpendicular from the Al-terminated α-$Al_2O_3$ surface. Each curve corresponds to data for a fixed tip-surface separation varying from 15 to 0.5 Å. Data in the inset show an enlargement of the first interfacial water layer. Only water molecules in a cylindrical density volume with diameter ~11 Å centered on the CNT were considered. The reference $z$ = 0 is the outermost plane of aluminum atoms. .....139

Figure 6.6: Same as Figure 6.5, but for water at the OH-terminated α-$Al_2O_3$ surface. The reference $z$ = 0 is the plane of hydroxyl group oxygen atoms. .....140

Figure 6.7: Charge density profiles of water as a function of the distance $z$ from Al-terminated (a) and OH-terminated (b) α-$Al_2O_3$ surfaces. The reference $z$ = 0 is the plane of aluminum and hydroxyl group oxygen atoms of the corresponding surface.

Continuous, dotted, and dashed lines correspond to different CNT-surface separations. .....142

Figure 6.8: Planar density distribution of oxygen water along the $x-z$ plane (parallel to the CNT) with slab thickness $dy$ = 3 Å. The average in-plane density shown in panels (a)-(c) corresponds to tip-surface distances at 12.0, 7.5 and 5.0 at the Al-terminated alumina surface. Data in panels (d)-(e) correspond separation distances 12.0, 8.5, and 5.5Å at the OH-terminated alumina surface.....144

Figure 6.9: Simulation snapshots of interfacial water at the Al-terminated alumina surface. In these simulation snapshots the CNT is located at 7.5 Å (left panel) and 5.5 Å (right panel) from the surface. The alumina surface is not shown for clarity. .....145

Figure 7.1: (a) Side view of the silica pore of width 10.67 Å. $Na^+$ (purple spheres) and $Cl^-$ (green spheres) ions in the silica pore are shown after 250 ns of simulation at 300 K. White, red, and brown spheres represent hydrogen, oxygen, and silicon atoms of the solid substrate, respectively. Water molecules are not shown for clarity. (b) Enlarged detail of one simulation snapshot illustrating one $Cl^-$ ion in contact with the silica surface. Only selected atoms from the solid substrate are shown to illustrate the reorientation of the surface hydroxyl groups near the $Cl^-$ ion.....154

Figure 7.2: Atomic density profiles for $Na^+$, $Cs^+$, and $Cl^-$ ions as a function of the distance $z$ from the fully hydroxylated silica surfaces. Panels a and b show data for NaCl and CsCl aqueous solutions, respectively. The reference ($z$ = 0) for these calculations is the first innermost plane of silicon atoms. All simulations are conducted at $T$ = 300 K, results are obtained as average during the last 40 ns of the 250 ns simulations.....156

Figure 7.3: Atomic density profiles for $Cl^-$ ions as a function of the distance $z$ obtained at different simulation time segments. The data shown are for the system with 64 pairs of NaCl ions. Dotted black, dashes blue, red, and green, and solid black correspond to density profiles at 20 ns, 40 ns, 60 ns, 100 ns and 140 ns, respectively. Each curve is obtained as average of simulations results observed during 40ns of simulation (eg., data obtained from 60 to 100 ns are shown as the green dashed line labeled "100 ns"). The reference ($z$ = 0) for this calculation is the first innermost plane of silicon atoms.....157

Figure 7.4: Atomic density profiles for water oxygen and hydrogen atoms as a function of the position $z$ across the silica pore. The reference ($z$ = 0) is the first innermost plane of silicon atoms. Results are identical in all system considered in this study. .....159

Figure 7.5: (a) Atomic density profiles of oxygen water with cations ($Na^+$, $Cs^+$) and oxygen water with anions ($Cl^-$) as a function of distance $z$ from the solid surface. The data are shown for the aqueous solution containing both NaCl and CsCl. The reference ($z$ = 0) for this calculation is the first innermost plane of silicon atoms. .....161

Figure 7.6: Simulation snapshots are illustrating the movement of cations in the silica nanopores. (a) The diffusion of $Na^+$ along its equilibrium positions. (b) The adsorption path for $Cl^-$ on the silica surface. Only the second (at 3.90 Å, see Table 7.1) layer of interfacial water is shown for clarity. .....162

Figure 7.7: In-plane mean square displacement of $Na^+$, $Cs^+$, and $Cl^-$ in the silica pores. The data are shown for NaCl and CsCl aqueous solutions. We note that the in-plane means square displacement curve for $Cl^-$ is identical in both systems. .....163

## Abstract

Interfacial water properties determine a number of phenomena in geology, biological systems, and ion-exchange processes. The behavior of water at the solid-liquid interface plays an important role in multiple applications including water desalination membranes, porous materials used in radioactive ion separations, and in the structure-function relationship in ion channels and biological membranes. Understanding the properties of interfacial water is therefore essential for securing progress in all these areas. Molecular dynamics simulations were performed to provide molecular level insights of the structural and dynamic behavior of interfacial water near various solid substrates. Density profiles, radial distribution functions, and in-plane density distributions were calculated to study the effect of silica, alumina, and graphite surfaces on the structure of interfacial water. Our results show the formation of two distinct structured water layers with in-plane density distributions highly dependent on the surface chemistry of the substrate. Our findings suggest that due to the surface, the perturbation of the water structure decreases as the distance from the solid substrate increases, becoming a non-factor for distances greater than ~14 Å from the surface. The in-plane organization of water molecules in contact with the surface also locally affects the hydrogen bond network and consequently the dynamic behavior of interfacial water. The dynamic properties were assessed in terms of residence and reorientation correlation functions. An anisotropic dynamic reorientation was observed for water at the silica surface. Towards deploying experimental techniques to validate our predictions, massive molecular dynamics simulations were utilized to study hydration forces near alumina surfaces. A single-walled carbon nanotube (CNT) was employed to

mimic an atomic force microscope (AFM) tip used in force spectroscopy. The results illustrate oscillatory hydration forces that act on the CNT at small separations. Changes on the local interfacial water density due to the presence of the CNT tip yield non-sinusoidal oscillations on the force profiles with a width of approximately the size of a water molecule. High local water density yields pronounced repulsive forces, while local density depletion yields attractive forces. Finally, we studied the behavior of aqueous electrolyte solutions in slit-shaped silica nanopores. The results support the existence of ion-specific effects under confinement, which can be explained by the properties of interfacial water.

# 1 Introduction

Water is one of the most important and essential molecules responsible for life. It has been extensively studied due to its importance, abundance in nature, and its interesting physical chemical properties. Water continues to fascinate the scientific community. Water at interfaces has generated, and continues to generate, significant research interest especially at nanoscale dimensions where unexpected physical phenomena may appear. These phenomena are typically classified as "hydrophilic" and "hydrophobic" and are important in biology, geology, and materials science. The understanding of interfacial water at the molecular level could potentially impact different fields ranging from nanotribology,[1-3] microfluidics,[4] lab-on-a-chip and molecular engineering.[5, 6] Structural properties of interfacial water are of significant importance in biological systems[7] and various processes such as the structure-function relationship of ion channels,[8-10] the dynamic behavior of biological membranes,[11, 12] and biolubrication.

Experimental studies have elucidated several features about the structural and dynamic properties of water in contact with various hydrophobic and hydrophilic substrates.[11, 13, 14] A number of data confirm significantly different behavior of interfacial water compared to that observed in the bulk. Such studies include backscattering spectroscopy,[15] quasi-elastic neutron scattering,[16] attenuated total reflectance infrared spectroscopy,[17] X-ray reflectivity measurements,[18] and ultrafast infrared spectroscopy.[19] For instance, Fenn et al. employed ultrafast infrared spectroscopy to study orientational dynamics of water at neutral and ionic interfaces.[19]

Their findings confirm a slower orientational relaxation of water at these interfaces compared to bulk water.

Computer simulations can play a synergistic role in fully describing and interpreting the experimental findings. Both molecular dynamics and Monte Carlo simulation techniques have been employed to study structural properties of interfacial water on surfaces such as silica and graphite,[20-31] inside and outside carbon nanotubes and fullerenes,[32-36] and near self-assembled monolayers exhibiting various terminal functionalities.[37] Among those contributions that assessed the dynamics of water at interfaces, Mamontov et al.[15] reported molecular dynamics simulations data, combined with experimental neutron scattering, for water on rutile. The data demonstrated that the rutile substrate determines not only the local structure of hydration water, but also its dynamic properties. The scattering experiments probed several types of molecular motions within the hydration layers, the features of which depend, as shown by the molecular dynamics simulations, on an interplay of water-water and water-surface preferential interactions. More recently, Romero-Vargas Castrillón et al.[38] showed that the rotational dynamics of interfacial water is slower than that of bulk water, but only for a distance of ~0.5 nm from a silica surface, while the translational dynamics, also slower at silica interfaces than in the bulk, is affected for up to ~1.0 nm from the silica substrate. Martí et al.[39] simulated water on flat graphitic substrates and showed that both the local dielectric constant, and the in-plane diffusion coefficient are significantly different compared to those observed in the bulk. In a recent study Debenedetti and coworkers[40] reported molecular dynamics simulations for interfacial water on a model silica-based surface. The surface polarity was adjusted to assess the relationship

between surface properties and dynamic behavior of interfacial water. The results showed that although the surface polarity affects both translational and rotational diffusion, the relationship is not monotonic because it is mediated by the structure of interfacial water.

Despite this wealth of research, a number of key issues remain unresolved. For instance, it is not clear how the solid structure perturbs interfacial water and how far from the solid this perturbation persists. The effect of surface chemistry and heterogeneity on the structural properties of interfacial water needs to be investigated further. Likewise, important dynamic properties of water need to be further explored and quantified. In particular, the rate of water reorientation and exchange rate of water molecules within the interfacial region are of particular importance in many scientific disciplines, however are still not fully understood.

In the first three chapters we employed molecular dynamics simulations to provide molecular level insight of the structural and dynamic behavior of interfacial water at different substrates. The main objective of Chapter 2 is to investigate properties of interfacial water and the hydrogen bonding network that develops when water molecules interact with different crystalline silica surfaces and graphite. This study focuses on the properties of water within the first few molecular layers from the substrate, where significant structural and dynamic changes are observed compared to bulk properties. In Chapter 3 and Chapter 4 we focus on structural and dynamic changes that occur on interfacial water when the degree of hydroxylation of the silica surface varies. A detailed layer-by-layer analysis is provided for structural and dynamic properties and how they depend on the solid surface properties.

In Chapter 5 we investigate the behavior of water at α-aluminum oxide (0001) surface. Alumina is used as a catalyst and catalyst support, as a substrate in microelectronic devices, and in many other applications. Complex surface hydroxylation and dehydroxylation phenomena are observed at the alumina surface in the presence of water. Numerous investigations have focused on changes in the surface chemistry of alumina in hydrated environments.[41-47] We employed all-atom equilibrium molecular dynamics simulations to probe the effect of aluminum-terminated and fully hydroxylated α-$Al_2O_3$ surfaces on the behavior of interfacial water.

The aluminum-terminated and fully hydroxylated alumina substrates were used in Chapter 6 for the investigation of hydration forces at the solid-liquid interface. Probing the properties of interfacial water has been the focus of several experimental studies, such as surface force apparatus[48] and atomic force microscopy (AFM).[49-51] AFM yields force profiles between the surface and the AFM tip. These profiles typically show oscillatory behavior with fixed periodicity of roughly the diameter of a water molecule and of increasing amplitude as the separation decreases. For instance, Jarvis et al. reported hydration forces with these features on a self-assembled monolayer by utilizing an AFM with tips made by multiwall carbon nanotubes.[49] In this study, we employed massive all-atom molecular dynamics simulations to mimic a capped carbon nanotube (CNT) tip that may be used as an AFM probe for the measurement of hydration forces at the alumina-water interface. Our results and molecular level insights will aid in the better interpretation of solvation forces obtained experimentally. These simulation results are also important for the interpretation of force-distance data that we collected on sapphire using a high-precision AFM.

The behavior of aqueous electrolyte solutions near charged surfaces under confinement is the focus of the material presented in Chapter 7. A number of applications related to biological membranes and ion-channels,[52, 53] design of ion-exclusion processes, and desalination membranes[54-56] require a detailed understanding of solvent-electrolyte properties under confinement. The widely used classical Poisson-Boltzmann (PB) theoretical approach is hampered by the mean-field approximation and the infinitesimal description of ions it implements. It is well known that these approximations could lead to an unsatisfactory description of the electric double layer. In Chapter 7 we utilize all-atom equilibrium molecular dynamics simulations for the study of the structure and dynamics of aqueous electrolyte solutions within slit-shaped silica pores. The data were analyzed after extensive equilibration times and reveal details on the distribution of ions in the nanopores. Our results suggest that water-ion correlations play an important role and to a large extent determine the properties of aqueous electrolytes under confinement.

# 2 Molecular Structure and Dynamics in Thin Water Films at the Silica and Graphite Surfaces

The material presented below was published in 2008 in volume 112, issue 35 of The Journal of Physical Chemistry C. This work was also featured as the cover art.

## 2.1 Abstract

The structure and dynamic properties of interfacial water at the graphite and silica solid surfaces were investigated using molecular dynamics simulations. The effect of surface properties on the characteristics of interfacial water was quantified by computing density profiles, radial distribution functions, surface density distributions, orientation order parameters, residence and reorientation correlation functions. In brief, our results show that the surface roughness, chemical heterogeneity and surface heterogeneous charge distribution affect the structural and dynamic properties of the interfacial water molecules, as well as their rate of exchange with bulk water. Most importantly, our results indicate the formation of two distinct water layers at the $SiO_2$ surface covered by a large density of hydroxyl groups. Further analysis of the data suggests a highly confined first layer where the water molecules assume preferential hydrogen-down orientation and a second layer whose behavior and characteristics are highly dependent on those of the first layer through a well-organized hydrogen bond network. The results suggest that water-water interactions, in particular hydrogen bonds, may be largely responsible for macroscopic interfacial properties such as adsorption and contact angle.

## 2.2 Introduction

Water at interfaces has generated, and continues to generate, significant research interest especially at nanoscale dimensions where unexpected chemical and physical phenomena may appear. The study of interfacial water has potential impact in many different fields ranging from geology,[57, 58] nanotribology,[1-3] microfluidics,[4] lab-on-a-chip and molecular engineering.[5, 6] Structural properties of interfacial water are of significant importance in biological systems[7] and various specific processes such as the structure-function relationship of ion channels,[8-10] the dynamic behavior of biological membranes,[11, 12] and biolubrication. Understanding the structure and behavior of water near different substrates can clarify a number of phenomena and processes, typically classified as "hydrophobic" and "hydrophilic" effects.

Experimental studies have elucidated several features about structural and dynamic properties of water in contact with various hydrophobic and hydrophilic systems.[3, 11, 13, 14, 59] Commonly, simulations have contributed to a better understanding and interpretation of experimental results.[13] Both molecular dynamics and Monte Carlo simulation techniques have been employed to study interfacial water on surfaces such as silica and graphite.[13, 20-29] A well-established conclusion is that both structural and dynamic properties of interfacial water depend on the atomic-scale geometry and heterogeneous chemical properties of the solid substrate. Computer simulation studies have also addressed the structural properties of water inside and outside carbon nanotubes and around fullerenes.[32-36]

Despite this wealth of research, a number of key issues remain unresolved. For instance, it is not clear how the solid structure perturbs interfacial water and how far

from the solid this perturbation persists.[60] Important dynamic properties such as the rate of water reorientation and exchange in the perturbed layer need to be investigated further. It is also of interest to identify the structural properties (e.g. atomic scale roughness and/or heterogeneous distribution of partially charged groups on the solid surface) that render a substrate hydrophobic and hydrophilic as determined from macroscopic observation (e.g. contact angle measurements). One possible route to answer this scientific question is to conduct simulations of thin water films on a number of well controlled surfaces with different degrees of hydrophilicity. Then, by analyzing how the structural and dynamic properties of the interfacial water molecules change as the substrate goes from hydrophobic to hydrophilic it is possible to provide a bridge between the atomic-scale properties of a solid surface and the macroscopic observations. This is the purpose of the present work. Our main objective is to investigate the structure and dynamics of water molecules and the hydrogen bonding network that develops when water molecules interact with a solid crystalline substrate. This study focuses on the properties of water within the first few molecular layers from the substrate, where significant structural and dynamic changes are observed compared to bulk properties. A detailed layer-by-layer analysis is provided below for structural and dynamic properties and how they depend on the solid substrates.

This chapter is organized as follows. In section 2.3 we provide simulation details and algorithms, in section 2.4 we discuss our main results, and in section 2.5 we summarize our conclusions.

## 2.3 Simulation Methodology and Details

The goal of this study is to investigate the behavior and structural properties of a thin water film in contact with three different solid surfaces. The surfaces are chosen to represent different degrees of hydrophilicity. The first surface considered is graphite, which is composed by three graphene sheets separated by 3.35 Å from each other. The solid substrates are aligned parallel to the $x$ and $y$ plane. Simulations were carried out in orthorhombic simulation boxes of constant volume. The $x$ and $y$ dimensions of the simulation boxes reflect the periodicity of the solid crystalline substrate. In the case of graphite the $x$ and $y$ dimensions are 29.5 and 34.1 Å, respectively. The second and third surfaces were obtained from the crystal structure of β-cristobalite $SiO_2$.[61] To obtain a realistic surface structure we followed the procedure of Pellenq and coworkers.[20] The crystal was cut along the (111) crystallographic face. All the silicon atoms that are part of an incomplete tetrahedral were removed and the non-bridging oxygen atoms (bonded to only one silicon atom) were saturated with hydrogen atoms. The hydrogen atoms were positioned 1 Å perpendicular to the surface and treated as rigid. By cutting the cristobalite crystal at different depths we obtained two surfaces with different hydroxyl surface density and thus different degree of hydrophobicity. The two surfaces are identified as low hydroxyl surface density (LD), with 4.54 OH/nm$^2$, and high hydroxyl surface density (HD) with 13.63 OH/nm$^2$. Albeit these models represent approximations of solid surfaces, they allow us to understand how the thermodynamic and structural properties of interfacial water depend on the presence, density, and orientation of hydroxyl groups on the solid substrate. In the case of silica surfaces the $x$ and $y$ simulation box dimensions are 30.2 and 34.9 Å, respectively. The solid slab thickness is

25.7 Å for the LD silica surface and 23.6 Å for the HD one. A thicker solid slab for the silica surfaces, compared to graphite, was considered because the electrostatic interactions are significant in these substrates. Top views of the silica surfaces are shown in Figure 2.1 where the surface hydroxyl groups can be seen.

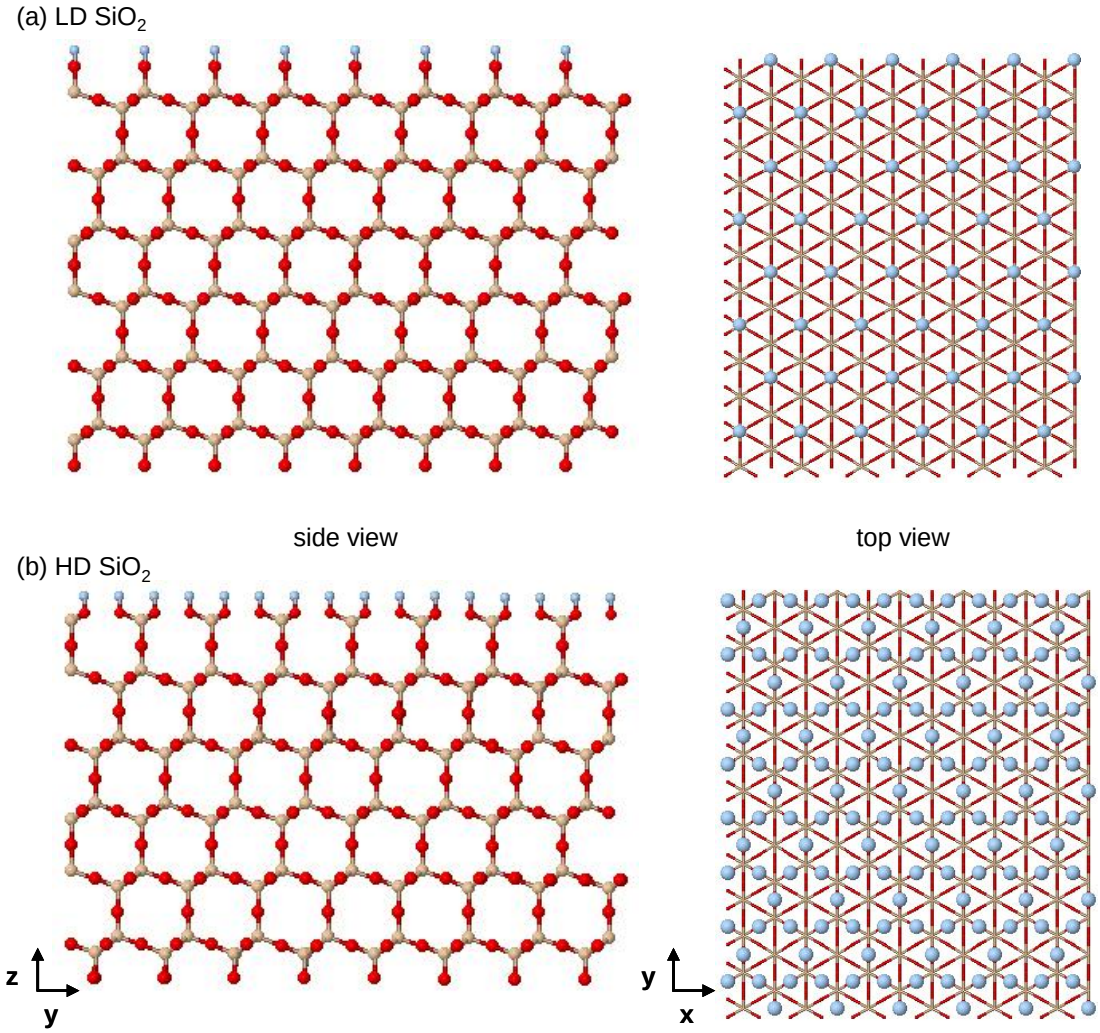


Figure 2.1: Side and top views of LD $SiO_2$ (a) and HD $SiO_2$ (b) surfaces. Blue, red and tan spheres represent the hydrogen atoms of the surface hydroxyl groups; oxygen and silicon atoms, respectively.

Two identical faces of the same rigid substrate were considered facing each other to represent a slit-shaped pore. Water was allowed in the space between the two solid surfaces. The simulation box was built by placing one slab of the solid substrates at the base and another, specularly symmetric, at a distance $H$ = 140 Å along the $z$-axis. To minimize interactions between the images of molecules along the $z$ direction an additional vacuum of thickness 30 Å was considered in the outermost side of the pores. The number of water molecules was 1000 and it was kept fixed, except when otherwise noted. Water molecules were placed in between the solid substrates as shown in Figure 2.2 for the case of graphite. Periodic boundary conditions were applied along the $x$, $y$ and $z$-axis.

The water molecules were simulated using the simple point charge/extended (SPC/E) model.[62] Carbon atoms of the graphite were held stationary and modeled as Lennard-Jones (LJ) spheres employing the parameters proposed by Chang and Steele.[63] The atoms of the silica substrates interact with water molecules by means of dispersive and electrostatic forces.[64] The dispersive interactions were modeled with a 12-6 Lennard-Jones potential. The LJ parameters for unlike interactions were determined using the Lorentz-Berthelot mixing rules.[65] The cutoff distance for all interactions is set to 9 Å and the long-range electrostatic interactions were treated using the Ewald summation method.[65] Bond lengths and angles in water molecules were kept fixed using the SHAKE algorithm.[66] In Table 2.1 we report all the parameters used to represent the force field in our simulations. Note that silicon atoms do not interact via dispersive interactions with water molecules.

Table 2.1: Parameters used within the force fields implemented in our simulations. In the case of silica, bO and nbO stand for bridging and non-bridging oxygen atoms, respectively.

| | Site | σ (Å) | ε (Kcal/mol) | q (e) |
|---|---|---|---|---|
| Water | O | 3.166 | 0.155402 | −0.8476 |
| | H | 0.000 | 0.000000 | 0.4238 |
| Graphite | C | 3.400 | 0.055700 | 0.0000 |
| Silica | Si | 0.000 | 0.000000 | 1.2830 |
| | bO | 2.700 | 0.456757 | −0.6290 |
| | nbO | 3.000 | 0.456757 | −0.5330 |
| | H | 0.000 | 0.000000 | 0.2060 |

The equations of motion were solved using the large-scale atomic/molecular massively parallel simulator (LAMMPS).[67] All simulations were performed in the canonical ensemble (NVT) where the number of particles ($N$), the simulation box volume ($V$), and the temperature ($T$) were kept constant. The system temperature was set at 300 K and controlled by a Nosé-Hoover thermostat with a relaxation time of 100 fs. The integration of the equations of motion was performed by the velocity-Verlet algorithm[65] with a time step of 1.0 fs. Each simulation ran for $10^6$ time steps that accounts for 1 ns of total simulation time. All the results presented in this study were obtained after 0.2 ns of equilibration time. During the production time, which last 0.8 ns, the atom positions were recorded every 200 time steps, corresponding to 0.2 ps, and retained for further analysis.

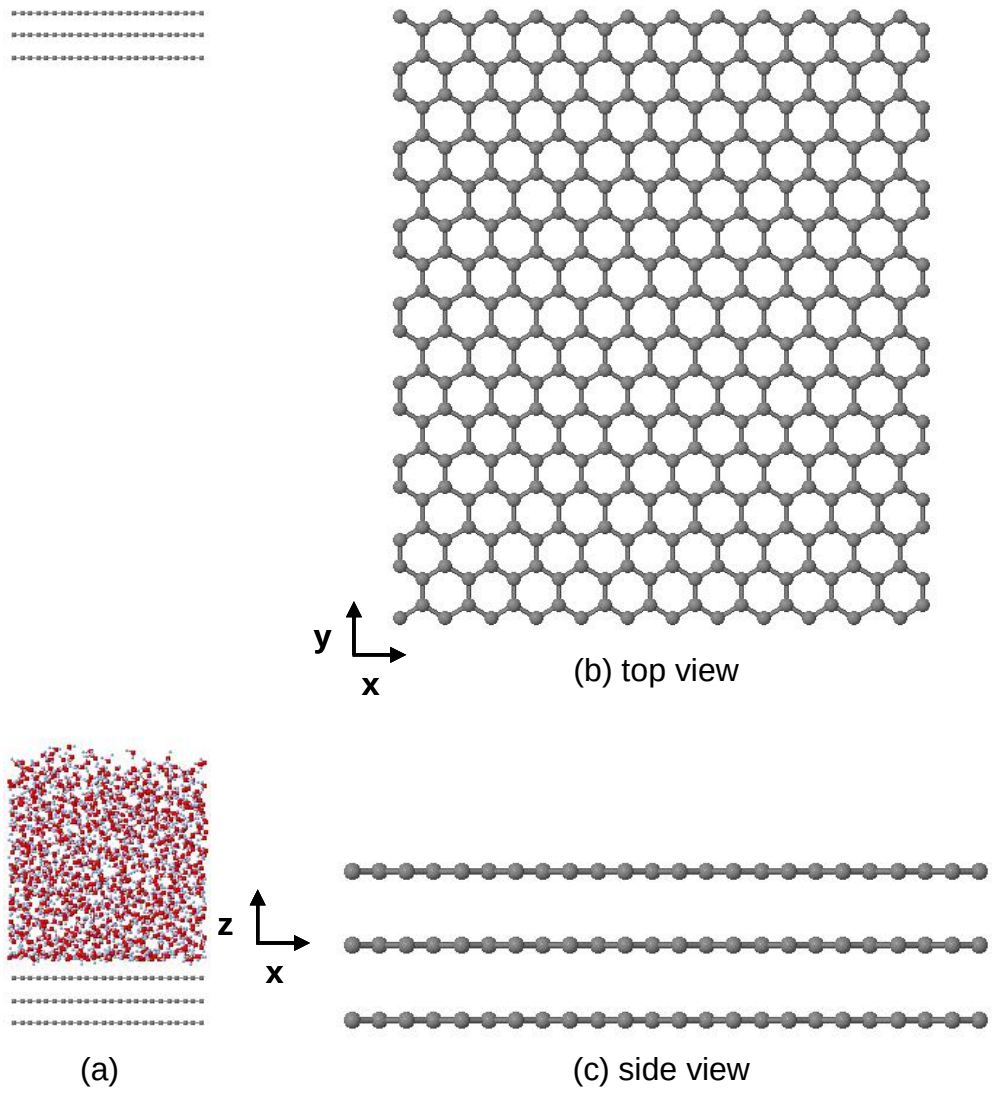


Figure 2.2: Snapshots of the graphite substrates used in our simulations. (a) Side view of the entire simulation box with water molecules in contact with the lower graphite surface. (b) Top and (c) side view of the graphite surface. In the top view only one of the graphene sheets is shown for clarity.

## 2.4 Results and Discussion

### 2.4.1 Atom Density Profiles

To assess the effect of film thickness on all properties of interfacial water molecules we conducted a number of simulations where the number of water molecules was reduced from 2592 to 1008. The results are shown in Figure 2.3 in terms of atomic density profiles of the oxygen atom of water molecules as a function of the distance from the graphite surface. As expected, the film thickness decreases as the number of simulated water molecules decreases, but our results indicate that the density profiles at the graphite-water interface, as well as that at the water-vacuum interface, do not depend on the film thickness. Further, the density profile at the center of the thin film is similar in all the cases considered. Thus, for economy of computational time we focused on thin films of 1000 water molecules at the solid-liquid interface in the remainder of this work.

In Figure 2.4 we show plots of the atomic densities of oxygen and hydrogen atoms of water molecules as a function of the distance $z$ perpendicular to the surfaces. Results are shown when the solid surface is graphite (solid line), LD $SiO_2$ (dotted line), and HD $SiO_2$ (dashed line). The reference point ($z$ = 0) for the density profile is the center of carbon atom in the outermost graphene sheet in the case of graphite and that of the non-bridging oxygen atoms in the LD or HD $SiO_2$ surfaces. The location of all the peaks that are observed in the density profiles in Figure 2.4 are reported and labeled in Table 2.2. This labeling will become useful in the following discussion. In the case of water on graphite (continuous line), the results presented in Figure 2.4a indicate one pronounced peak at 3.25 Å that clearly signifies the formation of one layer of water

molecules. In the same plot a second, less pronounced peak can be detected at 6.25 Å. In the case of the LD $SiO_2$ substrate, a distinct peak is located at 3.05 Å and a second, less pronounced peak appears at approximately 6.00 Å. Further, the appearance of a "shoulder" at 2.15 Å indicates the presence of structured water molecules very close to the LD $SiO_2$ surface. Interestingly, two pronounced layers of oxygen atoms are manifested at 2.15 and 2.95 Å on the HD $SiO_2$ surface. This suggests that a large amount of water molecules accumulate closer to the surface because of the increased surface hydroxyl density. In particular, we observe that the "shoulder" that appears at 2.15 Å on LD $SiO_2$ surface becomes a fully developed peak on the HD $SiO_2$. On the latter surface a smaller peak develops at 5.75 Å, closer to the surface than the peak at ~6.00 Å observed on the LD $SiO_2$ surface.

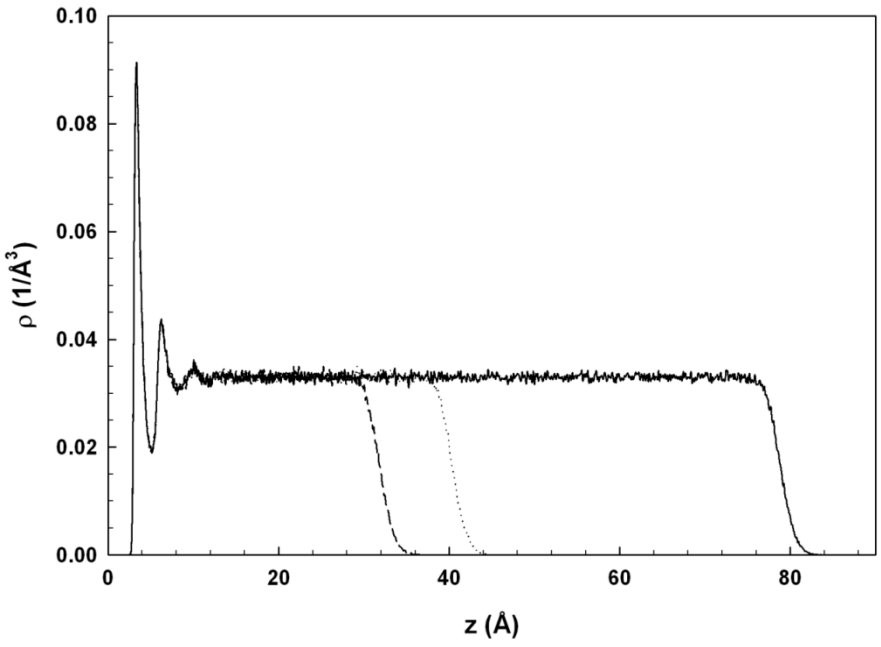


Figure 2.3: Oxygen atomic density as a function of distance *z* from the graphite surface. The oxygen atoms are those of water molecules. Three cases are shown in which 2592 (solid line), 1296 (dotted line), and 1008 (dashed line) water molecules were simulated. In all cases $T$ = 300 K.

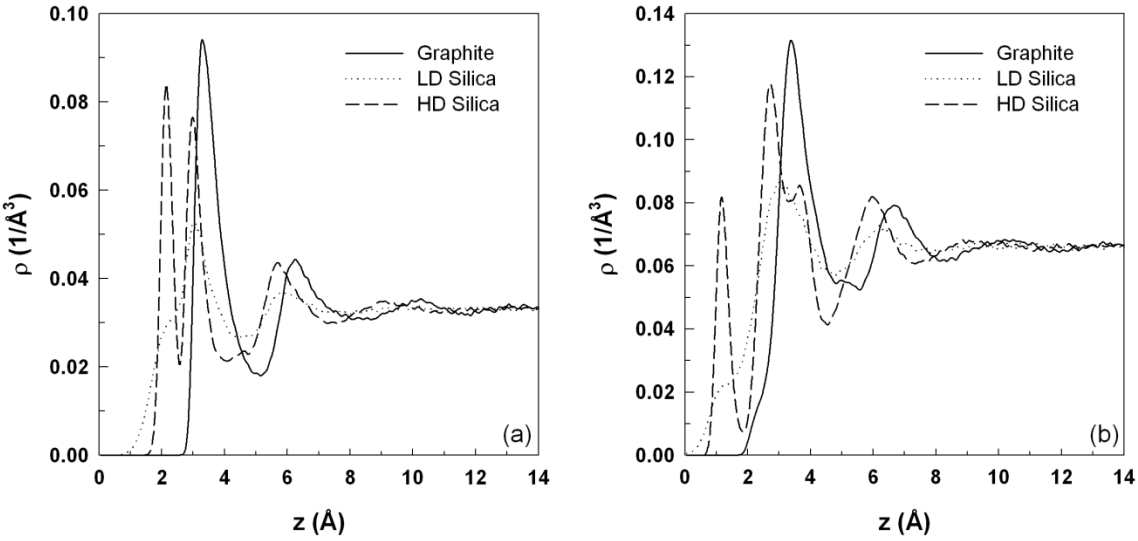


Figure 2.4: (a) Oxygen and (b) hydrogen atom density profiles as a function of distance $z$ from the solid surfaces. The reference $z = 0$ is the top plane of carbon atoms in the case of the graphite surface and the plane of non-bridging oxygen atoms in the case of both LD and HD silica surfaces.

Commensurate with the structuring of water evident from the oxygen atomic density profiles, in Figure 2.4b we observe layers of water hydrogen atoms. The most interesting data are those obtained on the HD $SiO_2$ surface. In this case (dashed line), four layers of hydrogen atoms appear at 1.15, 2.75, 3.65 and 6.05 Å. Consideration of the first peak (at 1.15 Å) on the HD $SiO_2$ surface in Figure 2.4b combined with the corresponding oxygen atoms located 1 Å above (the peak at 2.15 Å in Figure 2.4a) suggests a hydrogen-down orientation of the water molecules. Further, the highest peak (at 2.75 Å) on the HD $SiO_2$ in Figure 2.4b corresponds to the layer of hydrogen atoms that could belong to the water molecules of the first (at 2.15 Å) or second (at 2.95 Å) layer observed in the oxygen atomic density profiles in Figure 2.4a. Similarly to what observed for the oxygen atomic density profiles, we noticed that the first peak that appears in the hydrogen density profile at 1.15 Å at the HD $SiO_2$ is only a shoulder on

the LD $SiO_2$ surface. This indicates that increasing the surface density of hydroxyl groups has a very pronounced effect on the structure of interfacial water.

Table 2.2: Location (expressed at distance *z* from the surface) of the atomic density peaks of oxygen and hydrogen atoms on the various surfaces considered in Figure 2.4. On the fourth column we provide the labels used in our discussion to refer to the peaks. The first and second letters of the labels indicate the substrate and the atomic species, respectively. The number in the label corresponds to the layer, with layer 1 being the one closer to the substrate.

| Surface | Oxygen peak (Å) | Hydrogen peak (Å) | Layer label |
|---|---|---|---|
| Graphite (A) | 3.25 | 3.35 | AO-1 / AH-1 |
| | 6.25 | 6.65 | AO-2 / AH-2 |
| LD $SiO_2$ (B) | 2.15 | 1.15 | BO-1 / BH-1[α] |
| | 3.05 | 2.95 | BO-2 / BH-2 |
| | 6.00 | 6.25 | BO-3 / BH-3 |
| HD $SiO_2$ (C) | 2.15 | 1.15 | CO-1 / CH-1 |
| | 2.95 | 2.75 | CO-2 / CH-2 |
| | 5.75 | 3.65 | CO-3 / CH-3 |
| | - | 6.05 | CO-4 / CH-4 |

[α] this position corresponds to a "shoulder" in the density profile.

### 2.4.2 Planar Radial Distribution Functions

The results in Figure 2.4 clearly indicate that the presence of solid surfaces affect the density of the interfacial water, with the formation of layers of different density. This is in agreement with the work presented by a number of other groups.[13, 20, 25, 68] It is now of interest to determine whether or not water molecules belonging to each layer show pronounced differences when compared to the bulk. The results presented in Figure 2.5, Figure 2.6, and Figure 2.7 show in-plane oxygen-oxygen, $g_{OO}(r)$, hydrogen-hydrogen, $g_{HH}(r)$, and oxygen-hydrogen, $g_{OH}(r)$ radial distribution functions (RDFs). The RDFs are calculated in correspondence of slabs at several distances from the

surface. The thickness ($\delta z$) of the slab is 1 Å in all cases and the center of a slab corresponds to the peak of one specific layer as reported in Table 2.2. In some cases the center of the slab had to be displaced by 0.1 to 0.2 Å from the peak position in order to avoid interferences from atoms of adjacent layers. The in-plane RDFs obtained in correspondence to the interfacial peaks are compared to the RDFs calculated in the center of the thin interfacial water film ($z$ > 14 Å), which is identified as "bulk". The "bulk" RDFs are identical for all surfaces considered and are only shown in panel (a) of Figure 2.5, Figure 2.6, and Figure 2.7. According to the RDFs, the closer the water molecules are to the surface, the more structured the fluid becomes. Upon closer inspection, the results for the in-plane RDFs demonstrate that a solid surface affects the properties of interfacial water far beyond the mere increase of density shown in Figure 2.4. Further, it is clear from our results that these effects are surface-specific. In the case of graphite we observe that the peaks in all the RDFs become slightly more pronounced as we move from the center of thin films to the first layer on the solid surface. However, the position of the peaks in all RDFs does not change substantially. This indicates that the structure of water near graphite is substantially similar to that in the bulk, except for a slight increase in the density noted by previous studies and evident from the density profiles shown in Figure 2.4.[68, 69]

The behavior of water becomes more complex in the case of $SiO_2$ surfaces. Even on LD $SiO_2$ we note that the peak in the RDFs change shape as well as intensity. Because the RDFs (in particular the O-H and H-H ones) are representative of the hydrogen-bonding network, these results suggest that the presence of hydroxyl groups on the $SiO_2$ surfaces. Additionally, the atomic scale roughness affects the hydrogen-

bonding network between interfacial water molecules as they approach the solid surface. This behavior becomes more extreme in the case of the HD $SiO_2$ surface where it is not only obvious that water molecules in the first layer cannot form hydrogen bonds between themselves (the center-to-center corresponding to the first peak in layer CH-1 shifts to 5 Å, too far for hydrogen bonds to form), but they also exhibit typical features of solid-like structures. In particular the $g_{OO}(r)$ goes to zero between consecutive peaks. Because the main difference between LD and HD $SiO_2$ surfaces is the density of surface hydroxyl groups, it is clear that these perturb significantly the structure of water molecules, even at ambient conditions.

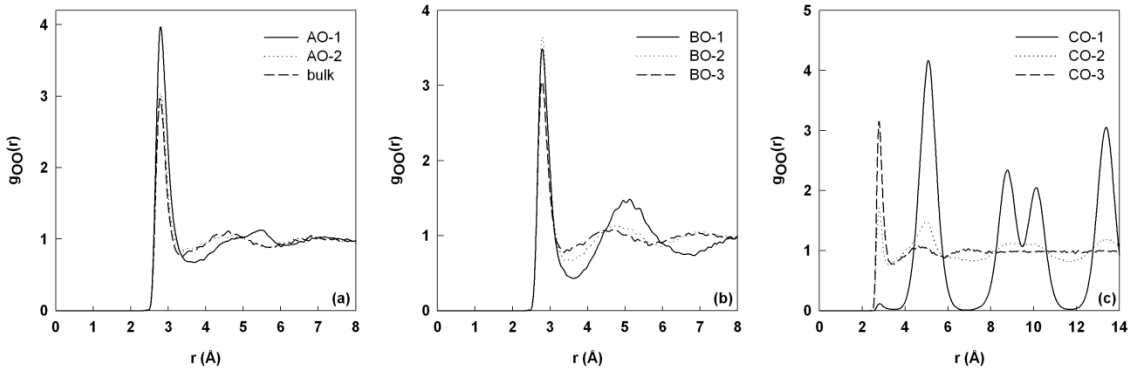


Figure 2.5: In-plane oxygen-oxygen radial distribution functions $g_{oo}(r)$ of graphite (a), LD $SiO_2$ (b), and HD $SiO_2$ (c). The dashed line of figure (a) corresponds to an in-plane RDF far from the surfaces ($z$ > 14 Å) and is identical in all cases.

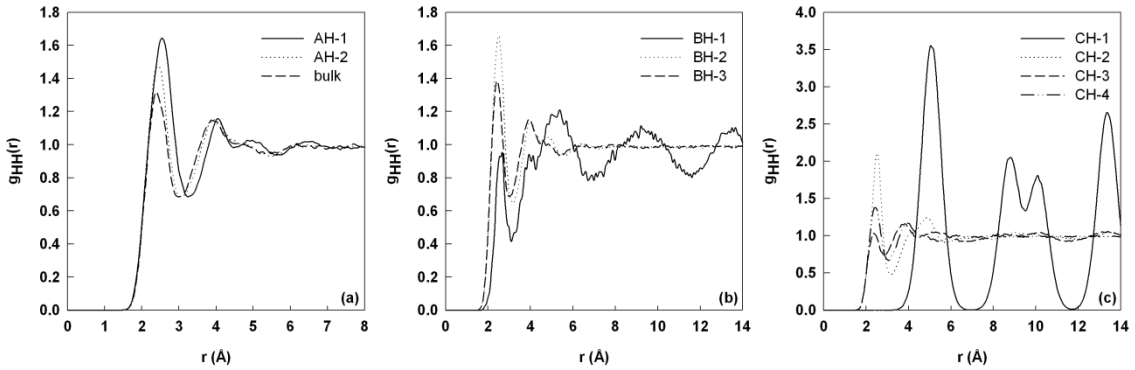


Figure 2.6: In-plane hydrogen-hydrogen radial distribution functions $g_{HH}(r)$ of graphite (a), LD $SiO_2$ (b), and HD LD $SiO_2$ (c). The dashed line of figure (a) corresponds to an in-plane RDF far from the surfaces ($z$ > 14 Å) and is identical in all cases.

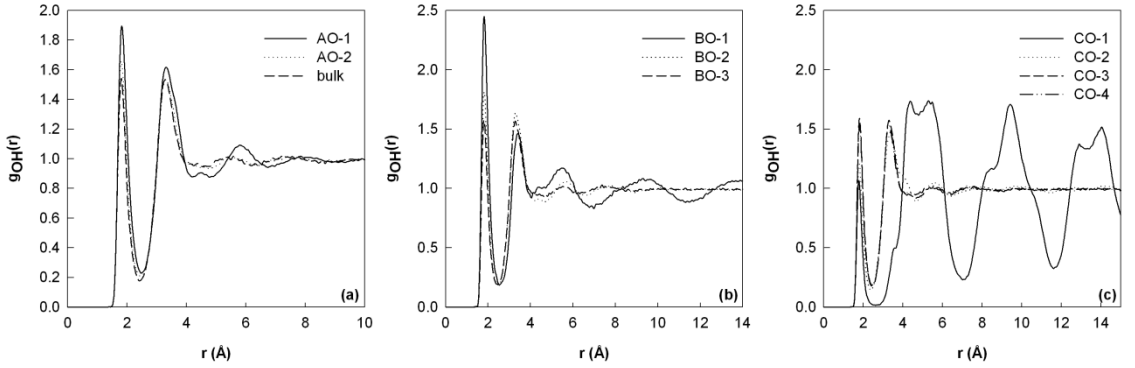


Figure 2.7: In-plane oxygen-hydrogen radial distribution functions $g_{OH}(r)$ of graphite (a), LD $SiO_2$ (b), and HD LD $SiO_2$ (c). The dashed line of figure (a) corresponds to an in-plane RDF far from the surfaces ($z$ > 14 Å) and is identical in all cases.

### 2.4.3 Surface Density Distributions

The results in Figure 2.5, Figure 2.6, and Figure 2.7 indicate that interesting properties of interfacial water develop near each solid surface. To further study the properties of water molecules within the first few molecular layers near a solid surface, we calculated the $x - y$ surface density distribution of oxygen and hydrogen atoms on planes whose location corresponds to the peaks of the density profiles (see Table 2.2). The results should be compared to the distribution of surface hydroxyl groups for HD

and LD $SiO_2$ shown in Figure 2.1. Similar to the radial distribution functions calculations, we considered slabs with thickness ($\delta z$) of 1 Å at different distances from the surface. When the calculation is performed for "bulk" water at the center of the thin film water film our results (not shown for brevity) indicate a uniform distribution of water molecules across the simulation box, as expected from both density profiles and in-plane RDFs discussed above. The effect of the surface on the water structure is negligible at distances larger than 14 Å from the surface for all surfaces considered.

To discuss the results we consider one surface at a time. In the case of graphite the in-plane RDFs did not indicate particular structure of interfacial water. The surface density distribution of oxygen atoms for layer AO-1 is shown in Figure 2.8a. The data presented in this contour plot indicate a uniform distribution of oxygen atoms in the first layer above the graphite surface. To clarify the results as well as the procedure adopted, in Figure 2.8b we show a drawing of the slab. The corresponding layer on the density profile is illustrated for better interpretation. A similar approach is followed in the calculations below.

In Figure 2.9 we provide data obtained on the LD $SiO_2$ surface. Panels (a) and (b) show the oxygen atom surface density profiles obtained in correspondence to peaks BO-1 and BO-2, respectively. The results presented in Figure 2.9a suggest a preferential distribution of oxygen atoms within layer BO-1. The high density areas of the contour plot indicate a highly structured layer where the oxygen atoms preferentially reside. The location of the high density areas is reminiscent of the hexagonal hydroxyl disposition on the solid substrate (see Figure 2.1a). In the second layer (BO-2), shown in Figure 2.9b, we observe some evidence of a preferential configuration. The oxygen atoms that

belong to this layer are located approximately 1 Å above the center of the hexagons observed in layer BO-1. The presence of distinct high density areas is in agreement with the corresponding $g_{OO}(r)$. However, the features of the $g_{OO}(r)$ found on the LD $SiO_2$ surface are similar to the ones for the bulk water, which explains the high translational freedom of oxygen atoms suggested by the contour plots shown in Figure 2.9.

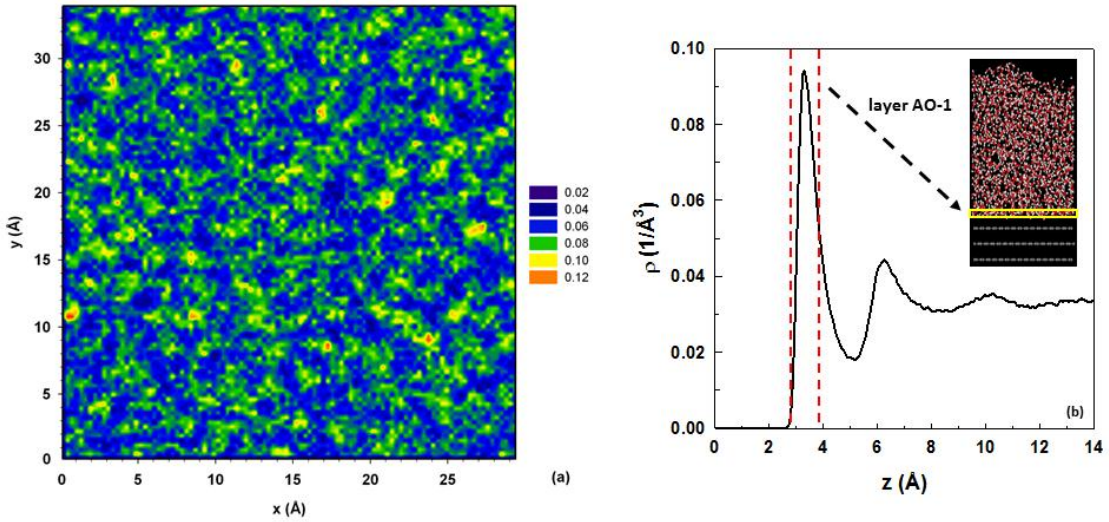


Figure 2.8: (a) Surface density distribution of oxygen atoms on graphite for the layer AO-1 that corresponds to the first peak of the density profile as shown schematically in panel (b). The surface density distribution is calculated on a slab of thickness 1 Å. See Table 2.2 for details on peak position. The units of the atomic density distribution (panel a) are given in $Å^{-3}$.

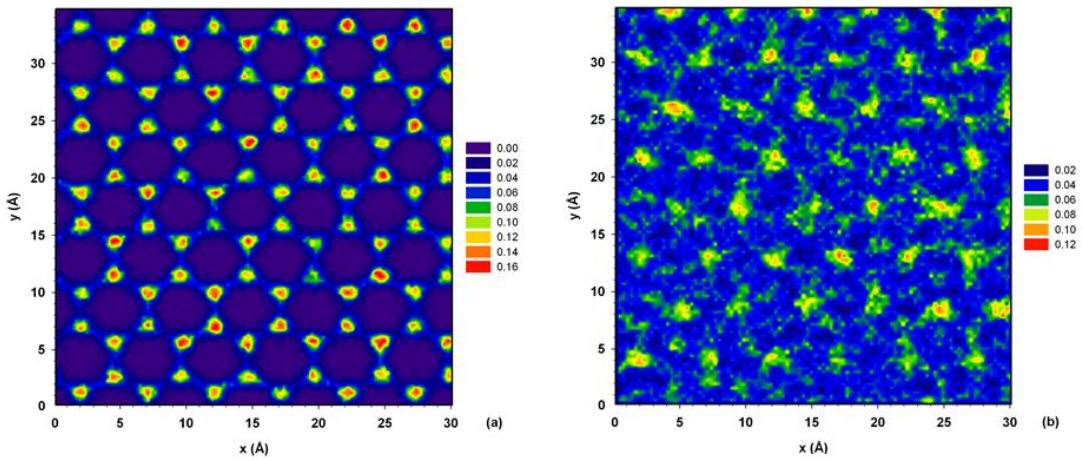


Figure 2.9: Surface density distribution of oxygen atoms on LD $SiO_2$ for the BO-1 (a) and BO-2 (b) layers. See Table 2.2 for details on peak position. The units of the atomic density distribution are given in $Å^{-3}$.

To complete the structural analysis in the case of water on LD $SiO_2$, we calculated the surface density distribution of the hydrogen atoms within specific layers. The results for hydrogen density distribution in layer BH-1 are presented in Figure 2.10. The data correspond to the layer located approximately 1 Å below the layer BO-1 of oxygen atoms of Figure 2.9a. Our results, complemented by the density profiles of Figure 2.4b, indicate the formation of a sparsely occupied layer where the hydrogen atoms reside along hexagonal structures. These data also suggest that water molecules in layer BO-1 form hydrogen bonds with those in layer BO-2. This molecular interaction may determine the distance *z* at which the surface manages to perturb the structure of interfacial water.

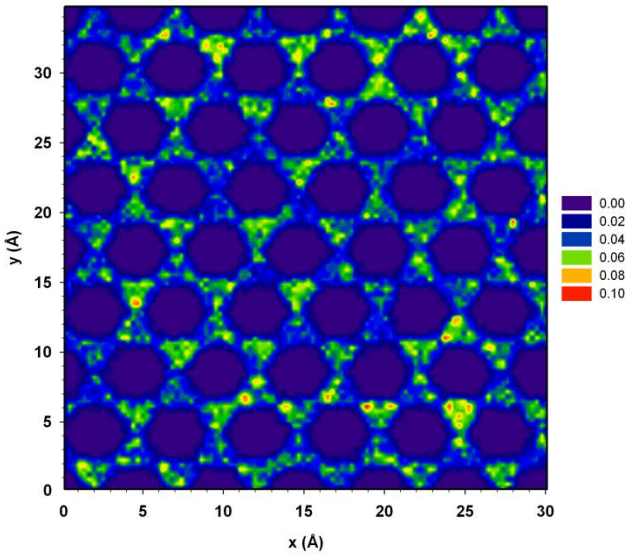


Figure 2.10: Surface density distribution of hydrogen atoms on BH-1 layer on LD $SiO_2$. See Table 2.2 for details on peak position. The units of the atomic density distribution are given in $Å^{-3}$.

As could be expected from the RDFs results, data on the HD $SiO_2$ are significantly different than those on all other substrates considered above. The results are shown in Figure 2.11 for the surface distribution of oxygen atoms in layers CO-1 (Figure 2.11a) and CO-2 (Figure 2.11b). The results indicate that oxygen atoms in layer CO-1 adopt a well-organized structure in which the oxygen atoms are highly confined within well-defined areas. The high density spots are very distinct and located above the center of hexagons formed by the surface hydroxyl groups shown in Figure 2.1a. It should be pointed out that the distance between the high-density areas in Figure 2.11a correspond to the distance between peaks in the in-plane RDFs shown in Figure 2.5c for layer CO-1. The pattern that appears in layer CO-2 (Figure 2.11b) suggests that the oxygen atoms have higher translational freedom than those in the layer CO-1. The contour plot reveals high density areas of hexagonal symmetry. The center of the hexagons observed in layer CO-2 corresponds to the location of the high density areas

for oxygen atoms observed in layer CO-1. However, the oxygen atoms of layer CO-2 primarily occupy every other vertex of the hexagon, and not every vertex, probably because of the establishment of a complex hydrogen-bonded network near the HD $SiO_2$ surface. Further, the results shown in Figure 2.11b suggest that all oxygen atoms located in layer CO-2 possess the ability to move along different directions in the $x - y$ plane.

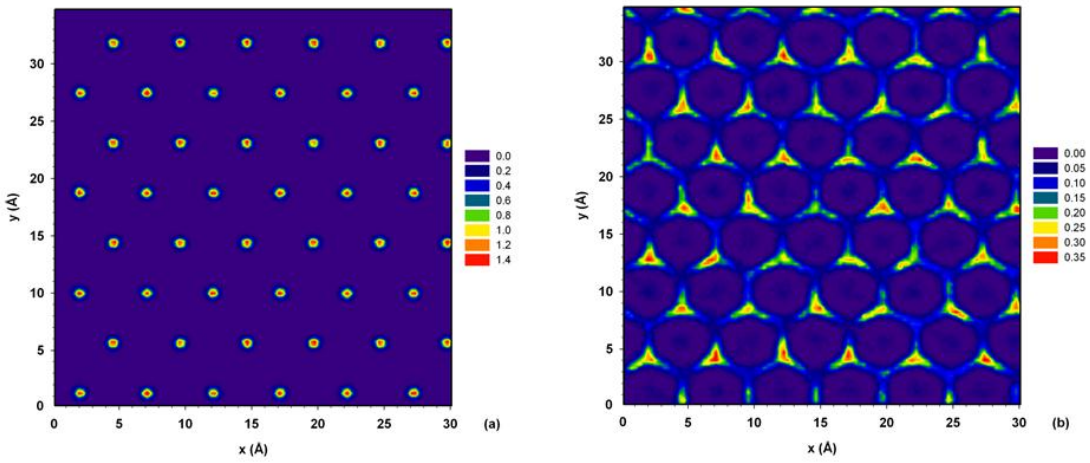


Figure 2.11: Surface density distribution of oxygen atoms on HD $SiO_2$ for the CO-1 (a) and CO-2 (b) layers. See Table 2.2 for details on peak position. The units of the atomic density distribution are given in $Å^{-3}$.

To complement the information gathered about the density distribution of oxygen atoms at the HD $SiO_2$ surface we report in Figure 2.12 the results for the surface density distribution for hydrogen atoms. Four peaks are considered: CH-1 (Figure 2.12a), CH-2 (Figure 2.12b), CH-3 (Figure 2.12c), and CH-4 (Figure 2.12d). The contour plots suggest a highly confined first layer of hydrogen atoms located 1 Å below the oxygen atoms of layer CO-1 (see Figure 2.12a). This finding corroborates the H-down configuration suggested by the observation of the corresponding hydrogen atomic density profiles (see Figure 2.4a and Figure 2.4b). The contour plot of Figure 2.12b identifies the high density areas where the hydrogen atoms exhibit preferential site

occupancy in layer CH-2. This diffuse distribution of hydrogen atoms is likely due to the fact that the hydrogen atoms in layer CH-2 are those covalently bonded to the oxygen atoms of layers CO-1 and CO-2. The hydrogen layer CH-2 has a higher atomic density than the hydrogen layers CH-1 and CH-3 due to the fact that it includes the hydrogen atoms of two adjacent water molecular layers. The pattern formed by the hydrogen atoms in layer CH-2 is circular and markedly different compared to the results obtained for the other layers discussed so far. The centers of the circles correspond to the position of the oxygen atoms in layer CO-1. The data analysis suggests that the first layer of water molecules is highly confined and one of the hydrogen, the one which belongs to layer CH-2, is involved in a rotational movement whose orientation is perpendicular to the surface axis formed by the second hydrogen (located in CH-1) and the oxygen (located in CO-1). The results presented in Figure 2.12c indicate that the hydrogen atoms within layer CH-3 are primarily located at every other vertices of a hexagonal pattern. The results shown in Figure 12a also suggest a strong limitation on translational movement for hydrogen atoms in the CH-3 layer. The results obtained in layer CH-4 (Figure 2.12d), located only at $z$ = 6.05 Å from the HD $SiO_2$ surface, indicate that any sort of surface-induced pattern for hydrogen atoms vanishes at distances larger than ~6 Å from the surface. This latter result helps us determine at what distance the surface effect is no longer strong.

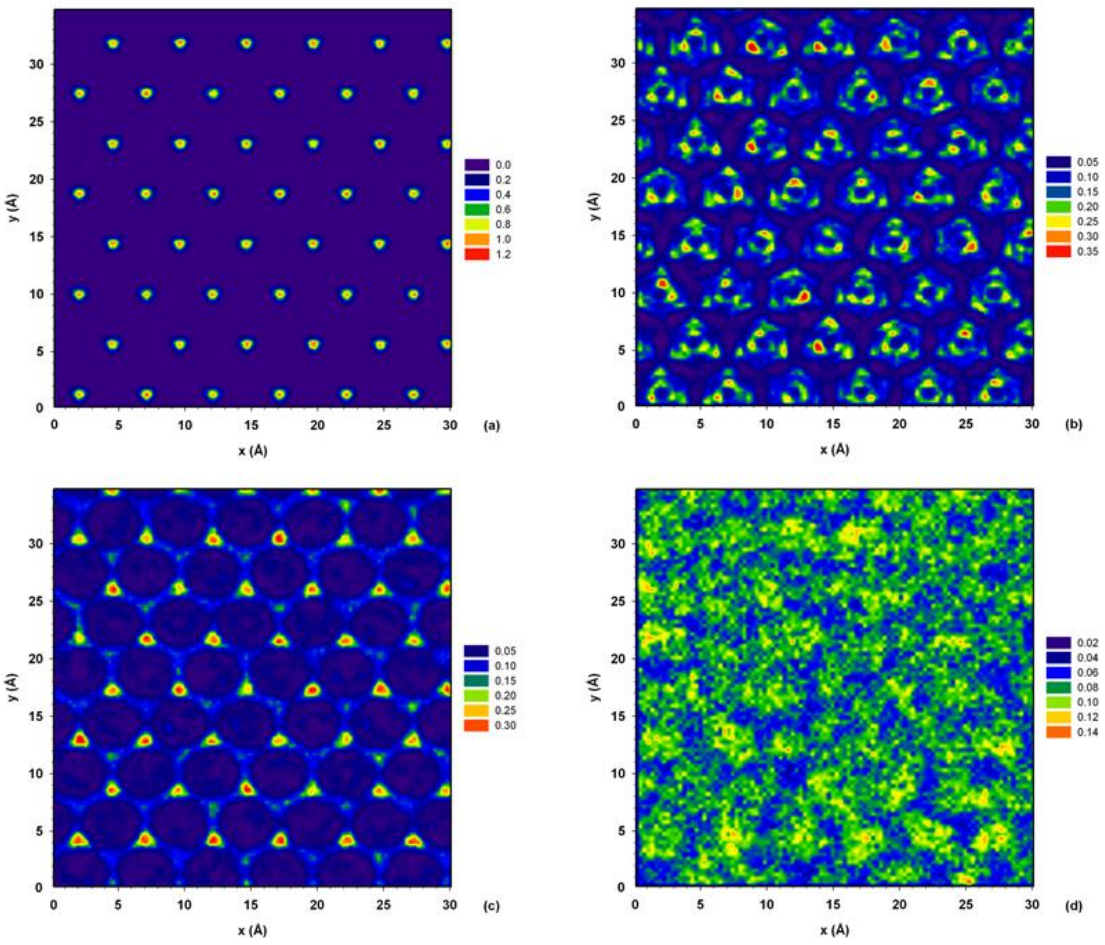


Figure 2.12: Surface density distribution of hydrogen atoms for the CH-1 (a), CH-2 (b), CH-3 (c), and CH-4 (d) layers on HD $SiO_2$. See Table 2.2 for details on peak position. The units of the atomic density distribution are given in $Å^{-3}$.

### 2.4.4 Water Orientation

The density profiles in Figure 2.4 indicate that the surface affects the axial distribution of water molecules. Similarly, in-plane RDFs and density distributions demonstrate that the mere presence of the surface may in some cases strongly affect the structure of water, generating even solid-like structures observed in the case of water on HD $SiO_2$. These results are by themselves important, but for a number of applications including lubrication and for the theoretical calculation of solvation forces it is

necessary to understand how the surface affects the orientation of interfacial water molecules. Thus we calculated the orientation order parameter $\langle cos(\theta) \rangle$ of water molecules as a function of their $z$ position. Angular brackets indicate ensemble averages. The angle $\theta$ is that between the opposite of the dipole moment vector and the vector normal to the surface. The order parameter equals zero in correspondence to an isotropic angular distribution. Nonzero values indicate a preferential orientation of the water molecules. Results for the order parameter obtained at the water-vacuum interface are in agreement with those of Thomas et al.[70] for all surfaces considered here, and are not shown for brevity. Those obtained at the solid-water interface are shown in Figure 2.13. Results are only shown for values of $z$ where water molecules are present. We observe a negative peak at approximately 2.15 Å and a positive peak at 2.85 Å for water on the HD $SiO_2$ surface. Similarly, we observe a negative and a positive peak for water on LD $SiO_2$, indicating preferential orientation of water molecules in the interfacial region. In the case of water on graphite the first broad peak that appears in Figure 2.13 suggests a weak preferred orientation for interfacial water molecules, as previously reported by others.[68, 69, 71] According to these results, the water molecules in contact with the graphite surface tend to project some hydrogen atoms toward the solid. Although no hydrogen bonds are possible with the surface, this configuration is thought to maximize the number of water-water hydrogen bonds.

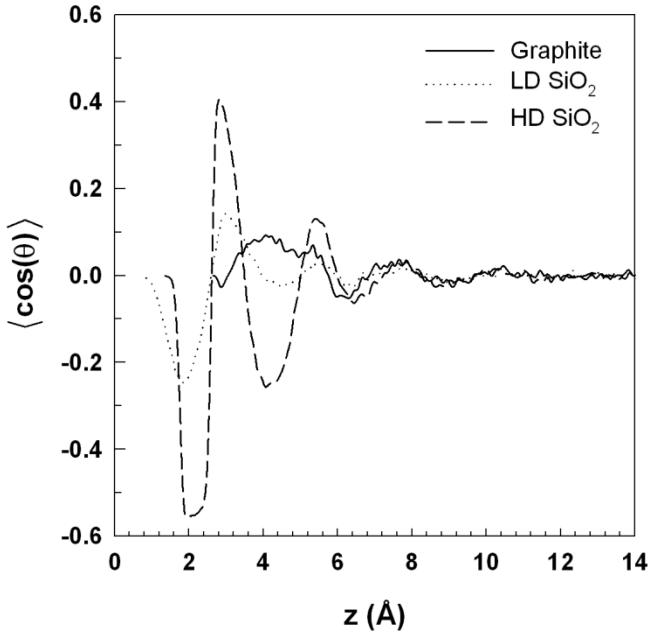


Figure 2.13: Order parameter $\langle cos(\theta) \rangle$ for water molecules as a function of their distance from the surface. The angle $\theta$ is that between the opposite to the dipole moment vector of water and the normal to the surface vector.

A more detailed picture of the orientation of interfacial water molecules is provided by the results presented in Figure 2.14 and Figure 2.15 where the time average of the angle θ is shown within $x - y$ planes at specific distances from the solid surface. In Figure 2.14 we show results for water on LD $SiO_2$ surface corresponding to layers BO-1 (Figure 2.14a) and BO-2 (Figure 2.14b). The data in Figure 2.14a suggest a hydrogen down orientation for the water molecules in layer BO-1 that occur in hexagonal patterns around the surface hydroxyl groups. These results should be interpreted in the context of the corresponding density contour plots. By doing so we conclude that water molecules that belong to the high density areas shown in Figure 2.9a have an average $\theta$ value of approximately 120º. However, when water molecules approach a surface hydroxyl group the angle decreases (light blue areas) because of a change in the orientation. A pattern similar to that obtained for layer BO-1 is observed

within the layer BO-2 (Figure 2.14b) with the difference that the regions with large oxygen densities that are characterized by small $\theta$. When water molecules migrate in the region of low oxygen density, the orientation changes and the angle increases.

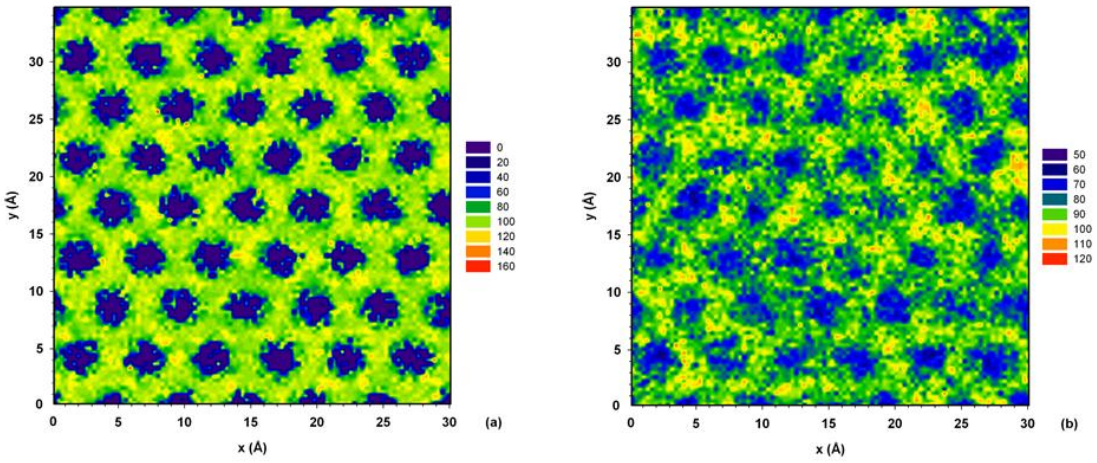


Figure 2.14: Contour plots showing the water orientation for water layers BO-1 (a) and BO-2 (b) on the LD $SiO_2$ surface. The average values of the angle $\theta$ between the vector opposite to the dipole moment of water and that normal to the surface are plotted in respect to the $x$ and $y$ direction. See Table 2.2 for details on peak position. The angle $\theta$ is in degrees.

The results obtained in the first layer (CO-1) on the HD $SiO_2$ surface, shown in Figure 2.15a, indicate a well-defined orientation for the interfacial water molecules. The oxygen atoms in this layer are highly confined and water molecules highly oriented with an average angle $\theta$ of approximately 120º. This finding corroborates the preferred hydrogen-down orientation observed for water molecules near the solid HD $SiO_2$ surface. According to the results in the same figure, water molecules maintain the same orientation even when they leave (not by much) the high density areas. The results also indicate that the angle $\theta$ is ~50º when water molecules occupy low density areas. Similarly in Figure 2.15b a small angle $\theta$ (< 80°) is observed in correspondence to the high density regions of the oxygen layer CO-2. The orientation changes significantly

when water molecules occupy the low density regions, $\theta$ increases above 80°, and in some cases reaches 120°. Similar calculations (not shown for brevity) were conducted for the graphite surface, but only a limited degree of preferential orientation was observed in the first two interfacial layers in agreement with all the data reported above. All the above results illustrate the impact of the substrate on the structural properties of water in the interfacial region. Significant and more pronounced are the effects on the water orientation on the HD $SiO_2$ surface. The large surface density of hydroxyl groups on this surface allows water molecules to adsorb in an organized manner within the first few molecular layers away from the surface. In the case of LD $SiO_2$ and graphite the surface effects are less pronounced and a lower degree of orientation is observed.

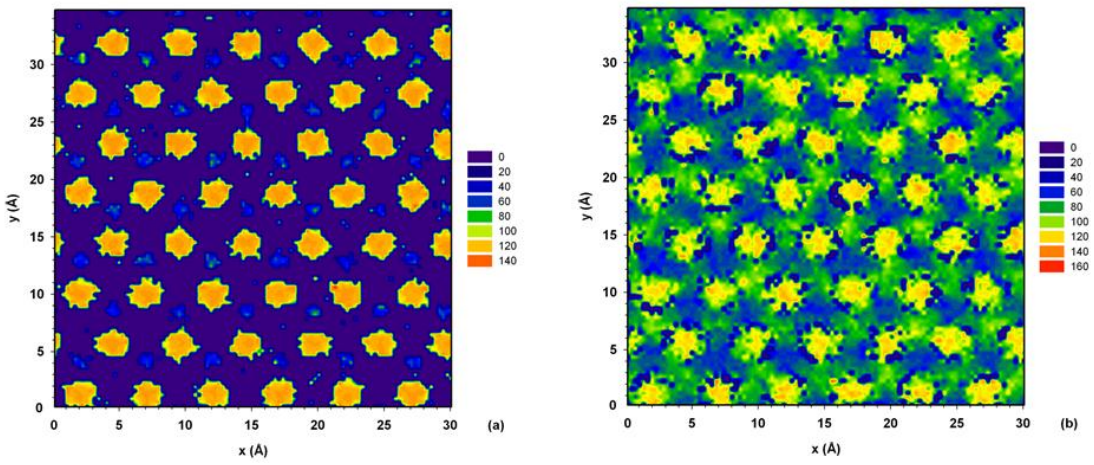


Figure 2.15: Same as Figure 2.14.The angle $\theta$ is calculated for water molecules on the HD $SiO_2$ surface for the oxygen layer CO-1 (a) and CO-2 (b). See Table 2.2 for details on peak position. The angle $\theta$ is in degrees.

### 2.4.5 Hydrogen Bonding

The results of the planar density profiles and orientation of water molecules suggest that the presence of a solid surface affects interfacial water directly by forming strong interactions. This behavior may lead to the formation of an extended and fairly stable hydrogen-bonded network away from the surface. We calculated the average numbers of hydrogen bonds established between water molecules as a function of distance from the surface. To define a hydrogen bond we used the geometric criterion proposed by Martí.[72] The position of the hydrogen bond was defined as that of the mid distance between the hydrogen of the donor and the oxygen of the acceptor molecule. The results are shown in Figure 2.16 in terms of the density of hydrogen bonds as a function of the distance *z* from the solid surface. The data indicate increased density of hydrogen bonds at specific distances from the three surfaces. In the case of graphite and LD $SiO_2$, the hydrogen bond density peaks are located at approximately 3.45 and 3.00 Å, respectively, which approximately correspond to the peaks of the oxygen atomic density profiles. This suggests that the large number of water molecules in the first layers form hydrogen bonds among themselves. The bonding environment of water on the HD $SiO_2$ surface is remarkably different. In this case a high hydrogen bond density is located at ~2.65 Å, which corresponds to the region in between the two oxygen layers (CO-1 and CO-2). This indicates that the formation and structural behavior of the second molecular layer is highly dependent on the hydrogen bond network. The highly confined water molecules of the first layer cannot establish hydrogen bonds between themselves. As a result they form hydrogen bonds with the water molecules of the second molecular layer, highly affecting their configuration. Compelling evidence of this is presented in Figure 2.16b where the in-plane hydrogen bond density distribution

that corresponds to the first peak of Figure 2.16a for water on the HD $SiO_2$ is shown as a function of the $x$ and $y$ direction. It is worth noting that the hydrogen bonds are located in specific positions and that these positions are in between the peaks of oxygen atom in the $x-y$ plane obtained in correspondence to the peak CO-1 and CO-2 (see Figure 2.4a, Figure 2.11a, and Figure 2.11b).

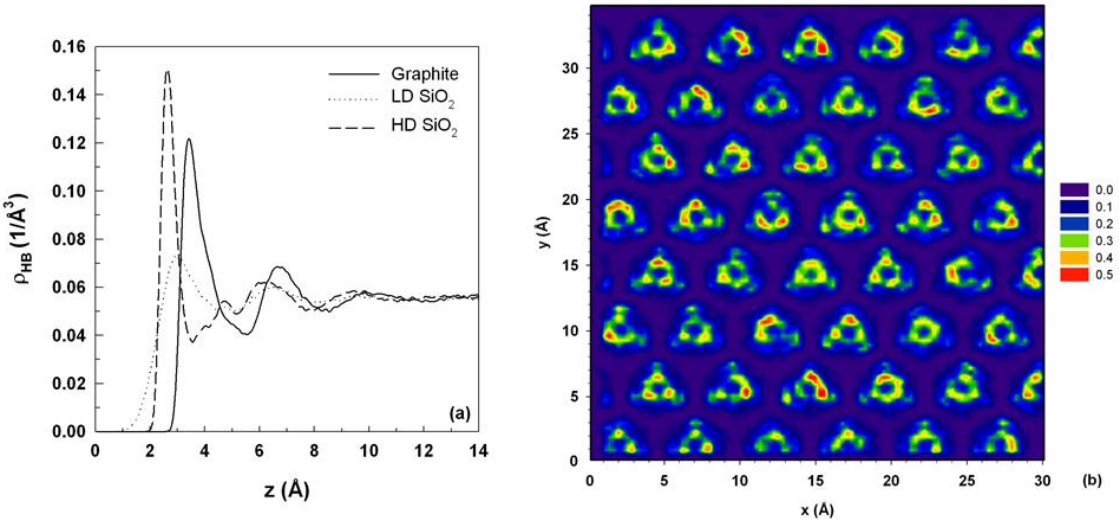


Figure 2.16: (a) Density profiles of the hydrogen bonds formed between water molecules as a function of distance from the solid surface. (b) Hydrogen bond surface density distribution correspondent to the first peak found for water on HD $SiO_2$, as shown in Figure 2.16a.

### 2.4.6 Residence Correlation Functions

The equilibrium properties discussed so far indicate that the surface, especially in the case of HD $SiO_2$, can profoundly affect the structure of interfacial water. It is also of interest to understand the residence times of water molecules within the layers and their exchange with those in the bulk. A residence correlation function $C_R(t)$ was employed to study the residence time of the water molecules in specific layers of interest. In each case a slab of thickness 1 Å was considered in correspondence to the

peaks that appear in Figure 2.4a (see Table 2.2 for peak position). The residence correlation function is then calculated as:

$$C_R(t) = \frac{\langle O_w(t) O_w(0) \rangle}{\langle O_w(0) O_w(0) \rangle} \tag{2.1}$$

where angular brackets designate ensemble averages. The term $O_w(t)$ describes whether an oxygen atom is, or is not, in the slab of interest at time $t$. The values for $O_w(t)$ are 1 or 0 when an atom belongs to the layer or not, respectively. The correlation function is expected to decay from 1 to 0 as time progresses in response to the movement of water molecules in and out of a specific layer. The slower the correlation function decreases, the longer the water molecules remain in the slab being examined. For example, based on the results shown in Figure 2.17a water molecules in the layer AO-1 on graphite remain longer in that layer than those in the AO-2 layer. The results regarding "bulk" water ($z$ > 14 Å) are identical for all three surfaces, further indicating that there is no impact of the surface on any of the water properties at that separation. In all cases, the autocorrelation function of the "bulk" decreases faster than any other calculated autocorrelation function.

The results presented in Figure 2.17 suggest that for most cases the water molecules close to the surface have the tendency to remain longer in that region compared to molecules found further from the surface. A different behavior is observed for water on LD $SiO_2$, in which case our results show that the residence time of water molecules in the layer BO-1 is not as long as in the denser layer BO-2. We ascribe this counter-intuitive result to the fact that the layer BO-1 is not really separated from the

layer BO-2 (it corresponds to a shoulder in the density profiles of Figure 2.4). Thus water molecules are relatively free to leave the layer BO-1. The dynamic behavior of water molecules at the HD $SiO_2$ surface is quantified in Figure 17c. The oxygen atoms of the first layer (CO-1) at the HD $SiO_2$ surface are highly confined, as suggested by the surface density distribution. In agreement with those calculations are the results of the correlation function that clearly indicate a significant residence time in the first interfacial layer. For the same system the results suggest a relatively long residence time in the second layer (CO-2) compared to water molecules on graphite and on LD $SiO_2$. This also suggests a limited exchange of water molecules between the first and the second molecular layers formed on HD $SiO_2$. Thus the restricted movement of the first layer molecules at HD $SiO_2$ in the $x$ and $y$ directions suggested by the contour plot of Figure 2.11a, is coupled to a slow exchange with bulk water molecules in the $z$ direction.

To quantify these qualitative observations we calculated the residence time as the time required for the autocorrelation function to decay from 1 to $1/e$ for all the cases considered in Figure 2.17. The results are presented in Table 2.3. We observe a significant difference between the residence times on the layer CO-1 on HD $SiO_2$ (~237.3 ps) compared to that in bulk water (~1.7 ps). It is also important to point out that the residence time for water in the first layer on graphite is significantly larger than that compared in any of the three layers considered on LD $SiO_2$. This latter result is quite surprising when we consider that graphite cannot establish hydrogen bonds with interfacial water molecules, and thus it is probably due to longer-lasting water-water hydrogen bonds formed at the water-graphite interface.

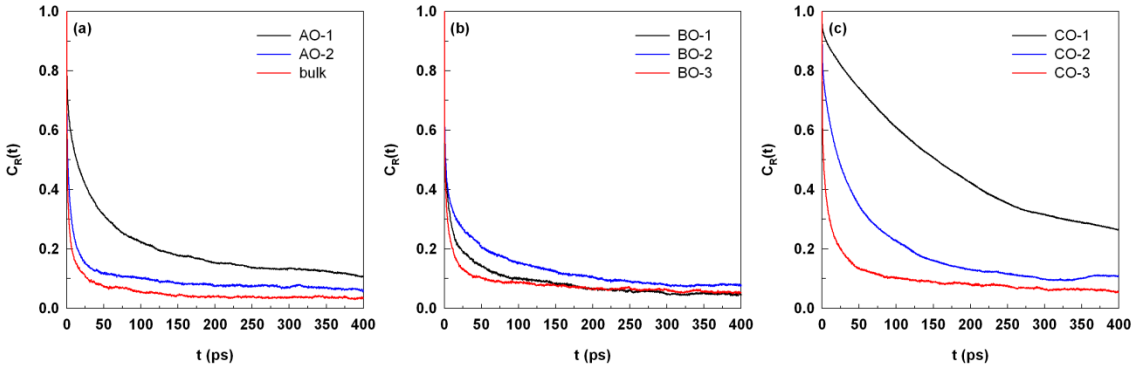


Figure 2.17: Residence correlation functions for oxygen atoms in the various layers at the graphite (a), LD $SiO_2$ (b), and HD $SiO_2$ (c) surfaces. See Table 2.2 for details on peak position.

Table 2.3: Time required for the autocorrelation function to decay from 1 to $1/e$ for all layers on the different surfaces considered. Results are obtained from the ACFs shown in Figure 2.17.

| Substrate | Layer | Time (ps) |
|---|---|---|
| Graphite | AO-1 | 34.9 ± 0.6 |
| | AO-2 | 3.9 ± 0.2 |
| LD $SiO_2$ | BO-1[α] | 4.7 ± 0.1 |
| | BO-2 | 6.8 ± 0.2 |
| | BO-3 | 2.4 ± 0.1 |
| HD $SiO_2$ | CO-1 | 237.3 ± 33.4 |
| | CO-2 | 45.1 ± 1.0 |
| | CO-3 | 5.8 ± 0.2 |
| Bulk (any substrate at $z$ > 14 Å) | Bulk | 1.65 ± 0.02 |

[α] this layer corresponds to a "shoulder" in the density profile.

### 2.4.7 Reorientation Correlation Functions

Another dynamic quantity of interest is the frequency by which water molecules change their orientation as a function of the distance from each of the solid substrates. To assess this property we computed reorientation autocorrelation functions for water molecules corresponding to different layers on the three substrates. In each case we

selected a slab of thickness 1 Å correspondent to the peaks in Figure 2.4a (see Table 2.2 for peak position). The reorientation of two vectors, defined by the geometry of a water molecule, was considered. The first vector is the opposite of the molecular dipole moment of one water molecule ($\overrightarrow{DM}$) and the second is the hydrogen-hydrogen vector ($\overrightarrow{HH}$). Each reorientation autocorrelation function was calculated as:

$$C_{\mu}(t) = \frac{\langle \hat{\mu}(t)\hat{\mu}(0) \rangle}{\langle \hat{\mu}(0)\hat{\mu}(0) \rangle} \tag{2.2}$$

where angular brackets designate ensemble averages. The symbol $\hat{\mu}$ represents the $\overrightarrow{DM}$ and $\overrightarrow{HH}$ unit vectors in each case. The corresponding correlation functions, $C_{DM}(t)$ and $C_{HH}(t)$, are shown in Figure 2.18 and Figure 2.19, respectively. Panels (a), (b), and (c) are results obtained on graphite, LD $SiO_2$, and HD $SiO_2$, respectively.

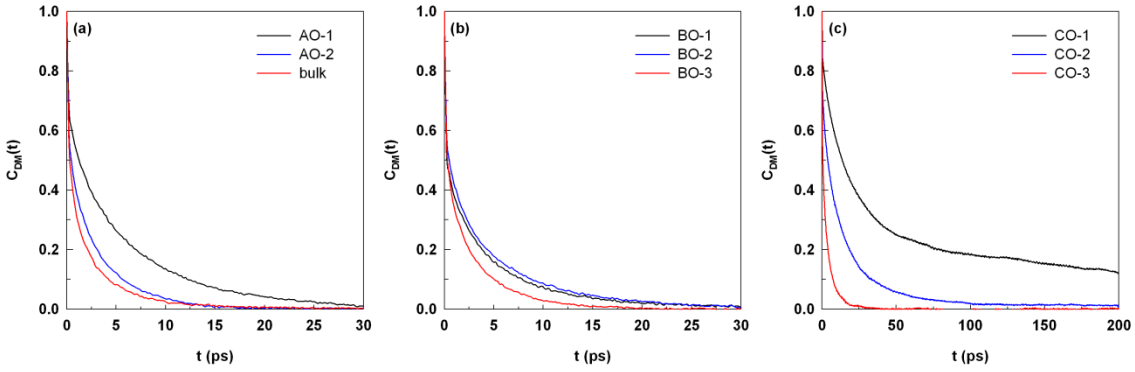


Figure 2.18: Reorientation autocorrelation function for the vector opposite to the molecular dipole moment of water. Results are shown in correspondence to various layers at the graphite (a), LD $SiO_2$ (b), and HD $SiO_2$ (c) surfaces. See Table 2.2 for details on peak position.

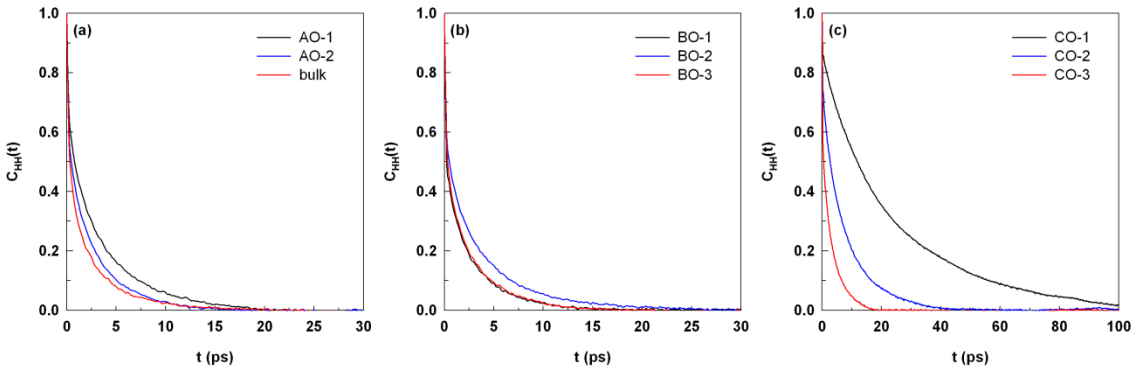


Figure 2.19: Reorientation autocorrelation function for the hydrogen-hydrogen vector of water. Results are shown in correspondence to various layers at the graphite (a), LD $SiO_2$ (b), and HD $SiO_2$ (c) surfaces. See Table 2.2 for details on peak position.

The results can be compared to those obtained for "bulk" water (panel (a) in both Figure 2.18 and Figure 2.19). Both bulk reorientation autocorrelation functions show fast decay from 1 to 0, and the two data sets do not differ. This indicates that the rotation of water molecules in bulk is isotropic. Because the results for "bulk" water do not depend on the surface, we again conclude that surface effects do not extend to 14 Å from the solid substrates under consideration. The results for the reorientation autocorrelation function for water in the various layers formed on the three substrates follow the general trend observed for the residence autocorrelation function of Figure 2.17. Namely, the closer a layer is to the solid surface, the slower the reorientation of the water molecules that belong to that layer. An exception, as in the case for the residence autocorrelation function, is observed in the case of water on LD $SiO_2$. In this case, the reorientation in layer BO-2 is the slowest of the three layers considered, whereas the reorientation in layer BO-1 is almost as fast as that observed in layer BO-2. In general, the reorientation autocorrelation function of the represents the $\overrightarrow{DM}$ vector is slower than that of $\overrightarrow{HH}$, suggesting that the presence of solid substrate determines anisotropic rotation of interfacial water molecules. The effect is very pronounced for

water molecules found within layer CO-1 on HD $SiO_2$. This observation is probably due to the fact that solid-water interactions determine, for the most part, the orientation of the $\overrightarrow{DM}$ of those water molecules at contact with the HD $SiO_2$. The $\overrightarrow{HH}$ orientation may be primarily determined by water-water hydrogen bonds, which can fluctuate rapidly.

## 2.5 Conclusions

We investigated structural and dynamic properties of water molecules within the first few molecular layers in contact with three solid surfaces. The surfaces (graphite and two $SiO_2$ substrates) were chosen to assess the effects of different degrees of hydrophobicity. In order to study the structural properties we calculated atomic density profiles, in-plane radial distribution functions, in-plane density distributions, preferential orientations, and hydrogen-bond density profiles. Our results confirm that the solid substrate perturbs interfacial water molecules for only a few molecular diameters away from the surface. In the case of graphite and $SiO_2$ with low density of hydroxyl groups, the interfacial water shows increased density compared to the bulk. When the density of hydroxyl groups increases we observe the formation of a highly ordered contact layer and of a second dense layer. The detailed analysis of the equilibrated structure revealed important results concerning the structure of the interfacial water molecules. Most significant are the results for the hydrogen bond network within the interfacial layer. These suggest that the properties of the second layer are determined by the water-water hydrogen bonds formed with the water molecules in the first layer.

Dynamic properties were assessed by calculating residence and reorientation autocorrelation functions for water as a function of the distance from the solid

substrates. Our results suggest a longer residence time for the water molecules found on the first layer on $SiO_2$ surface with high density of hydroxyl groups compared to all other cases. Results for the reorientation autocorrelation function follow trends similar to those observed for the residence autocorrelation function, suggesting that as the water molecules reside longer in specific locations close to the surface they also rotate less freely. In addition, we found evidence for anisotropic reorientation autocorrelation function. Namely, the vector identified by the two hydrogen atoms of a water molecule reorients significantly faster than the vector opposite to the water dipole moment. This behavior is particularly evident in the case of water in contact with HD $SiO_2$ surfaces. Our results also indicate that the dynamic behavior computed at 14 Å away from any surface is isotropic and identical for all three surfaces, further suggesting that there is no impact by the substrate on any of the water properties at distances larger than a few molecular diameters. The data presented here suggest that not only the solid surface, but also preferential interaction between interfacial water molecules may result in macroscopic phenomena typically used to discriminate between hydrophobic and hydrophilic surfaces. These new results provide a fundamental basis for investigating, in more detail, the molecular-scale phenomena relevant to nanofluidics and other nanotechnological applications.

# 3 Hydration Structure on Crystalline Silica Substrates

The material presented below was published in 2009 in volume 25, issue 14 of Langmuir.

## 3.1 Abstract

The structure of interfacial water at the silica solid surfaces was investigated using molecular dynamics simulations. Different degrees of surface hydroxylation where employed to assess the effect of the surface chemistry on the structure of interfacial water. Density profiles, in-plane radial distribution functions, in-plane density distribution, and hydrogen bond profiles were calculated to quantify these effects. Our results show that the surface hydroxylation affects the structure, orientation, and hydrogen bond network of interfacial water molecules. Data analysis suggests that the degree of hydroxylation controls the amount of water molecules in the first interfacial layer as well as the distance between the first adsorbed layer and the substrate. Well-organized and uniform structures of interfacial water appear on the homogeneously hydroxylated surface, while a heterogeneous interfacial structure, characterized by extensive water-water hydrogen bonds, forms on the partially hydroxylated surface. We demonstrate that both the local surface chemistry and water-water hydrogen bonds are the dominant factors that determine the structural properties of interfacial water.

## 3.2 Introduction

The study of water at interfaces continues to generate significant research interest especially at nanoscale dimensions where unexpected physical phenomena may appear. A fundamental understanding of interfacial water can provide new insights into processes important in geology,[57, 58] nanotribology,[1-3] microfluidics,[4] lab-on-a-chip, molecular engineering,[5, 6] and understanding biological systems[7] such as ion channels[8-10] and membranes.[11, 12] From a practical perspective, the condensation of a few molecular layers of water on solid surfaces is known to affect particle-particle interactions.[73, 74] Adsorbed water has been shown to form bridges between quartz surfaces separated by ~3.0 nm, bridges that induce a significant surface-surface attraction. This confined-volume attraction can be reduced by adding short alcohol molecules to the aqueous system.[75]

Experimental studies have elucidated several features about the structural and dynamic properties of water in contact with various hydrophobic and hydrophilic systems.[3, 11, 13, 14, 59] Simulations can play a synergistic role in better describing and interpreting the experimental findings.[13] Both molecular dynamics and Monte Carlo simulation techniques have been employed to study interfacial water on surfaces such as silica and graphite,[20-31] as well as inside and outside carbon nanotubes and fullerenes,[32-36] and near self-assembled monolayers exhibiting various terminal functionalities.[37] Although quantitative differences are substrate dependent, a well-established qualitative conclusion is that both structural and dynamic properties of interfacial water depend on the atomic-scale geometry and heterogeneous chemical properties of the substrate. However, a number of issues remain ambiguous. For example, it is not clear how the

solid structure perturbs interfacial water and how far from the solid this perturbation persists,[60] nor how the features of a solid surface (e.g. heterogeneous charge distribution) determine the residence time of water molecules at contact with a solid substrate.

Our objective is to investigate the structural properties of water molecules in the solid-liquid interfacial region and the hydrogen-bond network that develops when water molecules interact with a crystalline silica substrate. Our approach involves the use of molecular dynamics simulations of thin water films on a number of well controlled surfaces with different degrees of hydrophilicity. We recently compared the properties of interfacial water in contact with graphite and fully hydroxylated $SiO_2$ surfaces characterized by 13.6 or 4.5 hydroxyl groups per $nm^2$. In the present work three crystallographically equivalent $SiO_2$ substrates are considered. However, the degree of hydroxylation of the non-bridging oxygen atoms is altered to assess the importance of this surface feature on the properties of interfacial water. The degree of hydroxylation of the unsaturated oxygen atoms varied from 100, 50, and 0%, respectively. By analyzing how the structural properties of the interfacial water molecules change as the substrate varies we can provide a bridge between the atomic-scale properties of a solid surface and macroscopic observations. Our study is focused on a thin water layer supported by one silica surface, thus we do not interrogate the effect of confinement on the properties of interfacial water. The film thickness is chosen as a compromise to minimize the computational cost while allowing the establishment of an interfacial structure sufficiently thick that is independent on the film thickness. The analysis provided below is focused on the first few water molecular layers near the substrate,

where significant structural changes are observed compared to bulk properties. The significance of our results resides on the establishment of a direct connection between surface properties and the atomic-scale features of interfacial water. How these molecular-level features are related to the accumulation of simple electrolytes and/or surfactant molecules near solid surfaces is the subject of ongoing investigations.[76] Along these lines, a very recent contribution by Notman and Walsh[77] showed, using molecular dynamics simulations for aqueous solutions near fully hydroxylated α-quartz surfaces, that the local structure of water at the solid-liquid interface is related to the effective potential of mean force of methane and methanol as a function of the distance from the surface. In other words, this study showed that understanding water structure and dynamics at contact with a solid is important for predicting the adsorption of simple compounds on the solid substrate.

## 3.3 Simulation Methodology

The main objective of this work is to investigate the structural properties and behavior of a thin water film in contact with solid crystalline silica surfaces at three different degrees of hydroxylation. We selected the (111) crystallographic face from β-cristobalite $SiO_2$.[61] As we described earlier,[30] by cutting the β-cristobalite crystal along the (111) face, but at different locations it is possible to obtain surface 13.6 or 4.5 non-bridging oxygen atoms per $nm^2$. In our previous work, the most peculiar structures for interfacial water were observed when 13.6/$nm^2$ surface was fully hydroxylated. That surface has been chosen for the present study. We are now interested in how the interfacial water changes as the degree of hydroxylation varies. Following Pellenq and coworkers,[20] all the silicon atoms that are part of an incomplete tetrahedral were

removed and the non-bridging oxygen atoms (bonded to only one silicon atom) were saturated with one hydrogen atom positioned 1 Å perpendicular to the surface and kept rigid. We point out that allowing for the surface reconstruction would probably disrupt some of the interfacial water structures observed during our simulations. However, we consider our solid substrate a perfect system on which we can systematically add surface features (i.e., heterogeneous distribution of hydroxyl groups in the present work) and assess their effect on interfacial aqueous systems. The hydroxyl surface density of the fully hydroxylated surface is 13.6 OH/nm$^2$. A schematic representation of such surface is shown in Figure 3.1a. The second surface considered was 50% hydroxylated, with a hydroxyl surface density of 6.8 OH/nm$^2$, obtained by hydroxylating the necessary number of unsaturated oxygen atoms chosen at random. The surface is shown in Figure 3.1b. The third surface was completely not hydroxylated and it is represented in Figure 3.1c.

The solid substrate, a detailed description of which can be found in our previous report,[30] is maintained rigid during the simulation, thus we do not permit for the reconstruction of the surface, nor for the dissociation for the surface sites, which could be attained by employing the models developed by Garofalini[78] or by ab initio techniques. Although our models represent approximations of solid surfaces, they permit assessment of how the thermodynamic and structural properties of interfacial water vary as a function of the presence, density, and orientation of hydroxyl groups on the substrate. Throughout the manuscript we refer to both the 100 and 0% hydroxylated surfaces as "homogeneous" because all the non-bridging oxygen atoms are either hydroxylated or not, respectively. The 50% hydroxylated surface (center panel in Figure

3.1) is referred to as "heterogeneous" because some non-bridging oxygen atoms are hydroxylated, while others are not.

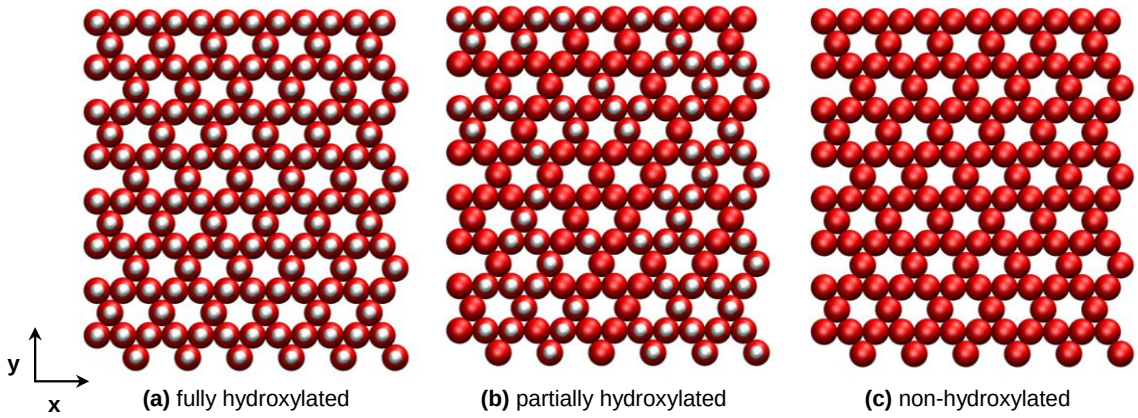


Figure 3.1: Top view of the fully hydroxylated (a), 50 % hydroxylated (b), and non-hydroxylated (c) $SiO_2$ surfaces. Only hydroxyl groups and non-bridging oxygen atoms are shown for clarity. White and red spheres represent hydrogen and oxygen atoms of the surface hydroxyl groups, respectively.

Because we are primarily interested in structural properties of interfacial water, water molecules were simulated using the simple point charge/extended (SPC/E) model.[79] This model yields structural properties for bulk water (e.g., radial distribution functions) that satisfactorily reproduce experimental data at ambient conditions. The atoms of the silica substrates interact with water molecules by means of dispersive and electrostatic forces.[64] The dispersive interactions were modeled with a 12-6 Lennard-Jones (LJ) potential. The LJ parameters for unlike interactions were determined using the Lorentz-Berthelot mixing rules.[65] These force fields are satisfactory for the scope of the present work, namely to assess how a model surface affects the structural properties of interfacial water. The cutoff distance for all interactions is set to 9 Å and the long-range electrostatic interactions were treated using the Ewald summation method.[65, 80]

Bond lengths and angles in water molecules were kept fixed using the SETTLE algorithm.[81]

The simulations were performed in the canonical ensemble where the number of particles ($N$), the simulation box volume ($V$), and the temperature ($T$) were kept constant. The $x$ and $y$ dimensions of the simulation box are 30.2 and 34.9 Å, respectively. This simulation box size is large enough to contain 144 hydroxyl groups in the fully hydroxylated surface. We simulated 1,000 SPC/E water molecules supported on each surface considered. These yield a supported water film of ~30 nm in thickness. The solid substrates are aligned parallel to the $x$ and $y$ plane. Simulations were carried out in orthorhombic simulation boxes, and periodic boundary conditions were implemented in the three directions. The system temperature was fixed at 300 K and controlled by a Nosé-Hoover thermostat with a relaxation time of 100 fs. The equations of motion were solved with the molecular dynamics package GROMACS[82-85] using the leap-frog algorithm[65] with a time step of 1.0 fs. After 0.5 ns of equilibration, the production time for all cases was 3 ns ($3 \cdot 10^6$ time steps) during which the atom positions were recorded every 200 time steps (0.2 ps) and used for further analysis. Additional details for the simulation setup and the force field parameters can be found in our previous report.[30]

## 3.4 Results and Discussion

### 3.4.1 Density Profiles

To assess the effect of the surface on the water structure, we calculated atomic density profiles in terms of density of oxygen and hydrogen atoms as a function of distance from the surface. The results are shown in Figure 3.2a and Figure 3.2b for

oxygen and hydrogen atoms, respectively. Note that these data are limited to oxygen and hydrogen atoms belonging to the water molecules. The solid, dotted, and dashed lines correspond to the results obtained on the fully hydroxylated (F), partially hydroxylated (P) and non-hydroxylated (N) silica surfaces, respectively. The fully hydroxylated surface, F in this work, corresponds to the "HD" surface in our previous report. The reference point ($z$ = 0) for the density profiles in Figure 3.2 is the plane of the non-bridging oxygen atoms of the silica surface. The surfaces perturb the structure of interfacial water as evidenced by peaks and valleys in the atomic density profiles. The exact positions of the atomic density peaks observed on the three surfaces are reported in Table 3.1. The labeling of the layers provided in Table 3.1 will be used throughout the text.

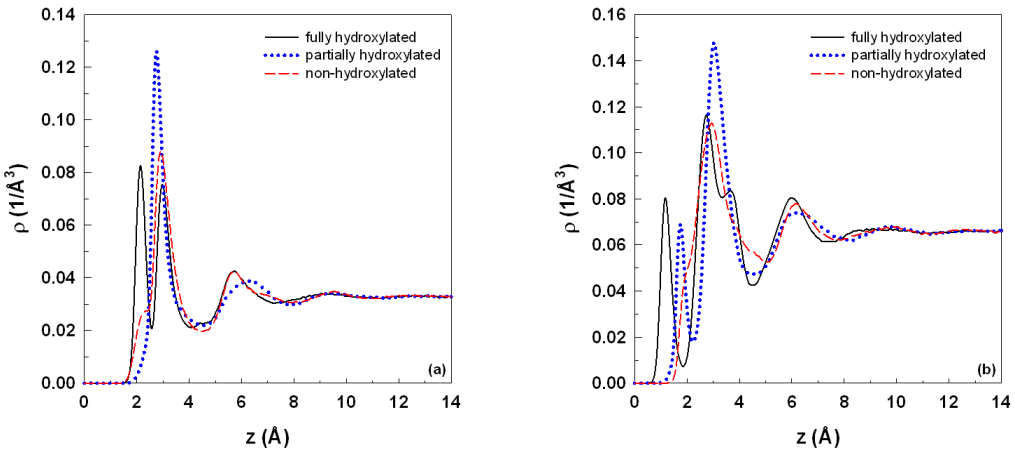


Figure 3.2: Oxygen (a) and hydrogen (b) atom density profiles as a function of distance $z$ from the solid surfaces. The reference $z$ = 0 is the plane of non-bridging oxygen atoms. Black solid, blue dotted, and red dash lines correspond to the fully hydroxylated, partially hydroxylated, and non-hydroxylated surfaces, respectively. Only oxygen and hydrogen atoms belonging to water molecules are considered here.

Table 3.1: Location (expressed as distance *z* from the surface) of the atomic density peaks of oxygen and hydrogen atoms on the various surfaces considered in Figure 3.2. On the forth column we provide the labels used in our discussion to refer to the peaks. First and second letters of the label indicate the substrate and the atomic species, respectively. The number in the label corresponds to the layer, number 1 being the one closest to the substrate.

| Silica surface | Oxygen peak (Å) | Hydrogen peak (Å) | Layer label |
|---|---|---|---|
| Fully hydroxylated (F) | 2.15 | 1.15 | FO-1 / FH-1 |
| | 2.95 | 2.75 | FO-2 / FH-2 |
| | 5.75 | 3.65 | FO-3 / FH-3 |
| | - | 6.05 | FO-4 / FH-4 |
| Partially hydroxylated (P) | 2.75 | 1.75 | PO-1 / PH-1 |
| | 6.30 | 3.05 | PO-2 / PH-2 |
| | - | 6.15 | PO-3 / PH-3 |
| Non-hydroxylated (N) | 2.35 | 1.95 | NO-1$^{\alpha}$ / NH-1$^{\alpha}$ |
| | 2.95 | 2.95 | NO-2 / NH-2 |
| | 5.75 | 6.15 | NO-3 / NH-3 |

$^{\alpha}$ this position corresponds to a "shoulder" in the density profile.

Our simulation results, presented in Figure 3.2, indicate that each surface perturbs interfacial water for distances approaching ~14 Å from the surface. The effect of the surface on the structure of water is more pronounced for distances less than ~8 Å where we observe a clear indication of the formation of distinct water layers at the interface. The bulk atomic density is retrieved at distances greater than 14 Å. Although these qualitative observations agree with a number of previous simulation studies,[28, 68, 69, 86] including ours,[30] the results presented in this work demonstrate that the degree of hydroxylation affects the interfacial water structure and possibly the orientation of interfacial water molecules. For the fully hydroxylated silica surface (solid line in Figure 3.2a) we observe two pronounced oxygen peaks at 2.15 and 2.95 Å that correspond to two distinct water layers, as described in detail in our previous work.[30]

The data suggest that the high density of surface hydroxyl groups is responsible for the accumulation of water on this surface. On the partially hydroxylated surface (dotted line in Figure 3.2a) we observe several O peaks, one of which is more intense and narrower than the others centered at 2.75 Å (Figure 3.2a). The water molecules associated with this peak do not oscillate significantly along the *z* direction. On the non-hydroxylated surface a broad oxygen peak is found at 2.95 Å, coupled to a shoulder at 2.35 Å. This suggests the formation of a thick layer within which water molecule oscillate significantly. It is likely that the water molecules closer to the surface have different structural properties than those located at the peak center. These observations indicate that the degree of surface hydroxylation determines the location of the first interfacial water layer. Specifically, the first oxygen peak on the fully, partially, and non-hydroxylated surfaces appears at 2.15, 2.75, and 2.95 Å, respectively, clearly demonstrating that a higher degree of hydroxylation leads to the formation of a water layer closer to the surface. It is, however, unexpected that one shoulder near the non-hydroxylated surface is located at 2.35 Å from the surface. Detailed structural analysis, provided below, addresses the water molecule in this location.

The results for the hydrogen atomic density presented in Figure 3.2b indicate the appearance of the first peak for hydrogen atoms belonging to water molecules at 1.15 Å on the fully hydroxylated surface. This layer of hydrogen atoms is 1 Å closer to the surface than the first layer of the corresponding oxygen atoms (2.15 Å), indicating a hydrogen-down orientation for the interfacial water molecules. As described in our previous study,[30] the hydrogen closest to the surface in those water molecules with a hydrogen-down configuration is located in the center of the hexagons formed by the

surface hydroxyl groups, thus minimizing the electrostatic repulsion between hydrogen atoms belonging to interfacial water and to the surface hydroxyl groups. The next three hydrogen peaks on the fully hydroxylated surface are located at 2.75, 3.65 and 6.05 Å. The highest peak (at 2.75 Å) corresponds to the layer of hydrogen atoms that belong to the water molecules of either the first (at 2.15 Å) or the second (at 2.95 Å) oxygen layer. This leads to the conclusion that the third hydrogen peak (at 3.65 Å) corresponds to the layer of the second hydrogen of water molecules whose oxygen atoms are located at 2.95 Å. On the partially hydroxylated surface (dotted line in Figure 3.2b) we observe one hydrogen peak at 1.75 Å suggesting a hydrogen-down orientation for some of the water molecules whose oxygen atoms are located at 2.75 Å. The intensity of the two peaks is ~0.07 and ~0.13 $Å^{-3}$ for hydrogen and oxygen atoms, respectively, implying roughly half of the water molecules in the first oxygen layer have a hydrogen-down orientation. The second hydrogen layer in the partially hydroxylated surface is located at 3.05 Å. This atomic layer contains at least one of the hydrogen atoms of the water molecules belonging to the first oxygen layer. Thus, some molecules in the layer show the hydrogen-down orientation, while others maintain both hydrogen atoms away from the surface. The simultaneous observation of both structures is probably due to the heterogeneous nature of the crystalline surface, which results in a heterogeneous behavior of the interfacial water molecules. Because there is evidence of hydrogen-down orientation in both the fully hydroxylated and partially hydroxylated surfaces, it is surprising that the location of the first hydrogen peak is different on the two surfaces, i.e., the first layer of hydrogen atoms forms closer to the surface on the fully hydroxylated than on the partially hydroxylated surface. In a similar manner, the

subsequent oxygen layer also forms at different positions on the two surfaces. Detailed analysis of water structure, provided below, will clarify these features.

The results for the hydrogen atomic density on the non-hydroxylated surface (dashed line in Figure 3.2b) indicate the formation of two atomic layers at 2.95 and 6.15 Å. The first peak (layer NH-1) is significantly broader than the first hydrogen peaks reported for fully (layer FH-1) and partially (layer PH-1) hydroxylated surfaces. The shoulder that appears at 1.95 Å (layer NH-1) indicates a structured layer of hydrogen atoms in contact with the non-hydroxylated surface. It is worth pointing out that a similar feature appears at ~3.5 Å, suggesting a different configuration of hydrogen atoms in the outermost part of the corresponding water layer. This result indicates that the thick interfacial layer on the non-hydroxylated surface contains water molecules characterized by multiple structural features, dependent on their location within the layer.

### 3.4.2 Planar Radial Distribution Functions

Planar radial distribution functions (RDFs) along the $x-y$ plane were calculated at different distances from the surface to assess the structural properties of interfacial water. In detail, in-plane RDFs calculations were carried out within bins 1 Å thick ($\delta z$) centered on each of the peaks reported in Table 3.1. For these calculations only atoms of different water molecules are considered. According to the density calculations displayed in Figure 3.2, the effect of the surface on water density is negligible at distances greater than 10-14 Å; above that distance we obtain "bulk" water density and uniform structure. For comparison purposes, the in-plane oxygen-oxygen, $g_{OO}(r)$, hydrogen-hydrogen, $g_{HH}(r)$, and oxygen-hydrogen, $g_{OH}(r)$ RDFs for "bulk"

water at 14 Å are presented in Figure 3.3. The results for distances greater than 14 Å from the surface are identical in all three substrates. These RDFs are consistent with the structure of bulk liquid water at ambient conditions.

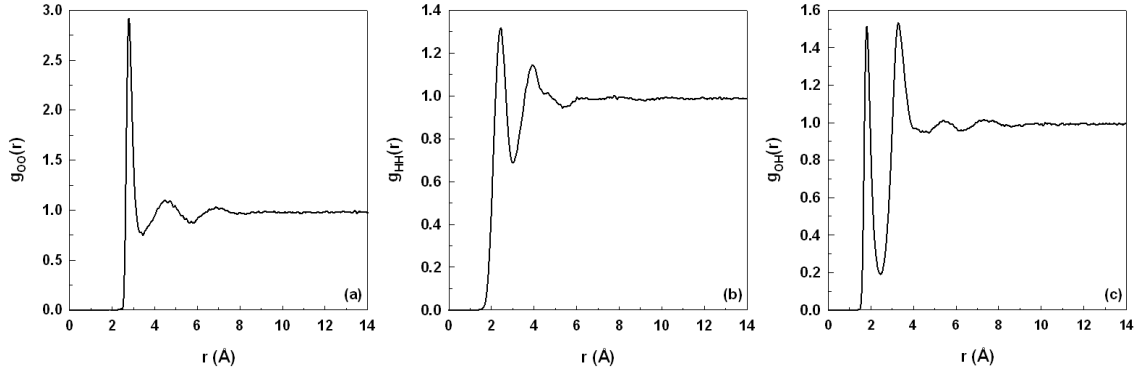


Figure 3.3: In-plane oxygen-oxygen (a), hydrogen-hydrogen (b), and oxygen-hydrogen (c) radial distribution functions. The RDFs shown in this figure were calculated along planes located 14 Å above the surface. The data are identical for all three surfaces considered here.

The in-plane RDFs reported in Figure 3.4, Figure 3.5 and Figure 3.6 correspond to oxygen-oxygen, hydrogen-hydrogen, and oxygen-hydrogen RDFs, respectively. Each figure includes in-plane RDFs results for the fully (left panel), partially (central panel), and non-hydroxylated surfaces (right panel). Data are obtained at several peaks, as identified in Table 3.1. The results elucidate the effect of the surface properties (i.e., degree of hydroxylation) on the structure of interfacial water, which exhibit more pronounced peaks closer to the surface. For example, on the fully hydroxylated surface the $g_{OO}(r)$ for FO-1 (solid line in Figure 3.4a) illustrates a solid-like structure, whereas the results for the layer FO-3 (dashed line in the same figure) are similar to those obtained for bulk water. On the partially hydroxylated surface (Figure 3.4b), the results are quite unexpected, since they suggest that in every layer considered the O-O RDF is similar to that obtained for bulk water (see Figure 3.3a). This effect is clearly due to the

heterogeneity of the surface and may explain why the first dense oxygen layer on this surface is located relatively far from the surface itself. On the non-hydroxylated surface (Figure 3.4c) we observe features similar to those obtained at the fully hydroxylated surface. In particular, the O-O RDF obtained at the NO-1 layer is identical to that obtained at the FO-1 layer, which is surprising when we consider that one surface is fully hydroxylated and the other is completely non-hydroxylated. However, it should be pointed out that the FO-1 and NO-1 layers correspond to a pronounced peak and to a shoulder in the respective density profiles. Because these features appear at similar distances from the surface, our results clearly indicate a preferential structure for oxygen atoms of the water molecules that are in contact with the two homogeneous surfaces considered here.

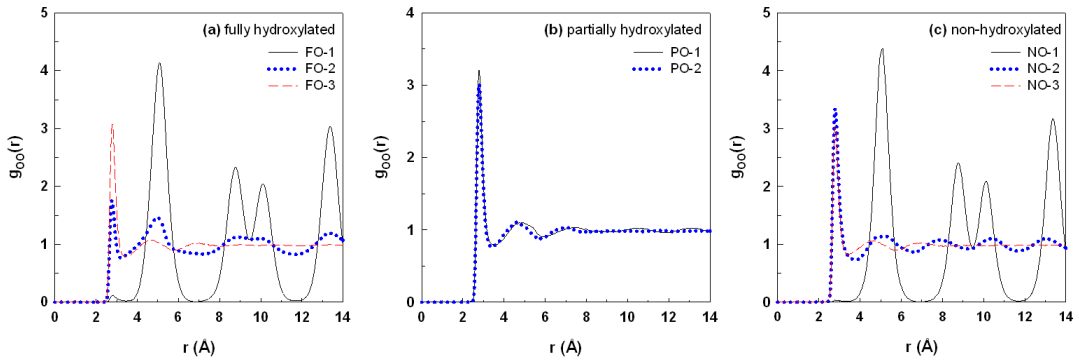


Figure 3.4: In-plane oxygen-oxygen radial distribution functions $g_{OO}(r)$ of the fully hydroxylated (a), partially hydroxylated (b), and non-hydroxylated (c) silica surface. Black solid, blue dotted, and red dash lines correspond to first, second, and third oxygen layer respectively. The location of each oxygen layers is given in Table 3.1.

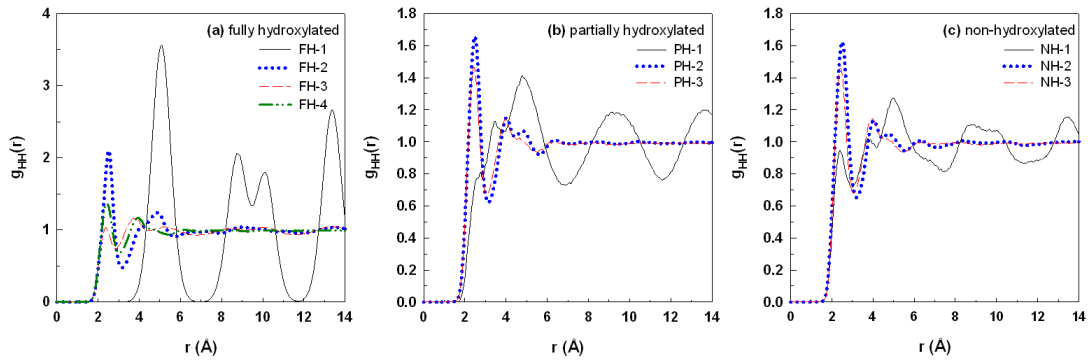


Figure 3.5: In-plane hydrogen-hydrogen radial distribution functions $g_{HH}(r)$ of the fully hydroxylated (a), partially hydroxylated (b), and non-hydroxylated (c) silica surface. Black solid, blue dotted, red dash, and green dash-dotted lines correspond to first, second, third, and fourth hydrogen layer respectively. The location of the hydrogen layers is given in Table 3.1.

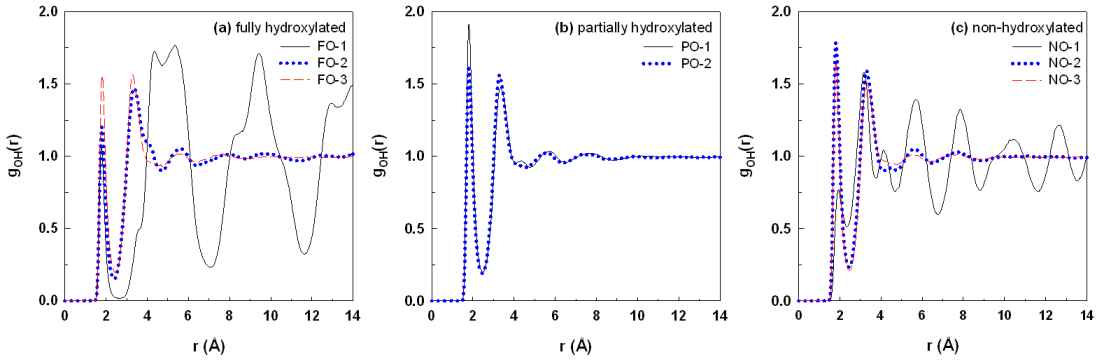


Figure 3.6: In-plane oxygen-hydrogen radial distribution functions $g_{OH}(r)$ of the fully hydroxylated (a), partially hydroxylated (b), and non-hydroxylated (c) silica surface. Black solid, blue dotted, and red dash lines correspond to first, second, and third oxygen layer respectively. The location of the oxygen layers is given in Table 3.1.

The data obtained for H-H and O-H RDFs (Figure 3.5 and Figure 3.6, respectively) emulate the observations described above. It is, however, worth pointing out that neither the H-H nor the O-H RDFs obtained in the first layer on the non-hydroxylated surface are identical to those obtained on the fully hydroxylated one. This indicates that although the relative position of water molecules within the first layer on the two surfaces is similar (the position is determined by the water oxygen atom), the

hydrogen-bond network obtained in the two cases is significantly different (the hydrogen bond network depends on the relative position of O and H atoms). It is also important to note that on the partially hydroxylated surface even the in-plane H-H and the O-H RDFs remain very similar to those obtained in the bulk, as was observed for the O-O RDFs discussed above. The RDFs are almost independent on the peak position, although some difference is observed in the H-H RDFs calculated for the first (PH-1), second (PH-2), and third (PH-3) layer. This suggests that interfacial water molecules on the partially hydroxylated surface maintain a structure very similar to that found in the bulk, a behavior that is clearly due to the heterogeneous nature of the substrate.

### 3.4.3 Planar Density Distributions

The in-plane atomic arrangement of oxygen and hydrogen atoms within the interfacial region is based on $x - y$ plane density distribution calculations. As with the in-plane RDFs calculations, the density bins are 1 Å thick ($\delta z$) and centered on the density peaks reported and labeled in Table 3.1. We point out that these results are strongly dependent on the arrangement of hydroxyl groups on the solid substrate. Relaxation and vibrations of surface atoms are likely to affect some of the features discussed below.

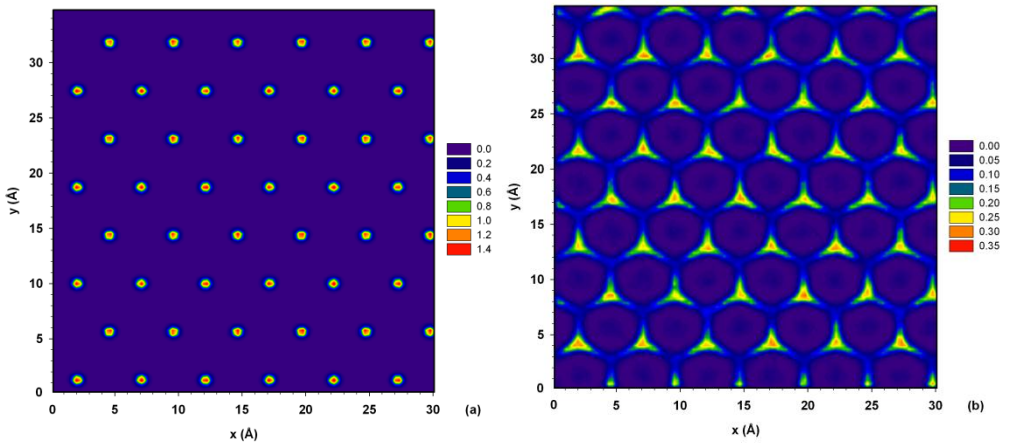


Figure 3.7: Surface density distribution of oxygen atoms for the FO-1 (a) and FO-2 (b) layers on the fully hydroxylated surface. Refer to Table 3.1 for location of the layers. The units of the atomic density distribution are given in $Å^{-3}$.

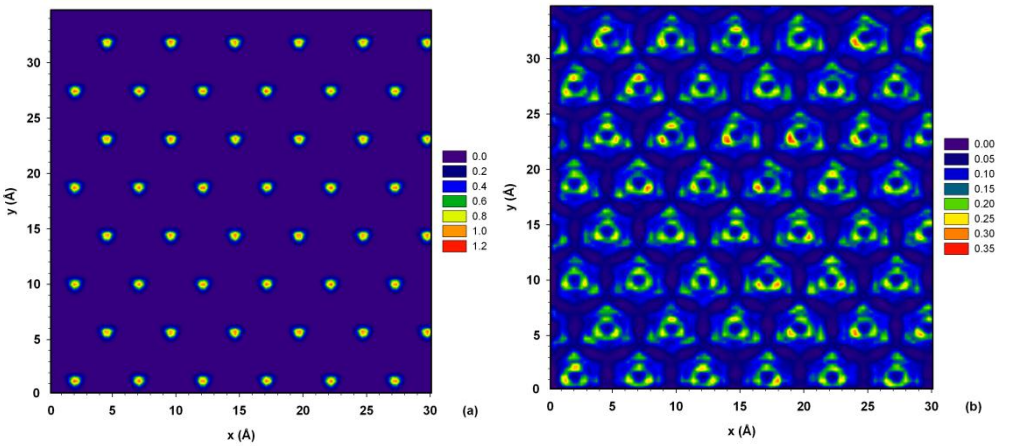


Figure 3.8: Surface density distribution of hydrogen atoms for the FH-1 (a) and FH-2 (b) layers on the fully hydroxylated surface. Refer to Table 3.1 for location of the layers. The units of the atomic density distribution are given in $Å^{-3}$.

The atomic density distributions of oxygen of the first (FO-1) and second (FO-2) atomic layers on the fully hydroxylated surface are reported in Figure 3.7. As discussed in our previous work,[30] the results suggest a highly structured first oxygen layer. We showed earlier that there is a connection between the $x-y$ plane atomic density distribution shown in Figure 3.7a and the arrangement of the surface hydroxyl groups shown in Figure 3.1. In short, the oxygen atoms that form one layer ~2 Å above the

surface are located at the center of the hexagons formed by the surface hydroxyl groups. This structure illustrates the strong effect of the substrate on the first molecular layer. The planar distribution of oxygen atoms in the FO-2 layer is shown in Figure 3.7b. The oxygen atoms yield a well-defined pattern, but exhibit a higher translational freedom in the $x - y$ plane compared to those in layer FO-1. The contour plot in Figure 3.7b reveals high density areas whose distribution reflects the hexagonal symmetry. The center of the hexagons in layer FO-2 corresponds to the location of the high density areas in layer FO-1.

The density distributions for hydrogen atoms in layer FH-1 and FH-2 are shown in Figure 3.8. The data presented for the layer FH-1 in Figure 3.8a suggest a highly restricted configuration whose structure is identical to that of the oxygen atoms in layer FO-1. The distance between the two layers (FO-1 and HO-1) is ~1 Å, clearly indicating that the water molecules in contact with the surface have one of the O-H bonds pointing towards the fully hydroxylated surface. The density distribution of hydrogen atoms in layer FH-2 is given in Figure 3.8b. The hydrogen atoms in this layer bond to either the oxygen atoms of layer FO-1 or FO-2, and occupy circular regions centered on the oxygen atoms of layer FO-1. A representative simulation snapshot to illustrate the relative arrangement of water molecules at the fully hydroxylated surface is shown in Figure 3.9. One water molecule from the first layer (FO-1) and three water molecules from the second layer (FO-2) are shown. The configuration of Figure 3.9 explains the circular region occupied by the hydrogen atoms that are located between the two oxygen atomic layers.

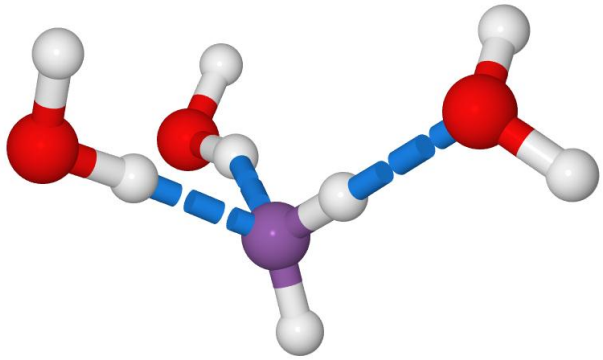

Figure 3.9: Simulation snapshot of four interfacial water molecules at the fully hydroxylated surface. The purple oxygen atom identifies the water molecule in layer FO-1, which is in contact with the surface. The water molecules with red oxygen atoms belong to layer FO-2. The blue dashed lines illustrate hydrogen bonds. The surface is not shown for clarity, but we point out that the hydrogen atom pointing towards the surface is at the center of the hexagons formed by the surface hydroxyl groups.

Oxygen and hydrogen atomic density distributions obtained on the partially hydroxylated surface are presented in Figure 3.10 and Figure 3.11, respectively. The density distribution of oxygen atoms in layer PO-1 shown in Figure 3.10a indicates the formation of one water layer with non-uniform structure. The variations in the atomic density within this layer are due to the surface heterogeneity (see Figure 3.1b). The results presented in Figure 3.10b show a uniform distribution of oxygen atoms in layer PO-2, suggesting that the partially-hydroxylated surface does not cause structuring of interfacial water within the layer PO-2, which is located 6.30 Å away from the surface. The data for the hydrogen density distribution in layer PH-1, shown in Figure 3.11a, is consistent with the presence of hydrogen-down oriented water molecules at the interface (the distance between PO-1 and PH-1 layer is 1 Å, which is the O-H distance within the SPC/E water). The results clearly indicate that the water molecules with one O-H pointing towards the surface are localized around hydroxyl groups that are surrounded by non-hydroxylated oxygen atoms. This finding is in qualitative agreement

with results reported by Giovambattista et al.,[25] who found that, for water confined within narrow slit pores, patches or single surface hydroxyl groups can function as local hydrophilic sites.

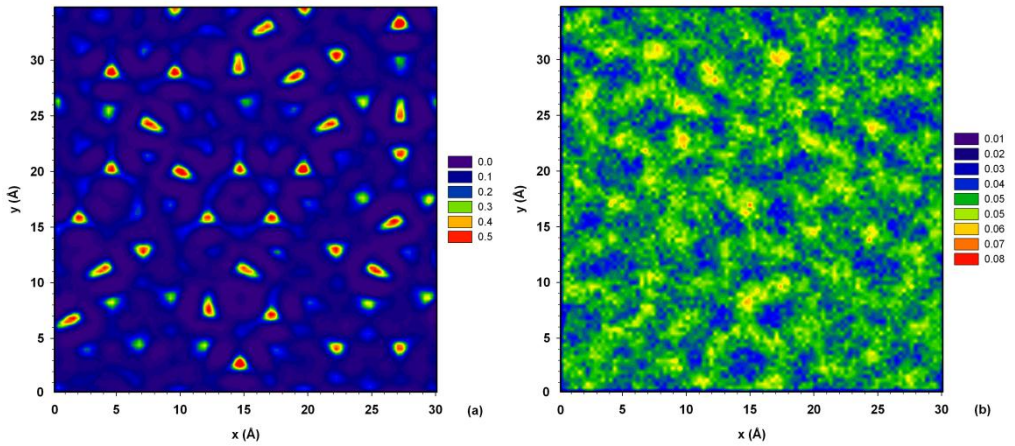


Figure 3.10: Surface density distribution of oxygen atoms for the PO-1 (a) and PO-2 (b) layers on the partially hydroxylated surface. The layers location is given in Table 3.1. The units of the atomic density distribution are given in $Å^{-3}$.

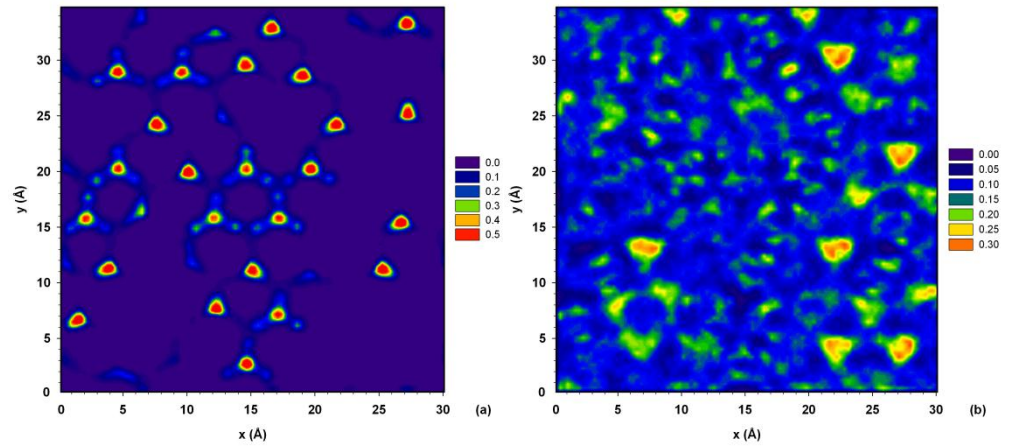


Figure 3.11: Surface density distribution of hydrogen atoms for the PH-1 (a) and PH-2 (b) layers on the partially hydroxylated surface. The layers location is given in Table 3.1. The units of the atomic density distribution are given in $Å^{-3}$.

By combining the oxygen density profiles in layer PO-1 and the hydrogen density profile of layer PH-1 (Figure 3.10a and Figure 3.11a, respectively) it appears that some water molecules in layer PO-1 are "anchored" to the surface with a hydrogen-down orientation. Other water molecules occupy well-defined areas identified by the contour plot of Figure 3.10a, but do not show a hydrogen-down orientation. The orientation of these latter water molecules can be assessed by analyzing the hydrogen density profiles within the layer PH-2, shown in Figure 3.2b. It appears that the typical circular pattern of hydrogen atoms observed in the case of the fully-hydroxylated surface (see Figure 3.8b) corresponds to those oxygen atoms of layer PO-1 that do not show a hydrogen-down orientation. Thus, the water molecules whose oxygen atoms lay within layer PO-1 can assume either a hydrogen-down, or a hydrogen-up orientation. Our results suggest that those molecules with a hydrogen-down orientation provide anchoring sites for the entire interfacial water structure on the partially hydroxylated surface, and are therefore identified in our discussion below as "anchoring" water molecules.

The simulation snapshot provided in Figure 3.12 clarifies the configuration of the interfacial water molecules on the partially hydroxylated surface. The water molecule with the purple oxygen corresponds to an "anchoring" molecule with the hydrogen-down orientation. The anchoring molecule is hydrogen bonded to (a) a second water molecule (far right in Figure 3.12) that belongs to layer PO-1 and shows the hydrogen-up orientation (b) to one water molecule (left) that belongs to neither the PO-1 nor the PO-2 layer, but occupies the region in between them.

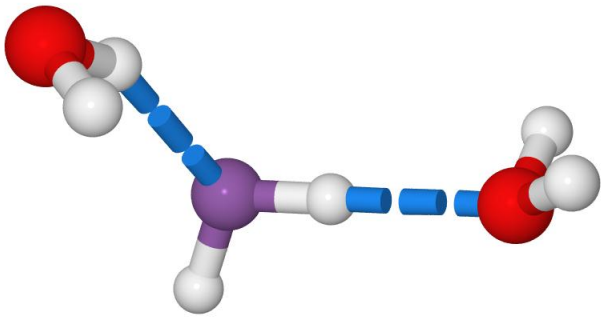

Figure 3.12: Simulation snapshot of three interfacial water molecules on the partially hydroxylated surface. The purple oxygen atom identifies the "anchoring" water molecule in layer PO-1 that is in contact with the surface. The far right water molecule belongs to layer PO-1 as well. The blue dashed lines illustrate the atomic species that are hydrogen bonded. The surface is not shown for clarity.

The results in Figure 3.13 show the in-plane distribution of oxygen atoms of water in layers NO-1 and NO-2 on the non-hydroxylated surface. The results for layer NO-1 (Figure 3.13a) illustrate a highly restricted structure identical to the structure in layer FO-1 (Figure 3.7a). Although water molecules in layers FO-1 and NO-1 are located at similar distances of 2.15 Å and 2.35 Å from the fully and non-hydroxylated surfaces, respectively, it is important to note that layer NO-1 corresponds to a shoulder in the density profile (dashed line in Figure 3.2a), whereas layer FO-1 is associated with a pronounced peak in the density profile (solid line in Figure 3.2a). Overall, the data in Figure 3.13a illustrate the effect of the arrangement of non-bridging oxygen atoms on the structure of the water-oxygen atoms that are in contact with the surface. This effect is not pronounced on the partially hydroxylated (heterogeneous) surface. The results in Figure 3.13b correspond to the dense layer of NO-2 oxygen atoms, and identify specific areas where the oxygen atomic density is significantly higher than others. These are the areas that correspond to the primary structure of the water at 2.95 Å from the surface.

The remaining features in Figure 3.13b correspond to the water molecules adjacent to layer NO-2. The areas of low density in Figure 3.13b are located at the same $x - y$ positions as the high-density areas in Figure 3.13a, suggesting that water molecules located in these positions oscillate along the $z$-direction, occupying both layer NO-1 (which is a shoulder in the density profile) and layer NO-2. This "oscillation" is consistent with the density profile in Figure 3.2a, which indicates the formation of a wide layer centered at 2.95 Å. The contour plot in Figure 3.13a characterizes the structure of water at the edge of the oxygen peak centered at 2.45 Å from the non-hydroxylated surface closest to the solid structure.

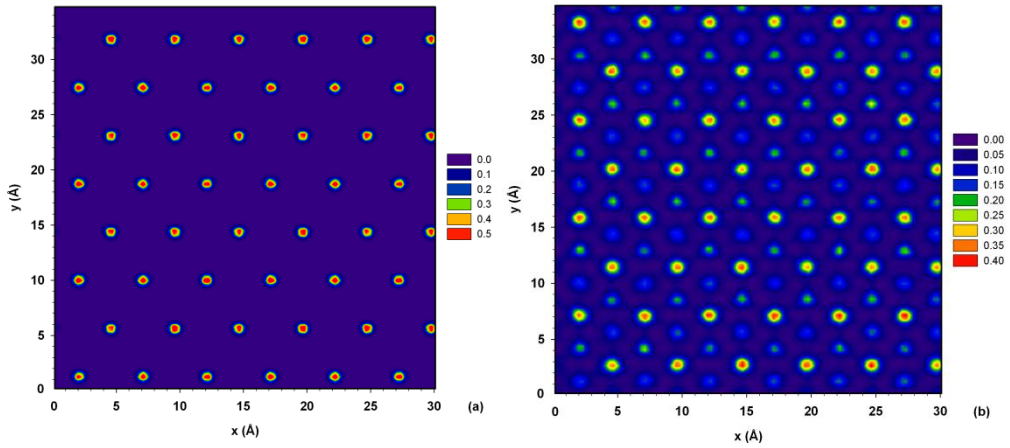


Figure 3.13: Surface density distribution of oxygen atoms for the NO-1 (a) and NO-2 (b) layers on the non-hydroxylated surface. The layers location is given in Table 3.1. The units of the atomic density distribution are given in $Å^{-3}$.

The in-plane density distribution of hydrogen atoms in Figure 3.14a reveals multiple well-defined patterns in layer NH-1. The distance between layers NH-1 and NO-2, located at 1.95 Å and 2.95 Å, respectively (see Table 3.1), suggests hydrogen-down-oriented water molecules at the interface. This finding is confirmed by the density distributions of layer NH-1 (Figure 3.14a) and NO-2 (Figure 3.13b). In fact the high

density areas in both plots appear at the same position in the $x-y$ plane and the distance along the $z$ direction is 1 Å. The less dense areas in Figure 3.14a correspond to the hydrogen atoms linked to oxygen atoms in NO-1. These circular areas whose centers correspond with the oxygen atoms of layer NO-1 (Figure 3.13a), indicate that the O-H bond orientation of these water molecules is almost parallel to the surface. The density distributions in Figure 3.14b show the structural properties of hydrogen atoms in layer NH-2. The hydrogen atoms in the thin layer form a well-defined pattern and become bonded with the oxygen atoms in both layers NO-1and NO-2.

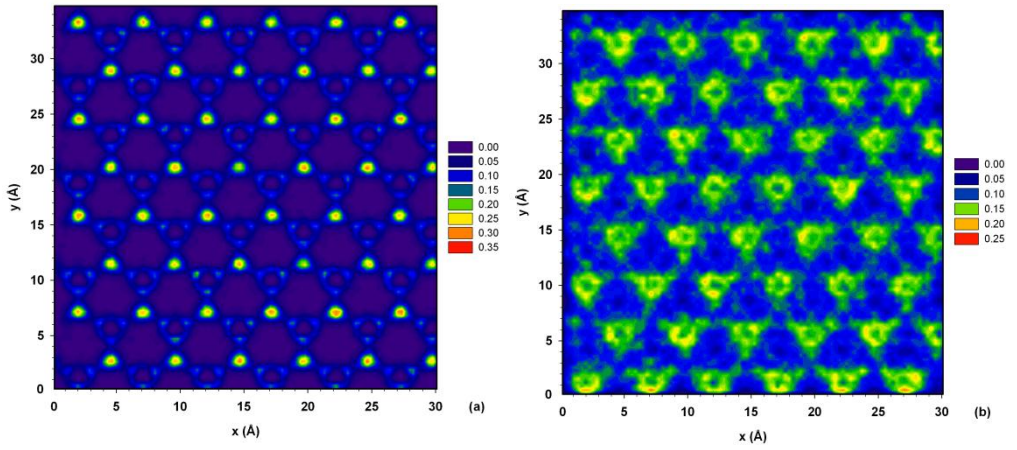


Figure 3.14: Surface density distribution of hydrogen atoms for the NH-1 (a) and NH-2 (b) layers on the non-hydroxylated surface. The layers location is given in Table 3.1. The units of the atomic density distribution are given in $Å^{-3}$.

One simulation snapshot for four water molecules on the non-hydroxylated surface is shown in Figure 3.15. The water molecule with the purple oxygen atom is located in layer NO-1 and is in contact with the surface. This snapshot shows one of the O-H bonds of the water molecule in layer NO-1 parallel to the surface. The remaining water molecules belong to layer NO-2 and are arranged in a triangular configuration above the water molecule of layer NO-1. The blue dashed lines represent the hydrogen bonds with which the four water molecules are associated. The far left and middle water

molecules of layer NO-2 have hydrogen-down orientation in contrast with the far right water that shows a hydrogen-up orientation. This snapshot, along with the analysis above, indicates that the configuration of water molecules in layer NO-2 is dependent on the orientation of layer NO-1 water molecules in contact with the surface. Note that the oxygen atom (purple in Figure 3.15) and two hydrogen atoms of the other water molecules are located at approximately the same distance from the non-hydroxylated surface. Thus our results show that on the non-hydroxylated surface interfacial water molecules assume hydrogen-down, hydrogen-parallel, and also hydrogen-up configurations, clearly because interfacial water molecules interact simultaneously with the surface, but also with other water molecules.

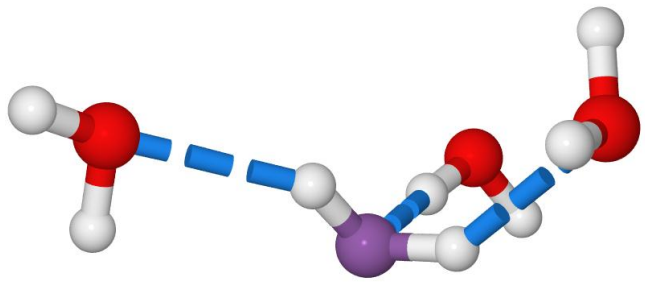

Figure 3.15: Simulation snapshot of four interfacial water molecules at the non-hydroxylated surface. The purple oxygen atom identifies the water molecule in layer NO-1 that is in contact with the surface. The remaining water molecules (red oxygen atom) belong to layer NO-2 and illustrate three different orientations. The blue dashed lines represent hydrogen bonds. The surface is not shown for clarity.

### 3.4.4 Hydrogen Bond Density Profiles

The structural properties of water molecules at the interface are greatly influenced by the surface chemistry. Furthermore, the hydrogen-bond network that forms among interfacial water molecules is responsible for determining equilibrium and transport properties at the interface. In order to better understand the relationship between the interfacial configuration of water molecules and the hydrogen-bond network we calculated the average number of hydrogen bonds established between water molecules as a function of the distance from the surface. In order to identify the hydrogen-bonded water molecules we employed the geometric criterion proposed by Martí,[72] as explained in details in our previous paper.[30] The position of the hydrogen bond was defined as the mean distance between the hydrogen of the donor and the oxygen of the acceptor water molecules. The hydrogen bond density profiles that are given in Figure 3.16 for the fully hydroxylated, partially hydroxylated and non-hydroxylated surface were calculated during the first 1 ns of the simulation production time. In the case of the fully hydroxylated surface, the first peak of the hydrogen-bond density is located at 2.65 Å, which corresponds to the region in between the oxygen layers FO-1 and FO-2. This finding illustrates the influence of the first highly confined water layer (FO-1) on the structural behavior of the second layer (FO-2) through a well-established, dense hydrogen-bond network. This is discussed extensively in our previous report.[30] The less pronounced peak that appears at 4.65 Å is associated with the hydrogen bonds formed between the hydrogen atoms of layer FH-3 and the oxygen atoms of layer FO-3.

The first peak on the partially hydroxylated surface (at 2.95 Å) is located very close to the position of the oxygen layer PO-1 (Figure 3.2a). This indicates that water molecules at this interface attain a maximum number of hydrogen bonds between water molecules within the same contact layer. In-plane density distribution calculations of hydrogen bonds in layer PO-1 indicate that the areas around the anchoring water molecules have a high hydrogen-bond density, as shown in Figure 3.17. In this figure we report on panel (a) the surface density distribution for hydrogen atoms in layer PH-1, and on panel (b) the in-plane hydrogen bond density profile in a layer of thickness 1 Å centered at 2.95 Å from the surface. This finding corroborates the observation that anchoring water molecules attract, through a hydrogen bond network, additional water molecules oriented towards layer PO-1.

The results on the non-hydroxylated surface show a broad peak centered at 2.95 Å. This peak appears at the same distance as the broad NO-1 layer. Thus water molecules within this layer are strongly correlated via hydrogen bonds. The shoulder that appears at ~3.65 Å in the hydrogen bond density profile on the non-hydroxylated surface suggests the formation of a few hydrogen bonds in the upper part of layer NO-1. These hydrogen bonds are likely to affect the structure of interfacial water farther from the surface.

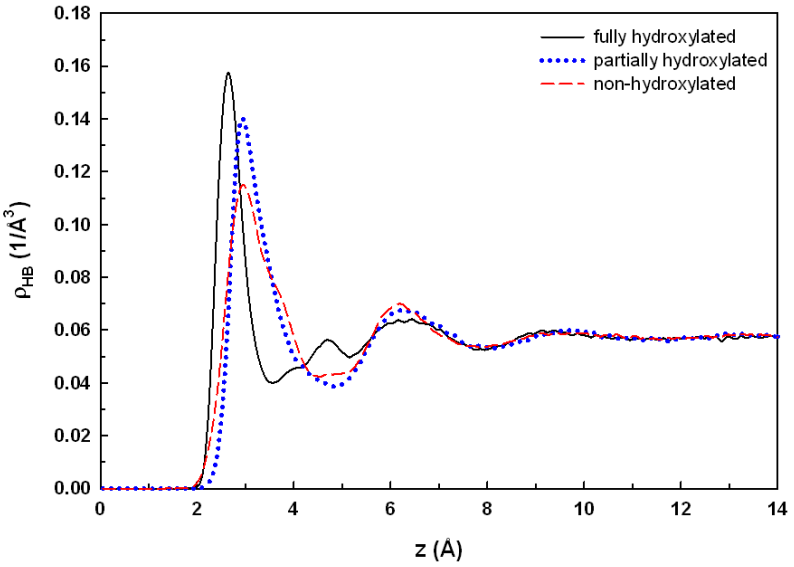


Figure 3.16: Density profiles of hydrogen bonds formed between water molecules as a function of distance from the fully hydroxylated (black solid line), partially hydroxylated (blue dotted line), and non-hydroxylated (red dashed line) solid substrates.

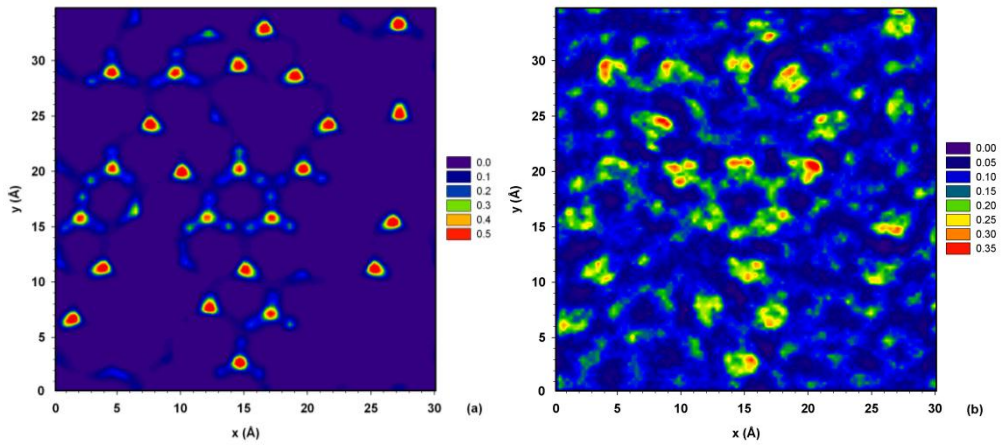


Figure 3.17: Surface density distribution of hydrogen atoms (a) for the layer PH-1 and in-plane hydrogen bond density distribution (b) in a layer of thickness 1 Å centered at 2.95 Å from the partially hydroxylated surface. The units of the density distributions are given in Å$^{-3}$.

## 3.5 Conclusions

The molecular structure of hydration water on three crystalline silica surfaces was investigated by conducting equilibrium molecular dynamics simulations. Three degrees of surface hydroxylation (fully, partially, and non-hydroxylated silica) were employed in our simulation to assess the hydration effect on the structure of interfacial water. We calculated density profiles away from the surfaces, in-plane radial distribution functions, in-plane density distributions, and hydrogen bond density profiles. The simulation results confirm that changes in the surface chemistry of the silica substrate affect the structural properties of interfacial water within the first few molecular layers. In all cases the perturbation of the structure of water due to the surface decreases as the distance from the solid substrate increases, becoming a non-factor for distances greater than ~14 Å.

Density profile calculations show that higher degrees of surface hydroxylation result in the formation of the first water layer closer to the solid substrate. The in-plane density distribution calculated for homogeneous (fully and non-hydroxylated) surfaces demonstrate that water molecules within the first two molecular layers are organized in well-defined patterns. However, different interfacial structures of liquid water are directly associated with the surface chemistry of the substrate. For example, the water molecules in the first layer at the fully hydroxylated surface have hydrogen-down orientations whereas non-hydroxylated surface water molecules in the contact layer have their O-H bonds parallel to the surface. Interestingly, the $x - y$ location of oxygen atoms located 2.15-2.35 Å from the solid substrate is the same on both surfaces illustrating that the position of the non-bridging oxygen atoms on the silica substrate

strongly affects the vicinal water. We observed that the structural properties of water molecules in contact with the surface affect the structural characteristic of water molecules in adjacent layers through well-defined hydrogen bond networks.

On the partially hydroxylated surface we observe a structural pattern for the hydration water that is not well organized due to the random distribution of the surface hydroxyl groups. The main factor that determines the interfacial water structure is the local density of hydroxyl groups. Areas of the solid substrate with high surface hydroxyl density promote hydrogen-up oriented water molecules, whereas areas with low density of surface hydroxyl groups promote hydrogen-down water molecules. The latter water molecules act as anchoring sites, attracting additional water molecules via the formation of a complex hydrogen-bond network. It is noteworthy that structural behavior on partially hydroxylated surface is not an “average” of interfacial water observed on the fully-hydroxylated and non-hydroxylated surfaces.

# 4 Dynamic Behavior of Interfacial Water at the Silica Surface

The material presented below was published in 2009 in volume 113, issue 45 of The Journal of Physical Chemistry C.

## 4.1 Abstract

Molecular dynamics simulations were employed to study the dynamic properties of water at the silica-liquid interface at ambient temperature. Three different degrees of hydroxylation of a crystalline silica surface were used. To assess the water dynamic properties we calculated the residence probability and in-plane mean square displacement as a function of distance from the surface. The data indicate that water molecules at the fully hydroxylated surface remain longer, on average, in the interfacial region than in the other cases. By assessing the dynamics of molecular dipole moment and hydrogen-hydrogen vector an anisotropic reorientation was discovered for interfacial water in contact with any of the surfaces considered. However, the features of the anisotropic reorientation observed for water molecules depend strongly on the relative orientation of interfacial water molecules and their interactions with surface hydroxyl groups. On the partially hydroxylated surface, where water molecules with hydrogen-down and hydrogen-up orientation are both found, those water molecules associated with surface hydroxyl groups remain at the adsorbed locations longer and reorient slower than the other water molecules. A number of equilibrium properties, including density profiles, hydrogen bond networks, charge densities, and dipole moment densities are also reported to explain the dynamics results.

## 4.2 Introduction

Understanding the physical chemical behavior of water is one of the great challenges the scientific community has always been fascinated by. One reason is that water is ubiquitous. Another is that water is responsible for life in this planet. Therefore understanding water and its subtle properties may let us understand several biological events such as structure-function relationships in proteins and cellular membranes,[9, 87, 88] and has important implications for a wide variety of disciplines extending from biology to geology, nanofluidics, materials science, etc.[4, 89, 90] As a practical example, recent theoretical developments suggest that the structure and local dynamics of water near an interface may be responsible for phenomena such as the accumulation of electrolyte ions at the interface.[91] These effects are due to, among other phenomena, changes in the local dielectric constant of water.[92] Such phenomena become important, for example, when the accumulation of electrolytes near a charged surface is to be used in designing ion-exchange or chromatographic processes.[93, 94]

Although a number of experimental and theoretical reports confirm that a solid surface affects the local structure of water via the formation of well-pronounced density layers and depletion regions,[27, 39, 69, 95, 96] the local value of the dielectric constant of water is determined not only by the water local density, but also by its local dynamics.[97] Not much attention has been traditionally given to this important aspect of interfacial water, presumably because of computing-power limitations and/or experimental difficulties. Among those contributions that assessed the dynamics of water at interfaces, Mamontov et al.[15] reported experimental neutron scattering data, combined with molecular dynamics simulations, for water on rutile. The data demonstrated that

the rutile substrate determines not only the local structure of hydration water, but also its dynamic properties. In particular, the scattering experiments probed several types of molecular motions within the hydration layers, the features of which depend, as shown by the molecular dynamics simulations, on an interplay of water-water and water-surface preferential interactions. More recently, Romero-Vargas Castrillón et al.[38] showed that the rotational dynamics of interfacial water is slower than that of bulk water, but only for a distance of ~0.5 nm from a silica surface, while the translational dynamics, also slower at interfaces than in the bulk, is affected for up to ~1.0 nm from the silica substrate. Ultrafast infrared spectroscopy was employed by Fenn et al.[19] to study orientational dynamics of water at neutral and ionic interfaces. Their findings confirm a slower orientational relaxation of water at these interfaces compared to bulk water.

Several simulation studies considered interfacial water in contact with carbon,[28, 35, 97] silica,[30, 40, 98-100] and other minerals.[13, 15] These investigations clearly show that the solid substrate perturbs the local structure of water up to 1.2-1.5 nm away from the surface. This perturbation is not only reflected in surface-specific density profiles, but also by a distribution of hydrogen bonds per water molecule different from that typically observed in bulk water. In particular, our group[30] demonstrated that the hydrogen-bond network formed between interfacial water molecules is in part responsible for determining the length scale away from the surface along which the surface perturbs the interfacial water. The importance of the hydrogen bond network near a surface has been reaffirmed by a recent theoretical framework proposed by Djikaev and Ruckenstein,[101, 102] which shows that the disruption of water-water

hydrogen bonds at interfaces may give rise to short range strong, attractive interactions between aqueous solutes.

In an attempt to quantify the local dynamics of interfacial water, Martí et al.[39] simulated water on flat graphitic substrates and showed that both the local dielectric constant, and the in-plane diffusion coefficient are significantly different compared to those observed in the bulk. Romero-Vargas Castrillón et al.[40] reported molecular dynamics simulations for interfacial water on a model silica-based surface. The surface polarity was adjusted to assess the relationship between surface properties, interfacial water structure, and interfacial water dynamics. The results showed that although the surface polarity affects both translational and rotational diffusion, the relationship is not monotonic because it is mediated by the structure of interfacial water.

Recently, our group reported equilibrium molecular dynamics simulation results for interfacial water in contact with model crystalline silica surfaces characterized by different degrees of surface hydroxylation.[98] Our results quantified how the surface heterogeneous properties affect structure, orientation, and hydrogen-bond network of interfacial water molecules. In this study the dynamic properties of interfacial water on the three surfaces are assessed by calculating residence probability, reorientation autocorrelation functions, in-plane mean square displacements and hydrogen bond lifetimes in the regions of interest.

## 4.3 Simulation Methodology

The (111) crystallographic face from β-cristobalite $SiO_2$ was selected to model the solid substrate. In our simulations all surface atoms are maintained rigid. This approximation yields a solid substrate that we consider an ideal system on which we can

systematically add surface features (e.g., heterogeneous distribution of hydroxyl groups) and assess their effect on interfacial aqueous systems. As we described earlier,[30] by cutting the β-cristobalite crystal along the (111) face, but at different depths it is possible to obtain surfaces with 13.6 or 4.5 non-bridging oxygen atoms per $nm^2$. The surfaces were prepared following the method described by Pellenq and coworkers.[20] We previously quantified how the interfacial water properties change as the degree of hydroxylation varies on the surface with 13.6 hydroxyl groups per square nanometer.[98] We focus here on quantifying the effect of surface degree of hydroxylation on the dynamic properties of interfacial water. The first surface considered is fully hydroxylated and it is characterized by 13.6 $OH/nm^2$. The second surface considered was 50% hydroxylated, with a hydroxyl surface density of 6.8 $OH/nm^2$, obtained by randomly hydroxylating the necessary number of non-bridging oxygen atoms. The third surface was completely not hydroxylated. Throughout the manuscript we refer to both the 100 and 0% hydroxylated surfaces as "homogeneous" because all the non-bridging oxygen atoms are either hydroxylated or not, respectively. The 50% hydroxylated surface is referred to as "heterogeneous" because some non-bridging oxygen atoms are hydroxylated, while others are not.

The solid substrate, a detailed description of which can be found in our previous reports,[30, 98] is maintained rigid during the simulation. Thus we do not account for the possible reconstruction of the surface, nor for the dissociation for the surface sites, which could be attained by employing, for example, the models developed by Garofalini[103, 104] or by ab initio techniques.[105]

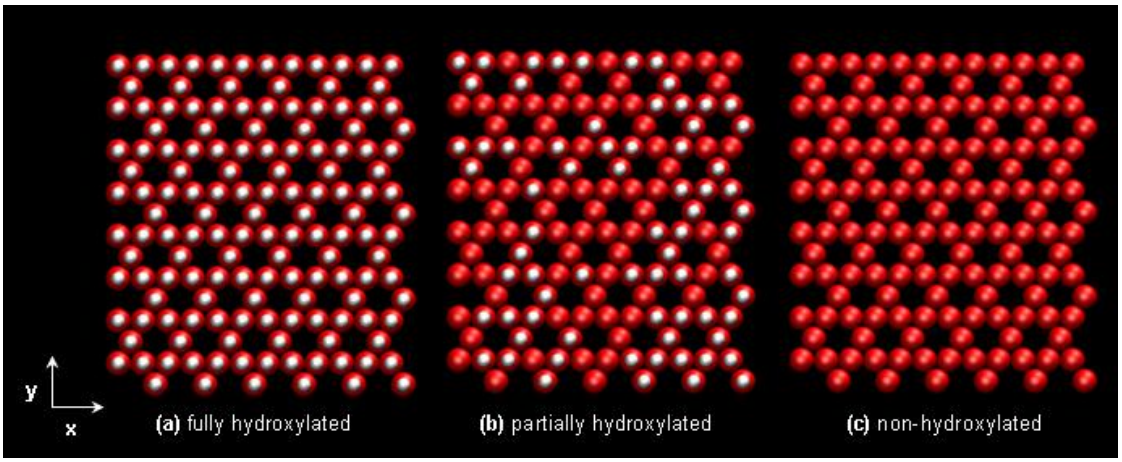


Figure 4.1: Schematic representation of top view of the fully hydroxylated (a), 50 % hydroxylated (b), and non-hydroxylated (c) $SiO_2$ surfaces. Only hydroxyl groups and non-bridging oxygen atoms are shown for clarity. White and red spheres represent hydrogen and oxygen atoms of the surface hydroxyl groups, respectively.

Water molecules were simulated using the simple point charge/extended (SPC/E) model.[79] This model yields structural properties for bulk water (e.g., radial distribution functions and self-diffusion coefficient) that satisfactorily reproduce experimental data at ambient conditions.[34] This rigid model however does not capture the effect of temperature on the structural properties of water, as recently demonstrated by Leetmaa et al.[106] The atoms of the silica substrates interact with water molecules by means of dispersive and electrostatic forces.[64] The dispersive interactions were modeled with a 12-6 Lennard-Jones (LJ) potential. The LJ parameters for unlike interactions were determined using the Lorentz-Berthelot mixing rules.[65] The implemented force fields are considered satisfactory for the scope of the present work, namely to assess how a model surface affects the dynamic properties of interfacial water. The cutoff distance for all interactions is set to 9 Å and the long-range electrostatic interactions were treated using the Ewald summation method.[65, 80] Bond lengths and angles in water molecules were kept fixed using the SETTLE algorithm.[81]

The simulations were performed in the canonical ensemble where the number of particles ($N$), the simulation box volume ($V$), and the temperature ($T$) were kept constant. All simulations were performed in orthorhombic simulation boxes, and periodic boundary conditions were implemented in all three dimensions. The solid substrate was aligned parallel to the $x$ and $y$ plane where the dimensions of the simulation box are 30.2 and 34.9 Å, respectively. We simulated 1,000 SPC/E water molecules supported on each surface type. These yield a supported water film of ~3.0 nm in thickness. The system temperature was fixed at 300 K and controlled by a Nosé-Hoover thermostat with a relaxation time of 100 fs. The equations of motion were solved with the molecular dynamics package GROMACS[82-85] using the leap-frog algorithm[65] with a time step of 1.0 fs. After 0.5 ns of equilibration, the production time for all cases was 3 ns ($3 \cdot 10^6$ time steps) during which the atom positions were recorded every 200 time steps (0.2 ps) and retained for further analysis. Additional details for the simulation setup and the force field parameters can be found in our previous reports.[30, 98]

## 4.4 Results and Discussion

### 4.4.1 Equilibrium Properties

A schematic representations of the three surfaces considered in this study is given in Figure 4.1. For clarity, we only report the oxygen (red) and hydrogen (white) atoms that are exposed to the aqueous phase. The hexagonal arrangement of the hydroxyl groups is clear from the left panel, in which we show the 100% hydroxylated surface. We also consider the 0% hydroxylated surface (right panel) and the 50% hydroxylated surface (center). We point out that none of the surface atoms (neither

surface hydroxyl groups nor silica atoms) is allowed to vibrate during our simulations. The structural properties of water on the three surfaces shown in Figure 4.1 have been discussed at length in our recent work,[98] but for clarity we report in Figure 4.2a the density profiles for oxygen atoms (top panel) belonging to water molecules as a function of the distance from the solid substrate. The results show that the atomic structure of the surface determines the distribution of water molecules at the interface, through the establishment of a complex hydrogen-bond network not only between water and surface, but also between water and water.[30, 98] Further details regarding the effect of the surface on the structure of interfacial water can be assessed by calculating the cumulative average density profile of the oxygen atoms (bottom panel in Figure 4.2), which allows us to quantify the depletion (or enrichment) of water molecules near the various surfaces considered here. Similar calculations have been employed by Wang et al.[100] to compare the water structure formed on mica and talc. Overall, our results confirm that the fully hydroxylated surface is more hydrophilic than the other two considered here, as indicated by the larger cumulative density observed at every distance from the surface up to ~14 Å from the surface.

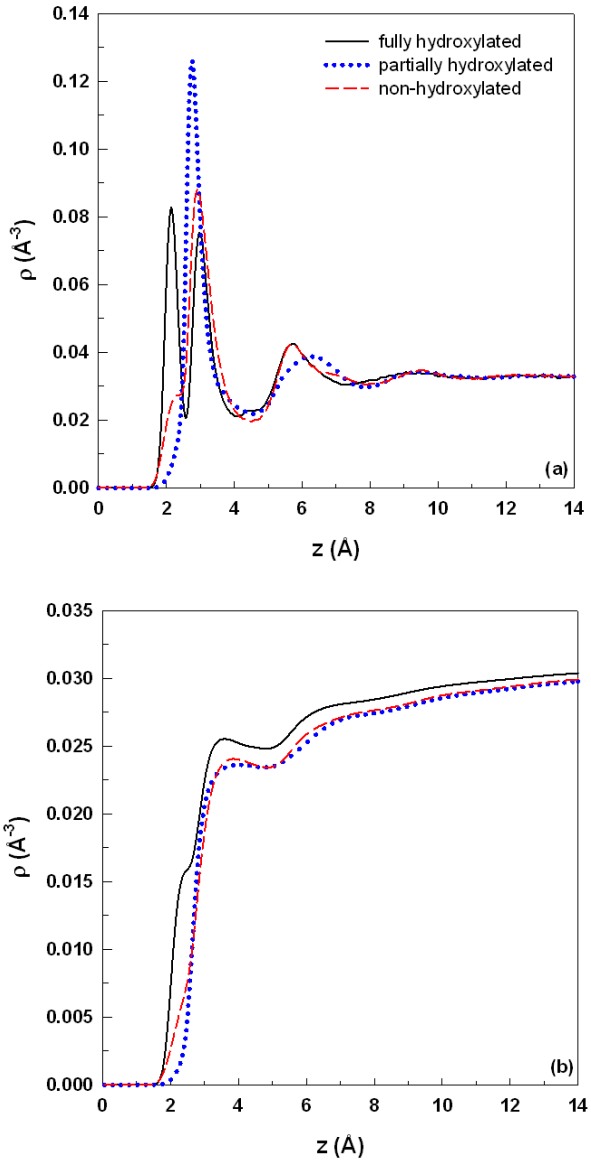


Figure 4.2: Atomic density profiles of water oxygen (panel a) as a function of distance *z* from the solid surfaces. The cumulative density profile of oxygen atoms as a function of distance is shown in panel b. The reference $z = 0$ is the plane of non-bridging oxygen atoms. Black solid, blue dotted, and red dash lines correspond to the fully hydroxylated, partially hydroxylated, and non-hydroxylated surfaces, respectively.

Table 4.1: Vertical distance of the atomic density peaks for oxygen atoms of water molecules (Figure 4.2a) from the plane of the non-bridging oxygen atoms of the fully, partially, and non-hydroxylated surfaces considered.

| Silica surface | Oxygen peak (Å) |
|---|---|
| Fully hydroxylated | 2.15 |
| | 2.95 |
| | 5.75 |
| Partially hydroxylated | 2.75 |
| | 6.30 |
| Non-hydroxylated | 2.95 |
| | 5.75 |

The charge density profiles of water molecules as a function of the distance from the solid surfaces were also obtained on the three surfaces, as shown in Figure 4.3. The charge of the oxygen atom for the SPC/E water model is −0.8476 e while that on each hydrogen atom equals +0.4238 e. The results in Figure 4.3 show that the solid surfaces perturb the interfacial water only for up to ~1.0 nm from the solid substrates. Further, the data in Figure 4.3 are consistent with a different orientation of the interfacial water molecules, due to surface features, which yield a pronounced structuring of interfacial water (Figure 4.2). For instance, at the fully hydroxylated surface, the positive peak at 1.15 Å and the negative peak at 2.15 Å in Figure 4.3 are due to the preferential hydrogen-down configuration for interfacial water molecules revealed by our previous calculations.[98] These local charge density profiles are expected to affect the distribution of charged species at solid-water interfaces, possibly contributing to the adsorption behavior of, for example, lactates[107] and amino acids analogues[77] on hydrated silica surfaces.

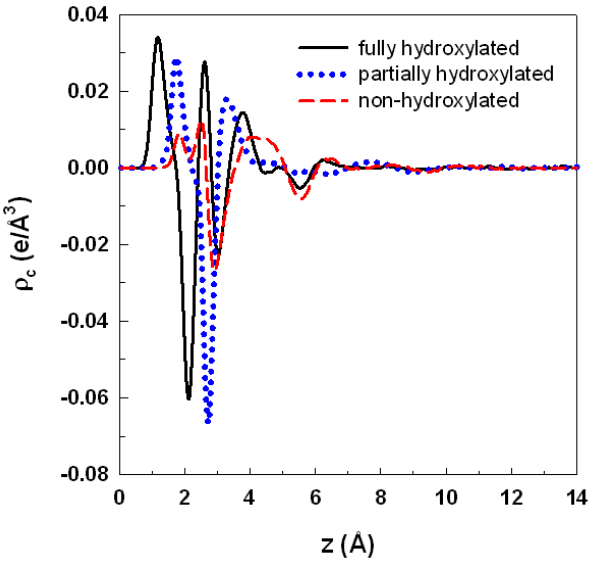


Figure 4.3: Charge density profiles of water as a function of the vertical distance $z$ from the three solid substrates considered. The reference $z$ = 0 is the plane of non-bridging oxygen atoms. Continuous, dotted, and dashed lines represent results obtained on the fully hydroxylated, partially hydroxylated, and non-hydroxylated surfaces, respectively.

Interfacial water molecules show preferential orientation.[98] To quantify these features we report in Figure 4.4 the $z$-component of the total dipole moment normalized by the surface area as a function of the distance from the surface. The total dipole moment in each slab is given by

$$\left\langle \mathbf{M}(z) \right\rangle = \left\langle \sum_{i \in slab} \boldsymbol{\mu}_i \right\rangle \tag{4.1}$$

where $\boldsymbol{\mu}_i$ is the dipole moment vector of water molecule $i$. The sum is extended to all the water molecules present in the calculation slab at distance $z$ from the surface. Angular brackets indicate ensemble averages. Corroborating the equilibrium properties discussed above, the results in Figure 4.4 show that the surfaces perturb the structure of water for up to ~1.0 nm. The $z$-component of the total dipole moment is due to both the local density of water molecules, and to their preferential orientation. Note that the

positive peak observed at 2.15 Å on the fully hydroxylated surface is in agreement with the hydrogen-down water orientation observed for the first layer of interfacial water molecules observed on that surface. The relative high intensity of the peak indicates a consistent orientation of all the water molecules within the first layer on that surface. On the non-hydroxylated surface a negative peak is observed at 2.15 Å, corresponding to a shoulder on the density profile (see Figure 4.2a), which illustrates a preferential oxygen-down orientation for those few water molecules in contact with the non-hydroxylated surface. On the partially hydroxylated surface we observe a positive value for the *z*-component of the total dipole moment in correspondence of the first interfacial water layer, which switches to a negative peak at slightly larger separations. These two consecutive peaks of opposite sign, observed also on the other surfaces, are the signature of layering of water molecules with opposite orientation on the various surfaces and are indicative of an attempt to maximize water-water hydrogen bonds. Fluctuations of the total dipole moment are responsible for local variations of the dielectric constant.[108, 109] For example, Martí et al.[97] reported an increase of the dielectric constant of water near graphite.

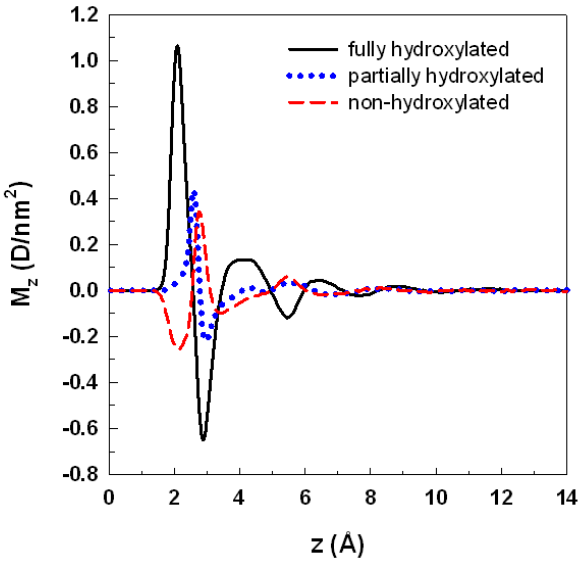


Figure 4.4: $z$-component of total dipole moment normalized by the surface area as a function of distance from the three surfaces types. Continuous, dotted and dashed lines represent water on the fully hydroxylated, partially hydroxylated, and non-hydroxylated surfaces, respectively.

### 4.4.2 Residence Probability

The charge density distributions shown in Figure 4.3 suggest that the local properties of interfacial water are varied, and are due to an interplay of density distributions and preferential orientations of interfacial water molecules. Because our objective is to determine water dynamic properties, it is of primary interest to quantify how long one water molecule that resides at a specific location away from a given surface type (e.g. fully hydroxylated) remains in that position. Previously we calculated residence correlation functions for water molecules on fully hydroxylated surfaces.[30] Our results showed that water molecules reside for very long times at contact with such surfaces, and that at distances larger than ~1.2-1.4 nm from the surface the dynamic behavior of water molecules is indistinguishable from that of bulk water. We now refine those calculations and quantify the residence probability, $P(t)$ as the probability of

finding one water molecule that continuously remains within a specific interfacial water layer (layer positions are given in Table 4.1). Once a water molecule leaves the respective layer, it may eventually return to the layer of interest, but our calculations do not account for such a possibility.

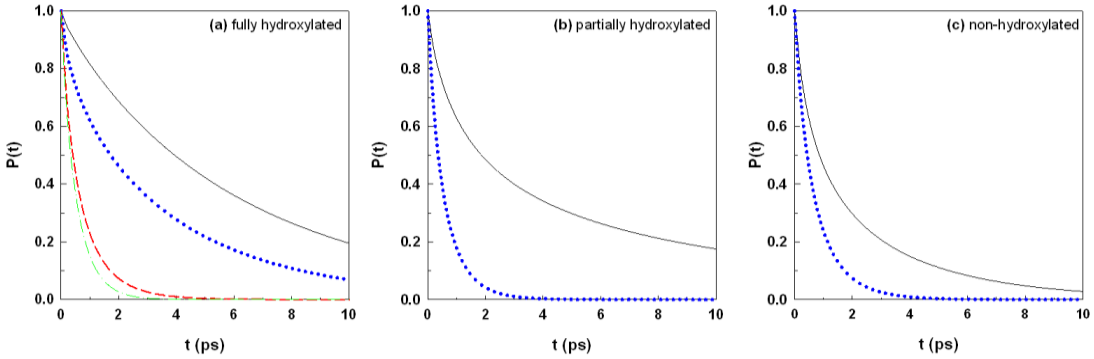


Figure 4.5: Residence probability for water molecules on distinct layers formed on the fully hydroxylated (a), partially hydroxylated (b), and non-hydroxylated (c) surfaces. Results are shown for the first layers formed on each surface. Black continuous, blue dotted, and red dashed lines represent water on the first, second, and third layer, respectively. The results for water molecules on the third layer are only shown on the fully hydroxylated surface. The position of each layer is shown in Table 4.1. The green dot-dash line represents the residence probability for water molecules located 14 Å above the surface, and corresponds to water with bulk properties.

The results shown in Figure 4.5 were obtained for water on the three surface types. From left to right, the panels are for water on the fully hydroxylated, partially hydroxylated, and non-hydroxylated surfaces, respectively. The width ($\Delta z$) of the calculation bins considered in this study is 1 Å. Each layer is centered at the peak positions given in Table 4.1. We also report in Figure 4.5 (left panel) $P(t)$ for water molecules 14 Å from the solid substrate at which bulk behavior is observed. $P(t)$ for water molecules at contact with each substrate decays more slowly than for bulk water. The decay is faster as the distance from the surface increases. For example, $P(t)$ on the third layer formed on the fully hydroxylated surface (red dashed line in Figure 4.5a)

decays only slightly more slowly than that for bulk water molecules (green dashed line). These results indicate that surface-water interactions in combination with water-water interactions effectively prevent interfacial water molecules from rapidly diffusing away from the surfaces.

To compare $P(t)$ for water on the three surfaces, in Figure 4.6 we report the results for water molecules found at a distance ~2-3 Å from the three surfaces. From the oxygen density profile shown in Figure 4.2a it is clear that at this distance water forms a well-defined layer in each of the surfaces considered. The results shown in Figure 4.6a indicate that water molecules reside for longer times on the fully hydroxylated surface compared to the non-hydroxylated one. The data obtained on the partially hydroxylated surface are unexpected. At short times (less than ~12 ps) $P(t)$ decays faster than it does on the fully hydroxylated surface, but at long times (more than ~12 ps) it decays more slowly than on the fully hydroxylated surface. This peculiar behavior (fast decay at short times, coupled with slow decay at long times) suggests that two populations of interfacial water molecules are found on the partially hydroxylated surface. This observation is in qualitative agreement with our recent structural analysis,[98] which indicates that some water molecules on the partially hydroxylated surface, located near the surface hydroxyl groups, assume a hydrogen-down orientation and provide anchoring sites for other interfacial water molecules with different orientation. These "anchoring" water molecules are responsible for the high intensity observed in the density profile for oxygen atoms (Figure 4.2) at the partially hydroxylated surface. The results in Figure 4.6a suggest that the anchoring water molecules are energetically stable and do not move frequently. To prove our phenomenological explanation, in

Figure 4.5b we compare $P(t)$ for water molecules found within the first layer on the partially hydroxylated surface, but we distinguish between those water molecules with a hydrogen-down orientation (anchoring water molecules) and the rest of water molecules (identified as "hydrogen-up" water molecules). The results show that the water molecules with hydrogen-down orientation reside on the layer for far longer times than the other molecules, clearly demonstrating their "anchoring" function.[98]

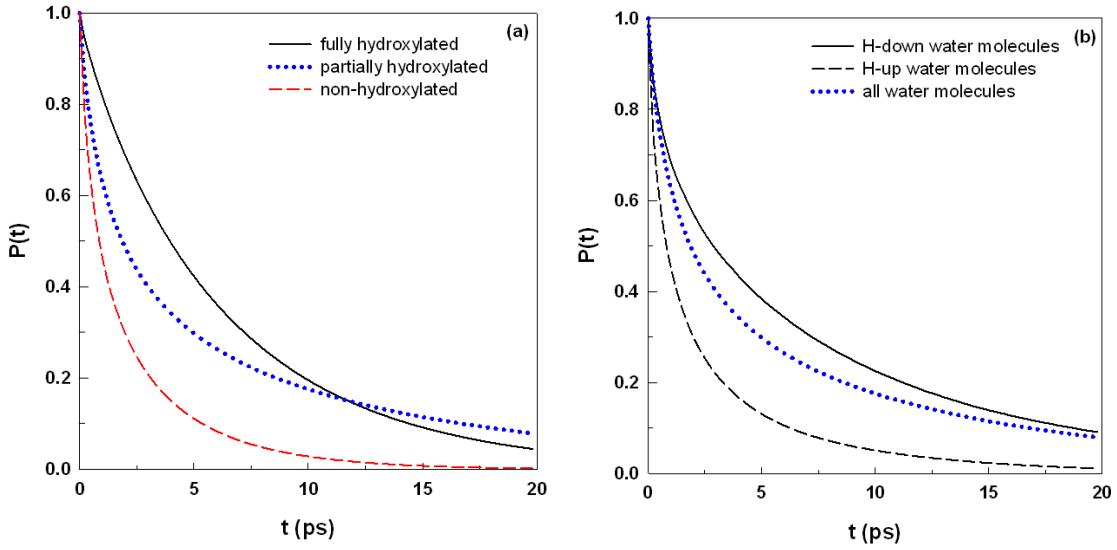


Figure 4.6: (a) Residence probability for the first interfacial oxygen atomic layers at the fully hydroxylated, partially hydroxylated, and non-hydroxylated surfaces. (b) Residence probability of the hydrogen-down (solid line), hydrogen-up water molecules (dashed line), and for all water molecules in the contact layer with the partially hydroxylated surface.

### 4.4.3 Translational Dynamics

The availability of reliable data for the residence probability permits assessment of layer-by-layer dynamics such as the in-plane translational diffusion. The time scale of the analysis considered in this study is reliable as long as the residence probability (Figure 4.6) is above 0.05, below which the statistics become unreliable. In Figure 4.7

we report the in-plane mean square displacement as a function of time along the plane parallel to the solid for water molecules on the three surfaces of interest. The in-plane mean square displacement for each layer is obtained as:

$$\left\langle \Delta \mathbf{r}(t)^2 \right\rangle = \frac{\left\langle \sum_{i \in slab} \left[ \left( x_i(t) - x_i(0) \right)^2 + \left( y_i(t) - y_i(0) \right)^2 \right] \right\rangle}{N(0)P(t)} \tag{4.2}$$

where $N(0)$ represents the number of water molecules that are present in the layer of interest at $t$ = 0. Once a water molecule leaves the layer of interest, its movements do not contribute any longer to the mean square displacement. Data are shown in Figure 4.7 only for as long as the residence probability is greater than 0.05. The mean square displacements data can be used to estimate self-diffusion coefficients. The faster the mean square displacement increases with time, the larger the self-diffusion coefficient. As expected, the translational mobility of interfacial water is faster on the layers farther from the surface, and the slowest on the first adsorbed layer. Data obtained on the first layer show that the translational diffusion is the slowest on the fully hydroxylated surface, and the fastest on the non-hydroxylated one, as expected from the analysis for the residence probability discussed above, as well as from the structural analysis discussed in our previous paper.[98] In every layer considered, water molecules on the fully hydroxylated surface appear to have slower translational diffusion than those on the other two surfaces. Our results, shown in Figure 4.7a, indicate that the water molecules in the first layer on the fully hydroxylated surface have very low mobility along the $x - y$ plane. All other water molecules considered show detectable translational diffusion. We note that the results for in-plane mean square displacement

are identical for water within the first layers on the partially and on the non-hydroxylated surfaces for up to ~8 ps.

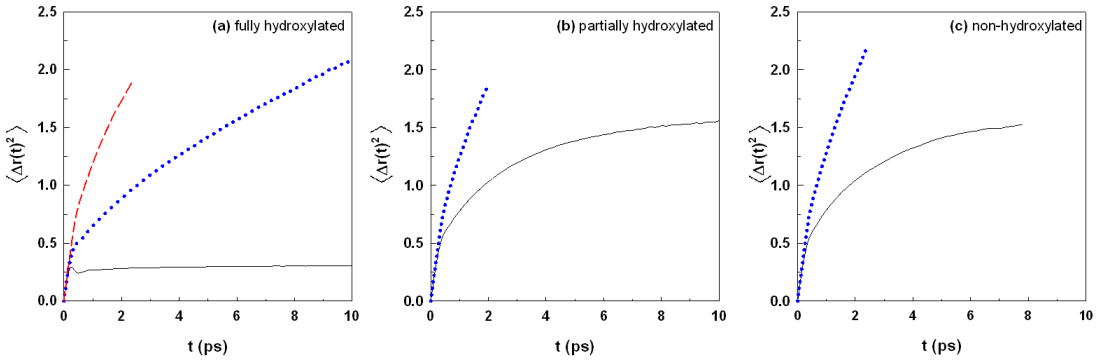


Figure 4.7: Layer-by-layer in-plane mean square displacement parallel to the solid surfaces for water molecules on the fully hydroxylated (a), partially hydroxylated (b), and non-hydroxylated surface (c). Solid, dotted, and dashed lines represent water on the first, second, and third layer (when considered), respectively. The position of each layer is shown in Table 4.1.

The observations just discussed for both the layer-by-layer residence probability and the layer-by-layer translational mobility for interfacial water can be combined by reporting the *z* location and corresponding distance traveled in the plane parallel to the surface for selected water molecules. We report the results for one representative water molecule on each of the surfaces in Figure 4.8. The bottom panels show the *z* position of the selected water molecule as a function of time. These positions correspond to the average *z* position during 20 ps of simulation time. The top panels show the mean square displacement observed within the plane parallel to the surface observed during the 20 ps used to calculate the average *z* position of the selected water molecule. Corroborating the results discussed above, the data in Figure 4.8 show that when a water molecule belongs to the first adsorbed layer on any of the surfaces considered it essentially does not move along the plane parallel to the surface. As the adsorbed water

molecule moves away from the first adsorbed layer (e.g., to the second layer and beyond), it shows a significant displacement parallel to the surface. This behavior is generally true on any surface, but it is particularly evident on the fully hydroxylated one (see enlargement on the left panels).

Another interesting observation from the data shown in Figure 4.8b is that in some cases water molecules adsorbed on the first layer on the fully hydroxylated surface ($z$ position ~2.15 Å) move to the second layer ($z$ position ~3.55 Å) and then return to the first adsorbed layer (detailed analysis of sequences of simulation snapshots demonstrates that the water molecule actually returns to exactly the same surface location). This observation is accompanied with a high mobility along the $x - y$ plane as observed at ~100, 250, and 650 ps in Figure 4.8a. In other cases, and more commonly, adsorbed water molecules that move to the second layer, leave after a few ps to the remainder of the thin water film. The interesting aspect of this observation is that when the water molecules adsorbed on the first layer leave, they seem to preferentially spend some time, although limited, on the second layer, before they either reabsorb on the fully hydroxylated surface, or leave the surface to reach the center of the water film. This behavior is probably dictated by the pronounced minima in the density profiles observed for oxygen atoms along the $z$ direction away from the surface (Figure 4.2a). It is also possible that the charge accumulation on the surface, discussed in Figure 4.3, introduces effective repulsions between water molecules that are attempting to move towards, or away from, the fully hydroxylated surface. Similar observations, although less pronounced, can be repeated for water molecules on partially and non-hydroxylated surfaces. Interfacial water molecules are highly

structured and thus they are located in specific sites lacking freedom to move along the $x-y$ plane primarily due to their interactions with the solid substrate. We also note that water molecules in the first layer of the non-hydroxylated surface have relative high mobility along the $z$-axis occupying different location in the same layer as can be observed in Figure 4.8f from ~2.2 to 2.6 ns. This may be due to the reduced structuring of interfacial water molecules, which allows them to more easily exchange position within the layer.

The discussion above becomes more interesting when the results are compared to those obtained on other surfaces. For example, molecular dynamics simulations, supported by backscattering neutron spectroscopy experimental data,[15] suggest that, contrary to the observations herein, water molecules adsorbed on the first layer of $TiO_2$ surfaces do not leave that layer, suggesting that surface properties, including the surface dielectric,[110] determine the dynamic behavior of interfacial water.

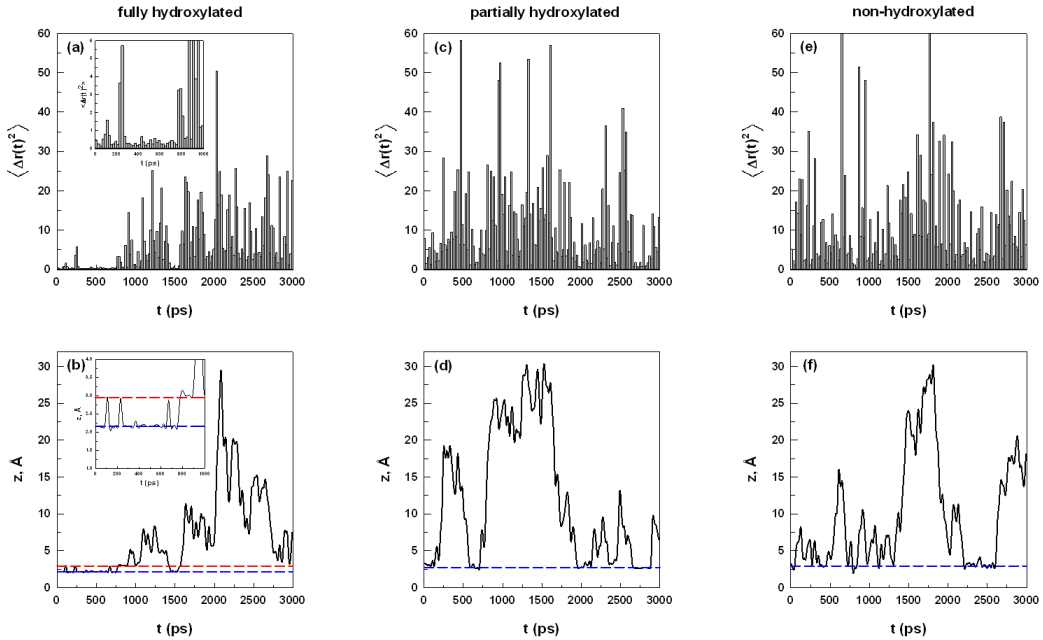


Figure 4.8: Average distance from the surface (bottom panels) and mean square displacement parallel to the solid surface (top panels) for one selected water molecule on each of the three surfaces considered. Data are shown for water molecules on the fully hydroxylated (left), partially hydroxylated (center), and non-hydroxylated surfaces (right). The dashed lines indicate the position of interfacial water layers reported in Table 4.1.

### 4.4.4 Rotational Dynamics

Another important quantity of interfacial water is the rotational diffusion. In our previous paper,[30] we showed how interfacial water on the fully hydroxylated surface shows anisotropic rotation. These observations are consistent with results reported in recent publications.[38, 100] Thus it is necessary to consider two vectors to fully characterize the rotation of interfacial water molecules. The water dipole moment vector and the vector identified by the two hydrogen atoms of each water molecule were considered in this study. To add to the assessment previously reported,[30] the analysis below is focused on those water molecules that reside within a specific interfacial layer long enough for the correlation function to be calculated. Thus only water molecules

that remain continuously present in the layer of interest for the total correlation length are considered. The correlation length considered is 10 ps in all cases. The autocorrelation function used for these calculations is:

$$C_v(t) = \frac{\langle \mathbf{v}(t)\, \mathbf{v}(0) \rangle}{\langle \mathbf{v}(0)\, \mathbf{v}(0) \rangle} \tag{4.3}$$

where $\boldsymbol{v}$ is either the dipole moment or the $\overrightarrow{HH}$ unit vector. We focus here on the first adsorbed water layer, where most differences compared to the bulk are expected.[19] In Figure 4.9 we report the autocorrelation function results for the dipole moment and the $\overrightarrow{HH}$ vector for water molecules in the first interfacial layers at the fully, partially and non-hydroxylated surfaces. The exact position of each layer is reported in Table 4.1. We also report the autocorrelation functions for water molecules located away from the surface ($z$ = 14 Å). For these latter calculations a 3 Å thick bin was employed to increase statistical accuracy. The analysis lasts 10 ps in all cases, short enough to ensure that, on each surface considered, the number of water molecules that remain within the layer of interest is sufficiently large to ensure reliable statistics. The data in Figure 4.9 suggest that both the dipole moment and $\overrightarrow{HH}$ vector autocorrelation functions decay more slowly at the three solid-liquid interfaces considered than they do in the bulk. In detail, the slowest rotational dynamics are observed for water molecules in the first layer of the fully hydroxylated surface and the fastest is observed at the non-hydroxylated surface. We further note that the reorientation of water molecules in the bulk region can be characterized as isotropic since the two autocorrelation functions are identical. On the contrary, the rotation of water molecules in the first interfacial layers

on any of the surfaces considered is anisotropic. The data suggest that in the case of the fully and partially hydroxylated surface the reorientation of the $\overrightarrow{HH}$ vector is slower than that of the dipole moment vector. In contrast, the dipole autocorrelation function at the non-hydroxylated surface decays more slowly than the $\overrightarrow{HH}$ one. We also included data from the second layer (~2.95 Å) on the fully hydroxylated surface (black dashed line in Figure 4.9) the results indicate a significantly faster decay of the $\overrightarrow{HH}$ autocorrelation function compared to the dipole moment. Thus, on this surface the anisotropic signature of the rotation of interfacial water molecules depends significantly on the layer position, probably because of the hydrogen-bond network established between interfacial water molecules. To quantify the difference between autocorrelation functions, we report in Table 4.2 the value of each autocorrelation function at time $t$ = 5 ps. The smaller this value is, the faster the corresponding autocorrelation function decays.

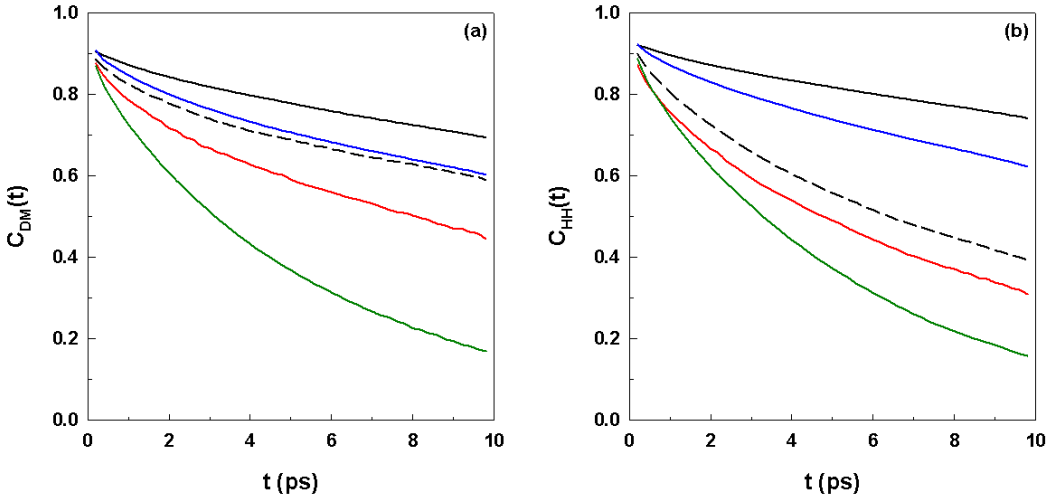


Figure 4.9: Dipole moment (a) and hydrogen-hydrogen vector (b) autocorrelation functions for interfacial water molecules on the fully hydroxylated (black), partially hydroxylated (blue), and non hydroxylated surface (red). Continuous and dashed black lines represent water in the first and second layers at the fully hydroxylated surface, respectively. The green line represents water molecules located 14 Å above the surface and have the bulk properties of water. In all cases $C(0) = 1$ (not shown for clarity). The position of each layer is shown in Table 4.1.

It is of interest to analyze further the data obtained at the partially hydroxylated surface because the structural characterization of the interfacial water molecules suggests that there are two different types of water molecules within the same layer.[98] The results for the dipole moment and $\overrightarrow{HH}$ vector autocorrelation function presented in Figure 4.10 illustrate the reorientation dynamics for those water molecules with hydrogen-down orientation, as opposed to those with hydrogen-up orientation. Hydrogen-down oriented water molecules have higher residence probability than the hydrogen-up ones as shown in Figure 4.6b. The data in Figure 4.10 suggest that the hydrogen-down oriented water molecules have a slower reorientation of the $\overrightarrow{HH}$ vector compared to the dipole moment vector. The opposite is observed for water molecules with hydrogen-up orientation, for which the $\overrightarrow{HH}$ autocorrelation function decays faster than that for the dipole moment. Our data suggest that those water molecules associated

with surface hydroxyl groups that have hydrogen-down orientation have a slow $\overrightarrow{HH}$ reorientation. In the case where water molecules are not highly associated with surface hydroxyl groups, they have higher reorientation freedom with respect to the $\overrightarrow{HH}$ vector. However, the data suggest that their dipole moment reorients at a slower rate because of electrostatic interactions with the surface.

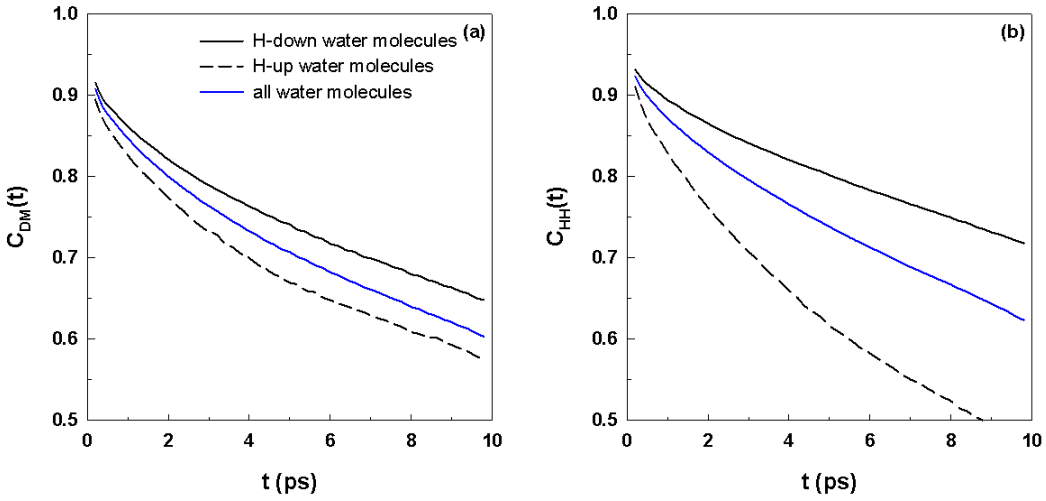


Figure 4.10: Dipole moment (a) and hydrogen-hydrogen vector (b) autocorrelation functions for water molecules in the first layer on the partially hydroxylated surface. Data for H-down water molecules (black solid line), H-up water molecules (dashed line), and all water molecules (blue solid line) in the first layer are provided in the figures. In all cases $C(0) = 1$ (not shown for clarity).

Table 4.2: Dipole moment and hydrogen-hydrogen autocorrelation functions calculated at time $t$ = 5 ps for interfacial water molecules (data shown in Figure 4.9 and Figure 4.10). The layer position is reported in Table 4.1. Properties for "bulk" water are estimated at 14 Å from the surface, and are independent on the surface considered herein.

| Silica surface | Layer | $C_{DM}(t)$ | $C_{HH}(t)$ |
|---|---|---|---|
| Fully hydroxylated | first | 0.78 | 0.82 |
| | second | 0.69 | 0.56 |
| Partially hydroxylated | first / H-down | 0.74 | 0.80 |
| | first / H-up | 0.67 | 0.62 |
| Non-hydroxylated | first | 0.59 | 0.49 |
| "bulk" behavior | 14 Å from surface | 0.37 | 0.37 |

### 4.4.5 Hydrogen Bond Dynamics

Our previous studies[30, 98] demonstrated that the structure of interfacial water is determined by both surface-water and water-water interactions. Water-water interactions are largely dominated by the formation of hydrogen bonds. In Figure 4.11 we report the hydrogen bond density profile and the average number of hydrogen bonds per water molecule as a function of the distance from the three surface types. To determine the formation of one hydrogen bond we adopt the geometric criterion proposed by Martí.[72] The position of one hydrogen bond is defined as the mid distance between the hydrogen and the oxygen atoms forming the hydrogen bond. The results in Figure 4.11a support our hypothesis that water-water hydrogen bonds are in large part responsible for determining the structure of interfacial layers, as discussed earlier.[30, 98] The results obtained for the average number of hydrogen bonds formed by each water molecule (Figure 4.11b) show minimal differences between the surfaces considered in this study. This observation may imply that the interfacial structure formed by water molecules on each surface (i.e., the data in Figure 4.2) is dependent on the surface

properties, but it appears that water molecules adopt whatever interfacial structure is necessary to allow for the breaking of fewer water-water hydrogen bonds. This observation may be important for further developments of the theoretical framework recently proposed by Djikaev and Ruckenstein.[101, 102] Our results show that the average number of hydrogen bonds per water molecule is 3.48 at distances larger than ~1.0 nm from the surface, in good agreement with simulation results reported for the SPC model of water in liquid bulk conditions.[111] In Figure 4.11b we also report the probability of finding hydrogen bonded water molecules as a function of distances from the surface. These data show that water molecules have a higher probability to be hydrogen bonded when located within high density layers.

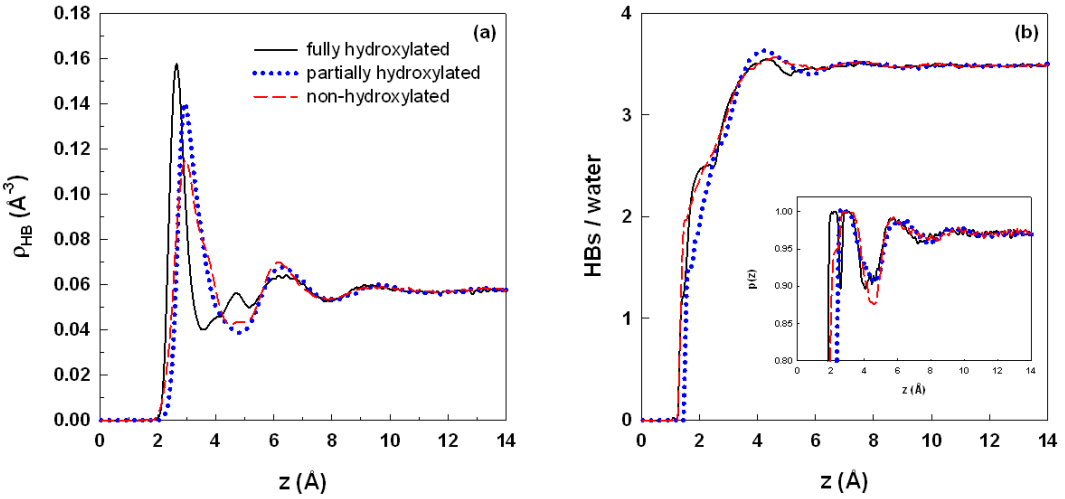


Figure 4.11: Hydrogen bond density profile (a) and number of hydrogen bonds per water molecule (b) as a function of the distance *z* from the three surfaces considered. The probability of finding hydrogen-bonded water molecules at a given distance from the three surfaces is given in panel b. Solid, dashed, and dotted lines represent water molecules on the fully hydroxylated, partially hydroxylated, and non-hydroxylated surfaces, respectively.

Table 4.3: Location (expressed as distance $z$ from the surface) of the hydrogen bond density peaks on the fully, partially, and non-hydroxylated surfaces as shown in Figure 4.11a.

| Silica surface | Hydrogen Bond peak (Å) |
|---|---|
| Fully hydroxylated | 2.65 |
| Partially hydroxylated | 2.95 |
| Non-hydroxylated | 2.95 |

For the scope of the present work it is of interest to determine the average lifetime of the hydrogen bonds as a function of their distance from the surface. To assess this quantity we calculate the continuous lifetime hydrogen-bond autocorrelation function associated with the various layers. Our results for bulk water are in quantitative agreement with those presented for SPC water by Martí et al.[111] The position of each of the hydrogen-bond layers considered is shown in Table 4.3. The results for the HB-HB autocorrelation functions, shown in Figure 4.12, indicate that the hydrogen bonds formed between water molecules near each of the three surfaces last far longer than water-water hydrogen bonds in bulk water. The time that the hydrogen bond autocorrelation function requires to decay from 1 to $1/e$ at the fully, partially and non-hydroxylated surfaces and in the bulk region is 1.73, 1.07, 0.68, and 0.42 ps, respectively. This is not too surprising, considering that interfacial water molecules show slower translational and rotational diffusion when compared to bulk water, as discussed in Figure 4.7 and Figure 4.9, respectively. Water-water hydrogen bonds last the longest when water is near the fully hydroxylated surface and the shortest when water is near the non-hydroxylated surface. Contrary to what has been observed before, we did not find evidence of cross-over behavior for water near the partially hydroxylated surface. Instead, the hydrogen bond correlation function exhibit decays

that are intermediate between the results obtained on the fully and on the non-hydroxylated surfaces.

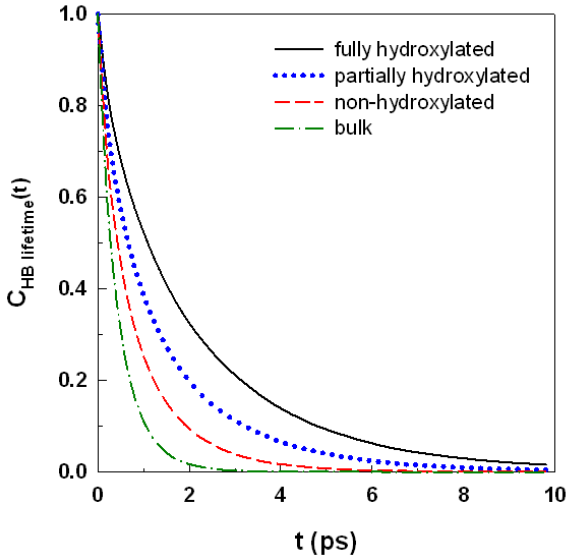


Figure 4.12: Hydrogen bond – hydrogen bond autocorrelation functions on the three surfaces considered. Solid, dashed, and dotted lines represent hydrogen bonds on the fully hydroxylated, partially hydroxylated, and non-hydroxylated surfaces, respectively. The layer position is reported in Table 4.3. The green dash-dot line corresponds to hydrogen bonds formed between water molecules 14 Å above the surface, where the results are identical on all three surfaces and resemble those obtained for bulk water.

## 4.5 Conclusions

Equilibrium molecular dynamics simulations were employed to study the dynamic behavior of interfacial water on crystalline silica surfaces with three different degrees of hydroxylation. Fully hydroxylated, partially hydroxylated and non-hydroxylated silica surfaces were used to assess the effect of the substrate on dynamic behavior of interfacial water. We calculated the residence probability of water in the interfacial layer as well as the in-plane mobility at the region of interest. The rotational dynamics were evaluated by calculating the dipole moment and $\overrightarrow{HH}$ vector

autocorrelation functions. The dynamics of the hydrogen bond network were evaluated by means of continuous lifetime hydrogen bond autocorrelation functions. Additional equilibrium properties such as atomic and cumulative density profiles, local charge density, hydrogen bond density profile, and total local dipole moment were also presented.

Our simulation results indicate that the solid substrate not only affects the structural properties of water, but also strongly alters its dynamic behavior. Our data indicate that interfacial water molecules at the fully hydroxylated surface remain longer on average in the interfacial region than water molecules at partially and non-hydroxylated surfaces. The data illustrate a relative low in-plane displacement on water molecules that are strongly associated with the solid surface. We provide evidence for significantly different rotational dynamics for water molecules that have hydrogen-down orientation compared to the others. For instance, water molecules at the fully hydroxylated surface have a slower reorientation of the $\overrightarrow{HH}$ vector than that exhibited by the dipole moment. At the partially hydroxylated surface water can have a fast reorientation of the dipole moment or the $\overrightarrow{HH}$ vector depending on its in-plane position in contact with the solid substrate. Interfacial water molecules at the non-hydroxylated surface have a slow reorientation of the dipole moment probably because of the absence of surface hydroxyl groups. Lower hydrogen bond lifetimes are found at the non-hydroxylated surface, where we observe shorter residence probability with respect to results obtained on the other substrates.

# 5 Molecular Dynamics Studies of Interfacial Water at the Alumina Surface

The material presented below was accepted to The Journal of Physical Chemistry C for publication.

## 5.1 Abstract

Interfacial water properties at the alumina surface were investigated via all-atom equilibrium molecular dynamics simulations at ambient temperature. Al-terminated and OH-terminated alumina surfaces were considered to assess the structural and dynamic behavior of the first few hydration layers in contact with the substrates. Density profiles suggest water layering up to ~10 Å from the solid substrate. Planar density distribution data indicate that water molecules in the first interfacial layer are organized in well-defined patterns dictated by the atomic terminations of the alumina surface. Interfacial water exhibits preferential orientation and delayed dynamics compared to bulk water. Water exhibits bulk-like behavior at distances greater than ~10 Å from the substrate. The formation of an extended hydrogen bond network within the first few hydration layers illustrates the significance of water-water interactions on the structural properties at the interface.

## 5.2 Introduction

Properties of water at the solid-liquid interface play an important role in ion adsorption/desorption processes on solid substrates, diffusion of ions in nanopores, biological membranes, and ion channels.[52-54, 112] A number of experimental[15, 19, 113] and theoretical[30, 98, 100, 114, 115] studies have provided molecular-level insights on the behavior

of interfacial water. It has been reported that the structural and dynamics properties of interfacial water are significantly affected by the solid substrate characteristics, resulting in different behavior compared to that of water in the bulk.[116, 117] In general, these effects occur at short distances from the solid substrate.[118]

A widely used material in catalysis is aluminum oxide, often referred to as alumina. Alumina is used as a catalyst and catalyst support, as a substrate in microelectronic devices, and in many other applications. The surface chemistry of crystalline and amorphous $Al_2O_3$ under various conditions has been previously investigated both experimentally and theoretically.[119-124] It has been observed experimentally that the $\alpha$-$Al_2O_3$ (0001) surface can be terminated with an aluminum layer in the absence of water.[119] A single aluminum termination is predicted to be the most energetically stable in the absence of water by Garofalini and co-workers.[125] Complex surface hydroxylation and dehydroxylation phenomena are observed at the alumina surface in the presence of water. Numerous investigations have focused on changes in the surface chemistry of alumina in hydrated environments.[41-47] For instance, Eng et al. investigated experimentally the surface properties of the hydrated $\alpha$-$Al_2O_3$ (0001) surface and reported an oxygen-terminated surface coupled with the formation of an ordered contact water layer.[126] Coustet et al. confirmed that when exposed to humid atmospheres the $\alpha$-$Al_2O_3$ surface is hydroxylated.[127] Barth et al. employed dynamic scanning force microscopy techniques to image the atomic structure of the hydrated $\alpha$-$Al_2O_3$ (0001) surface. The results are consistent with the formation of hydroxide clusters, suggesting surface reconstruction at high temperatures.[128] An ab initio molecular dynamics study by Hass et al. revealed,[129] in agreement with previous

ab initio calculations by Hase and co-workers,[43] that dissociative adsorption of water is energetically favored on the Al-terminated (0001) α-$Al_2O_3$ surface compared to molecular physisorption.

Surprisingly, molecular dynamics simulation studies with focus on the properties of interfacial water at alumina surfaces are not common, although the effect of water adsorption on the structure of the alumina surface has been reported.[130] The present work stems from the necessity of better understanding the structure of interfacial water on this technologically very important material. In this study we report properties of interfacial water on the α-aluminum oxide (0001) surface with two surface terminations. We employed all-atom equilibrium molecular dynamics simulations to probe the effect of aluminum-terminated and fully hydroxylated α-$Al_2O_3$ surfaces on the behavior of interfacial water. The effect of surface chemistry on the structure of interfacial water was assessed by the study of two extreme degrees of hydroxylation on the alumina surfaces. Although it is more likely to observe extensive surface hydroxylation of an alumina substrate in a humid environment, it is of interest to understand the behavior of interfacial water near aluminum sites that may coexist with hydroxyl groups on a realistic alumina surface. This approach allows us to explore the structure and dynamics of adsorbed water and reveals atomic-level insights of the phenomena occurring at the solid-liquid interface. The results are briefly compared to those available for water on other substrates.

## 5.3 Simulation Details

The (0001) crystallographic face of corundum α-$Al_2O_3$ (space group $R\bar{3}c$)[131] was used to model the alumina solid substrate. The CLAYFF force field was

implemented to simulate the solid substrate.[132] Two fully flexible (0001) α-$Al_2O_3$ surfaces were considered. One is Al-terminated, the other OH-terminated (the fully hydroxylated surface shows ~15 OH/$nm^2$). A top view of the two surfaces with the aluminum and hydroxyl group terminations are shown in the left and right panels of Figure 5.1, respectively. The $x$ and $y$ dimensions of the solid substrate were both approximately 9.1 nm, for a total surface area of ~82 $nm^2$. The total length of the simulation box along the $z$ direction is ~160 Å.

The SPC/E model was used to simulate water.[79] The model is known to reproduce well structural and dynamic properties of bulk water. When results obtained implementing either the SPC/E or the SPC models for water at contact with silica substrates are compared, no observable differences were reported.[133] The bonds and angles of water molecules were kept fixed by employing the SETTLE algorithm.[81] Non-bonded interactions were modeled by means of dispersive and electrostatic forces. The electrostatic interactions were modeled by a Coulombic potential. The dispersive interactions were modeled with a 12-6 Lennard-Jones (LJ) potential. The LJ parameters for unlike interactions were determined by Lorentz-Berthelot mixing rules.[65] The cutoff distance for all interactions was 9 Å. Long range corrections to electrostatic interactions were treated using the particle mesh Ewald (PME) method.[134]

All simulations were performed in the canonical ensemble where the number of particles ($N$), the simulation volume ($V$), and the temperature ($T$) were held constant (NVT ensemble). The system temperature was fixed at 300 K and controlled by a Nosé-Hoover thermostat[135, 136] with a relaxation time of 100 fs. Periodic boundary conditions were applied in the three directions. The equations of motion were solved with the

simulation package GROMACS[83, 85] by using a leapfrog algorithm[137] with time step of 1.0 fs. Data analysis was performed for the last 1 ns of our simulation, after we completed 3 ns of equilibration.

We simulated 15,000 water molecules in order to create a thin water film in contact with the solid surface of thickness ~55 Å along the *z*-axis. An empty gap remains between the thin film and the periodic image of the alumina substrate, similarly to our prior studies.[30, 98, 116] Additional simulations were conducted for the estimation of the contact angle. In these simulations 1000 water molecules were considered on each of the two surfaces. The simulated system is similar to that used previously to study water on silica.[98, 116, 133]

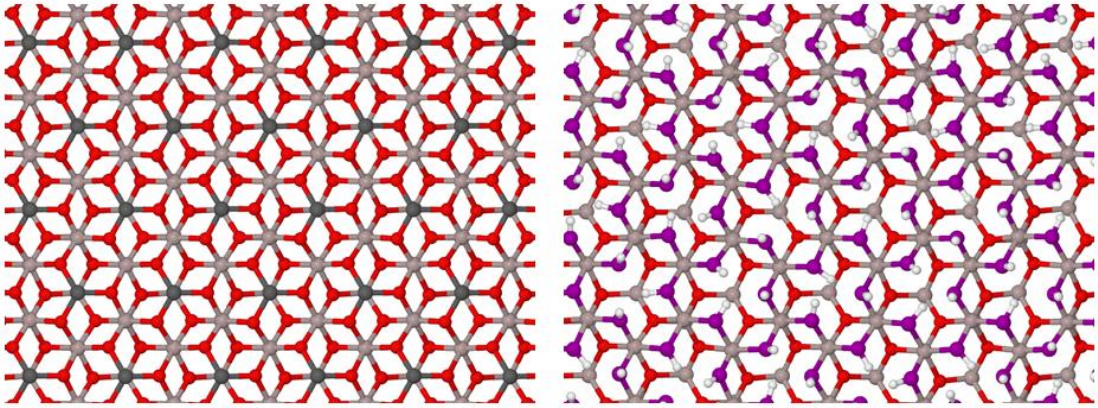

Figure 5.1: Top view of the Al-terminated (left panel) and OH-terminated (right panel) alumina surfaces. Tan and red spheres represent aluminum and oxygen atoms, respectively. Top layer aluminum atoms at the Al-terminated alumina surface are shown in grey. Surface hydroxyl groups are shown with purple for oxygen and white for hydrogen atoms. Only the upper five atomic layers are shown for clarity. The thickness of the alumina surface along the *z*-axis (perpendicular to the planes shown herein) is approximately 12.75 and 12.10 Å for the Al-terminated and OH-terminated surfaces, respectively.

## 5.4 Results and Discussion

### 5.4.1 Density Profiles

In Figure 5.2a we report atomic density profiles of water oxygen (solid black line) and water hydrogen atoms (dashed blue line) as a function of the distance from the Al-terminated alumina. The reference ($z$ = 0) corresponds to the top plane of aluminum atoms on the substrate. The oxygen atomic density data show the formation of two water layers at 1.90 and 4.50 Å, respectively. The first peak in the hydrogen atomic density profile (Figure 5.2a) appears at 0.95 Å. Comparing the intensities of the first oxygen peak to that of the first hydrogen peak suggests hydrogen-down preferential orientation for roughly half of the water molecules found within the first hydration layer at the Al-terminated surface.

The second atomic hydrogen layer appears at 2.15 Å. The width of this peak, its intensity, and the proximity to the first peak suggest a complex structure for the water molecules in the first hydration layer. As mentioned earlier, about half of these waters have a hydrogen-down orientation, while the rest tends to maintain the OH vectors parallel, and slightly pointing away from the surface. The second pronounced peak for oxygen atoms in Figure 5.2a appears at 4.5 Å. This peak is accompanied by two peaks in the corresponding atomic hydrogen density profile at 3.6 and 4.85 Å. As the distance approaches 10 Å, and further, the density profiles become smooth, suggesting bulk-like behavior.

The minimum at ~2.5 Å in the oxygen density provides evidence of a region depleted of water in between the two primary hydration layers. It should however be pointed out that our results show the presence of water hydrogen atoms in this

"depleted" region, suggesting that water molecules in the first hydration layer interact, probably via hydrogen bonds, with water molecules in the second hydration layer. However, it should be pointed out that, as discussed later, our results show much larger density of hydrogen bonds formed between water molecules belonging to the first hydration layer, suggesting that only a few bonds form between water molecules of the first hydration layer, and those in the second hydration layer.

Atomic density profile data at the OH-terminated alumina surface are shown in Figure 5.2b. The reference $z$ = 0 for the OH-terminated surface is the plane of the hydroxyl group oxygen atoms of the substrate. In these results the first water oxygen layer forms at 2.6 Å and the first two water hydrogen atomic layers occur at 1.65 and 2.9 Å, respectively. The distance between the first hydrogen and oxygen atomic layers is ~1 Å, equal to the OH bond distance in a water molecule. Our results suggest a preferential orientation for ~70% of the water molecules within the first hydration layer with one OH bond pointing towards the surface.

The results obtained at the two alumina surfaces indicate that the Al-terminated surface promotes the formation of a very dense first water layer, almost isolated, via a depletion layer, from the second hydration layer. On the OH-terminated surface the first water layer is less dense than that observed at the Al-terminated surface. The water molecules in the first layer on both surfaces are to a large extent characterized by H-down orientation. On both surfaces, it appears that the perturbation in the local water density due to the presence of the solid flat substrate occurs within less than 10 Å from the substrate, in qualitative agreement with results obtained for water at other substrates.[30, 138-141] This is in stark contrast with results obtained, for example for

acetonitrile near a silica surface[142] where the silica surface promoted structuring of interfacial acetonitrile for up to ~22 Å.

The charge density profiles away from both surfaces, presented in Figure 5.2c, show an oscillatory trend with alternating positive and negative peaks. The peaks correspond to the positively and negatively charged atomic layers due to layering and orientation of interfacial water molecules. Atomic density and charge density profile data reveal strong perturbation on the water structure due to the presence of the alumina surface that extends up to approximately 10 Å from the solid substrate. For distances greater than 10 Å the variations on the density profiles are significantly less pronounced, suggesting bulk-like behavior. Similarly in the charge density profiles we observe zero net charge that provides evidence for isotropic water properties at such distances. The data presented in Figure 5.2c lay the foundation for the study of adsorption of electrolytes on the surfaces.[112]

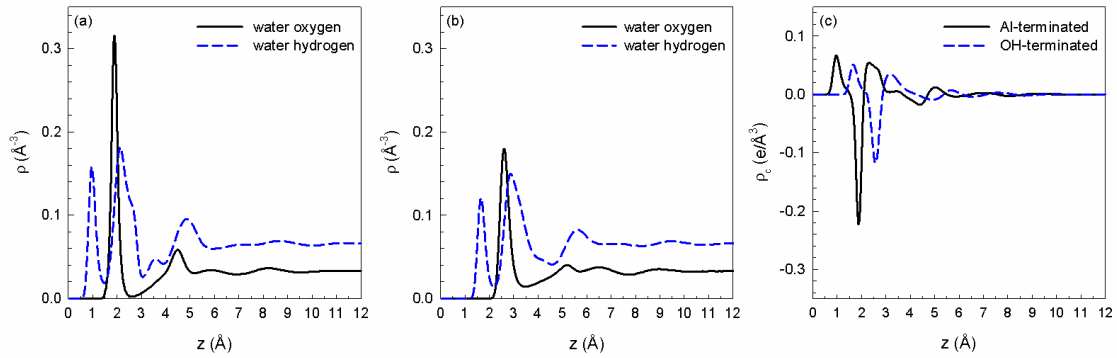


Figure 5.2: (a) Atomic density profile of oxygen and hydrogen atoms on Al-terminated alumina surface. (b) Atomic density profile of oxygen and hydrogen atoms on OH-terminated alumina surface. (c) Atomic charge density profile of water molecule on Al-terminated and OH-terminated alumina surfaces in solid black and dashed blue lines, respectively.

### 5.4.2 Planar Density Distributions

To understand and relate the behavior of interfacial water to the properties of the solid substrate we calculated planar density distributions of water. The results are shown in Figure 5.3 and Figure 5.4. The distributions of oxygen and hydrogen atomic species were calculated in layers parallel the surface ($x - y$ plane) and of thickness $dz$ = 1 Å. These layers were centered at the primary atomic layers, based on data shown in Figure 5.2a and b.

The density distribution data of the first oxygen layer at the Al-terminated surface, given in Figure 5.3b, shows a well-defined structure. We observe highly confined water molecules distributed along the $x - y$ plane. The aluminum atoms on the surface (see Figure 5.1a) provide adsorption sites for interfacial water. We observe the formation of a hexagonal pattern with water molecules occupying all vertices. This structure repeats periodically throughout the interface. In each hexagonal configuration we observe the adsorption of three water molecules above the three terminal aluminum atoms present on the surface. The other three water molecules occupy the other adsorption sites on the hexagon. The planar distribution data for the first hydrogen layer (Figure 5.3a) reveal that absorbed water molecules exhibit a hydrogen-down orientation, which is in agreement with the density profile data shown in Figure 5.2a. We note that the two types of adsorbed water molecules alternate within the hexagonal pattern (this structure is discussed in detail below). The data in Figure 5.3c show the position of hydrogen atoms at 2.15 Å from the alumina surface. The hydrogen atoms in this layer belong primarily to those water molecules whose oxygen atoms form the first layer. In Figure 5.3b we also observe a few circular-like density distribution patterns.

These correspond to water molecules adsorbed on surface oxygen sites that become exposed due to the rearrangement of some surface aluminum atoms. Although the rearrangement observed for some Al surface atoms may be a consequence of the instability of the Al-terminated substrate in water, a detailed discussion of such behavior is beyond the scope of the present paper.

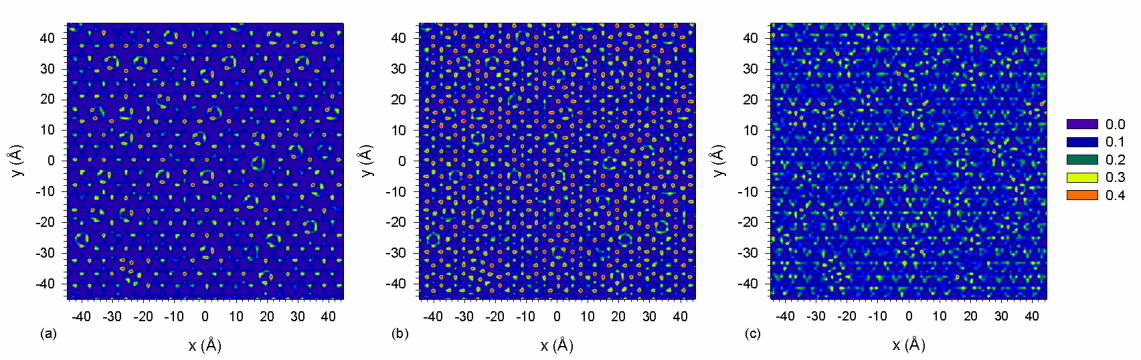


Figure 5.3: Surface density distributions along the $x-y$ plane (parallel to the surface) for water oxygen in the first layer (b) and water hydrogen in the first layer (a) and second layer (c) at Al-terminated alumina surface. The positions of the atomic layers are shown in Figure 5.2a. Densities are expressed in $Å^{-3}$.

In Figure 5.4b we provide oxygen density distribution data for the first water layer on the OH-terminated alumina surface. The first layer forms at 2.6 Å from the surface (see Figure 5.2b). From the oxygen density distribution results (Figure 5.4b) we observe that water molecules are organized with high density areas near the surface hydroxyl groups, yielding a distinct hexagonal pattern. However, the results suggest higher transitional freedom along the $x-y$ plane than the data obtained at the Al-terminated surface. Data for the first hydrogen atomic layer, at 1.65 Å from the alumina surface (Figure 5.4a), suggest a preferential H-down orientation for water molecules whose oxygen atom is found within specific adsorption sites (see Figure 5.4b). Similarly, data for the second layer of hydrogen atoms at 2.9 Å, shown in Figure 5.4c,

are consistent with a less organized structure with high density areas primarily forming at regions where the hydrogen density in the first layer (Figure 5.4a) is low or zero. This finding suggests that the adsorption site ($x-y$ position) of a water molecule in the first interfacial layer determines its orientation, and potentially its ability for hydrogen bonding with surrounding water molecules.

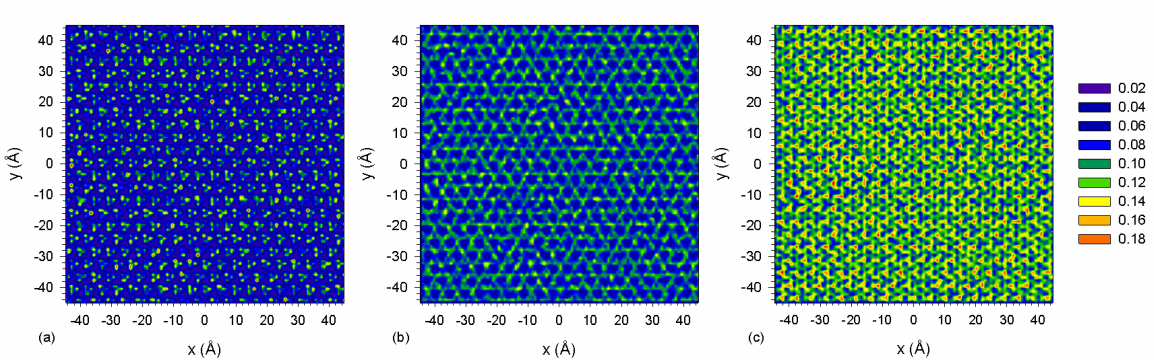


Figure 5.4: Surface density distributions along the $x-y$ plane (parallel to the surface) for water oxygen in the first layer (b) and water hydrogen in the first layer (a) and second layer (c) at OH-terminated alumina surface. The positions of the atomic layers are shown in Figure 5.2b. Densities are expressed in $Å^{-3}$.

Simulation snapshots of two representative equilibrium interfacial water structures at the Al-terminated (left panel) and OH-terminated surfaces (right panel) are shown in Figure 5.5. The simulation snapshot obtained on the Al-terminated surface (left panel in Figure 5.5) highlights the presence of water molecules with two distinct orientations within the first hydration layer. As expected from the planar density profiles (Figure 5.3b), the interfacial water molecules are organized within hexagons, in which one water molecule occupies each of the vertexes. Three water molecules project one OH bond each towards the surface (confirming the H-down orientation for half of the water molecules in the first hydration layer discussed above), while the other three maintain both OH bonds somewhat parallel to the surface. The three molecules with

both OH bonds parallel to the surface (purple in Figure 5.5) are located approximately on top of the Al atoms. Because of the proximity of these exposed Al atoms to each other, the six water molecules within the hexagon highlighted in the simulation snapshot are strongly interacting via hydrogen bonds (highlighted as broken blue lines). Our analysis confirms that the distribution of atomic species at the solid substrate determines the distribution and orientation of water molecules within the first adsorbed layer of interfacial water.

On the OH-terminated surface (right panel), we observe a much less defined structure of hydration water. Some water molecules point one of their OH bonds towards the surface (red water oxygen atoms), while others do not (purple). Water molecules in this hydration layer possess larger translational freedom than those on the first hydration layer on Al-terminated surfaces, although reorientation dynamics have not been explicitly assessed herein.

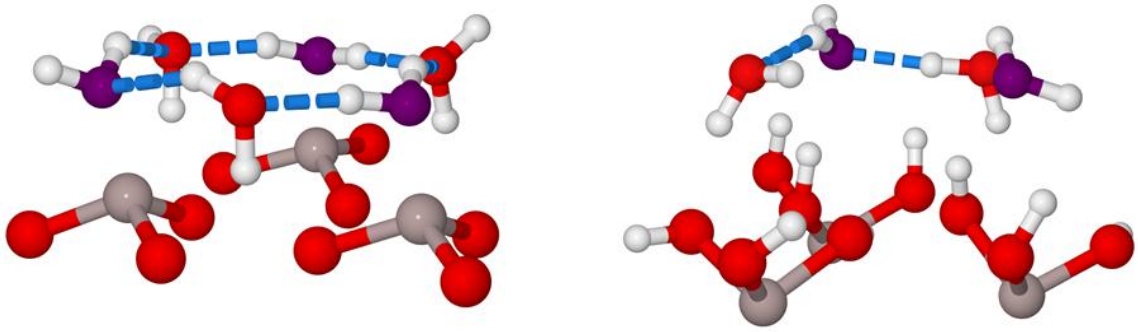

Figure 5.5: Simulation snapshots of selected interfacial water molecules at the Al-terminated (left panel) and OH-terminated (right panel) alumina surfaces. Only the first few atomic layers of the alumina surface are shown for clarity. Tan, red, and white spheres represent aluminum, oxygen, and hydrogen atoms, respectively. Water molecules with no OH bonds pointing toward to the surface are shown with purple oxygen atoms. The blue dashed lines represent hydrogen bonds.

### 5.4.3 Molecular Orientation

The orientation of interfacial water was assessed in terms of an order parameter, defined as the angle $\theta$ between the water dipole moment and the vector normal to surface. In Figure 5.6 we report the ensemble average of $cos(\theta)$ as a function of the distance from the two alumina surfaces. The results confirm the preferential orientation of water in contact with both alumina surfaces. The data show that surface effects on interfacial water orientation are more pronounced at the Al-terminated surface. For water molecules in contact with this surface we observe positive and negative peaks at ~1.65 and 1.90 Å, respectively. This finding suggests an opposite dipole moment orientation for the two types of water molecules found within the first water layer. The pronounced peak at ~2.3 Å (black solid line) shows that the water dipole moment and the normal to the surface vector form on average a ~50° angle. This is consistent with a molecular orientation in which at least one OH bond point towards the solid substrate. We note that this peak corresponds to a region with low atomic density (see Figure 5.2a). Further analysis indicated that the few water molecules that reside at this distance have that distinct orientation. Similar positive-negative oscillatory behavior of the order parameter as function of distance from the OH-terminated is shown in blue dashed line. The first peak at ~2.6 Å suggests that water molecules in the first interfacial layer (see Figure 5.2b) have a consistent orientation of their dipole moment. We also note preferential orientation at the ~3.1 Å which corresponds to a region with low atomic density. This orientational configuration at the depletion zone may be due to strong water-water interaction by the two adjacent layers. The order parameter converges to zero at the bulk-like region found at distances larger than 10 Å from the substrate, where water exhibits isotropic behavior. It should be pointed out that the results shown

in Figure 5.6 are not sufficient to characterize the orientation of interfacial water molecules. More complete analysis is provided for example by Marry et al.[143] for water at a negatively charged clay surface and by our group for water on silica.[116] For the present case, a reliable interpretation of the structure of interfacial water can be attained when the density profiles described above are combined with the results shown in Figure 5.6.

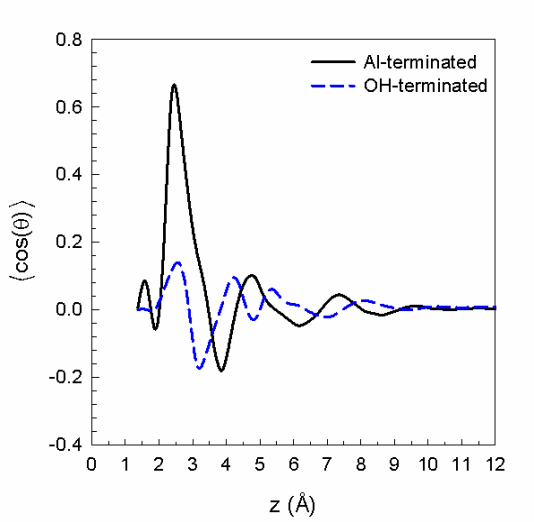


Figure 5.6: Order parameter $\langle \cos(\theta) \rangle$ for water molecules as a function of distance from the Al-terminated (black solid) and OH-terminated (blue dashed line) surfaces. The angle $\theta$ is the one formed between the water dipole moment vector and the vector normal to the surface.

### 5.4.4 Hydrogen Bond Network

We determined hydrogen bond density profiles as a function of distance from the Al-terminated (solid black line) and OH-terminated (dashed blue line) surface. The results are shown in Figure 5.7. The geometric criterion proposed by Martí[72] was adopted to determine the formation of hydrogen bonds between water molecules. The position of one hydrogen bond is defined as the mid-distance between the hydrogen and

oxygen of the two hydrogen-bonded water molecules. Our data show a pronounced peak on the hydrogen bond density profile for Al-terminated surface at ~2.0 Å. This position corresponds to hydrogen bonds formed between water molecules located within the first hydration layer on the Al-terminated surface, as shown in the simulation snapshot provided on the left panel of Figure 5.5. The peak at ~4.85 Å suggests increased hydrogen bonding among water molecules in the second layer. The position and sizeable width of this peak indicate that water molecules at the second hydration layer (~4.5 Å) could hydrogen bond with water molecules that belong to a layer at distances further from the alumina surface. The data also reveal lesser peaks at ~2.75 Å and 3.45 Å at the Al-terminated surface, which suggest hydrogen bonding between first and second layer water molecules. The density of these hydrogen bonds is much less than that of hydrogen bonds between water molecules within the first hydration layer. This observation provides evidence of the structural relationship between adjacent water layers, qualitatively in agreement with previous results for water on silica.[30] The results of Figure 5.7 suggest the presence of only a few water-water hydrogen bonds between water molecules in the first and second layer at the Al-terminated surface, which is consistent with the snapshots shown in Figure 5.5. Unlike the results observed on fully hydroxylated crystalline silica surface, the results for hydrogen bond density profiles (Figure 5.7), especially on the Al-terminated alumina substrate, are consistent with pronounced hydrogen bonding between water molecules belonging to the first hydration shell. Analysis of simulation snapshots (left panel of Figure 5.5) as well as of the planar density distribution of water within the first hydration layer (Figure 5.3b) demonstrate that the pronounced hydrogen bonding between water molecules in the first layer is

possible because the preferential adsorption sites on this surface are relatively close to each other. In contrast, the structure of silica used in our previous simulations[9] provides strong adsorption sites for water molecules in the first hydration shell that are ~5 Å apart from each other. The distance is too large to form hydrogen bonds.

The data provided in Figure 5.7 for the OH-terminated alumina surface show two pronounced peaks at ~2.75 and 5.85 Å. The first peak indicates an increased number of hydrogen bonds for water molecules within the first water layer at 2.6 Å. The second peak suggests extensive hydrogen bonding between the second and third water layers, as suggested by Figure 5.2b for the oxygen atomic density. It should be pointed out, however, that a well-defined third water layer is not evident from the density profile data (see Figure 5.2b). We also note shoulders on peaks in Figure 5.7 at approximately 3.25 and 4.0 Å (dashed blue line) indicative of hydrogen bonding between first and second layer water molecules. At distances greater than ~10 Å we observe a uniform hydrogen bond density distribution, representative of bulk-like water behavior. This finding is also in good quantitative agreement with previous studies on different substrates.[30, 100]

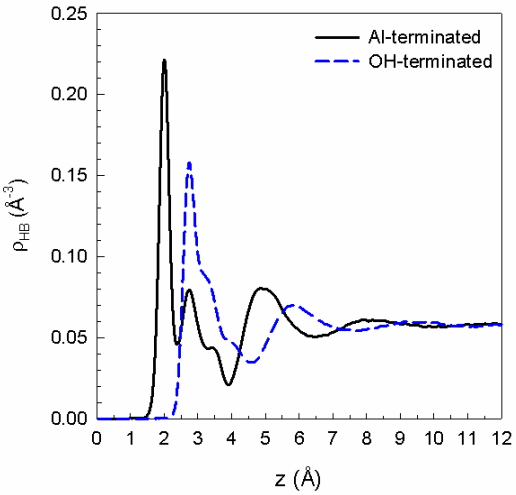


Figure 5.7: Hydrogen bond density profiles as a function of distance $z$ from the alumina surface. Solid black and dashed blue lines represent hydrogen bonding between water molecules at the Al-terminated and OH-terminated surfaces, respectively.

### 5.4.5 Residence Time

In Figure 5.8 we provide results on the residence probability $P(t)$ of water molecules within the various interfacial layers formed on the two surfaces. These data allows us to quantify how long one water molecule, on average, continuously resides within a distinct interfacial layer formed at the alumina surfaces. The results for the Al-terminated surface (Figure 5.8a) suggest that water molecules in the first hydration layer (black solid line) reside at specific adsorption sites (Figure 5.3b) significantly longer than water molecules in the second interfacial layer (blue dashed line). This slow dynamic behavior, supported by the structural properties of first layer water molecules, previously discussed, indicate energetically stable configurations with pronounced water-surface correlations. As water molecules in layers further from the surface are considered, the dynamic properties approach that of bulk water (red dotted line in Figure 5.8a). Similar qualitative behavior is observed at the OH-terminated alumina

surface (Figure 5.8b), although pronounced differences are noted in the $P(t)$ profiles obtained for water molecules on the first interfacial layers formed on the two alumina surfaces. For example, the time for $P(t)$ to decay to $1/e$ is approximately 130.4 and 10.8 ps for water molecules in the first layer on the Al-terminated and OH-terminated surface, respectively. This difference is primarily due to the different alumina surface terminations. Data show a slower decay of the $P(t)$ for the second layer at the Al-terminated surface than the OH-terminated one, although the difference is not as significant as in the case of water molecules belonging to the first hydration layer. Our results suggest that the perturbation of the surface on water dynamic properties diminishes at distances greater than ~10-12 Å from the solid substrate, as was observed for water on crystalline silica.[116] The residence time of water within the first hydration layer on the Al-terminated alumina surface (left panel in Figure 5.8) is significantly longer than that obtained for the first hydration layer on the fully hydroxylated crystalline silica surface, discussed in our prior study.[116] On both surfaces our results show a delayed dynamics for interfacial water, with very long residence times. Both results are due to strong substrate-water interactions, with both surfaces providing patterned sites that promote the formation of an ordered first hydration layer. In addition to this, on the Al-terminated alumina surface considered in the present work, the exposed Al atoms provide adsorption sites for interfacial water that are close enough to allow the formation of hydrogen bonds between water molecules belonging to the first hydration layer (see left panel of Figure 5.5). This behavior was not possible on the silica surface considered in a previous study[116] because of the intrinsic structural properties of the substrate.

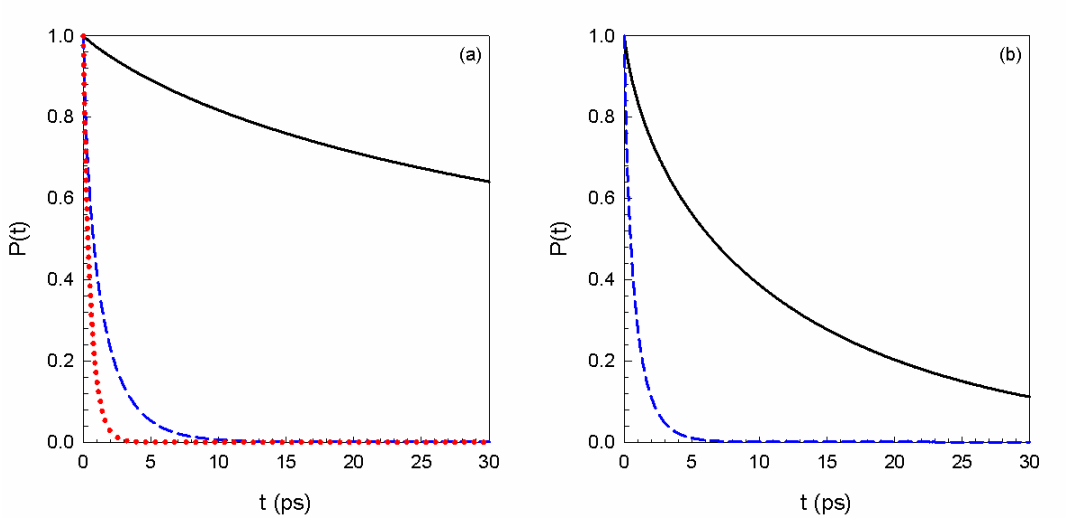


Figure 5.8: Residence probability for water molecules in the first (solid black line) and second (blue dashed line) interfacial layers at the Al-terminated (a) and OH-terminated (b) alumina surfaces. Data in red dotted line corresponds to water molecules located at 14 Å above the surface and are identical for both surface terminations. As detailed in our prior work,[116] water molecules within a layer formed at 14 Å above the surface essentially reproduce bulk-like behavior.

### 5.4.6 Surface Wettability

The degree of hydrophobicity of the alumina surfaces was qualitatively assessed via the estimation of a water nanodroplet contact angle. We conducted simulations with 1000 water molecules placed on the alumina with a surface area ~82 $nm^2$. Although this number of water molecules is sufficient for the qualitative characterization of the surfaces considered, our study cannot provide sufficient details for predicting contact angles that could be verified experimentally because it is well-known that the contact angle calculation depends on the droplet size.[144, 145] Simulation snapshots obtained after 4 ns of simulation, presented in Figure 5.9, reveal that both Al-terminated and OH-terminated alumina surfaces considered herein are very hydrophilic. The nanodroplets of 1000 water molecules completely wet both substrates. Small differences exist between the two nanodroplets, but we have not collected significant statistics to discuss

these differences in more details. Additional simulations with 2000 water molecules at the two alumina surfaces (see Figure 5.10) also show similar behavior of water on the two surfaces. In particular, the top views (right panels in Figure 5.10) clearly show that the first hydration layer spreads uniformly on the entire available surface. Excess water molecules form a smaller droplet adsorbed on the first hydration layer (left panels in Figure 5.10). Because water molecules easily spread and form a complete first hydration layer when either 1000 or 2000 water molecules are simulated, our results suggest that both surfaces present hydrophilic properties.

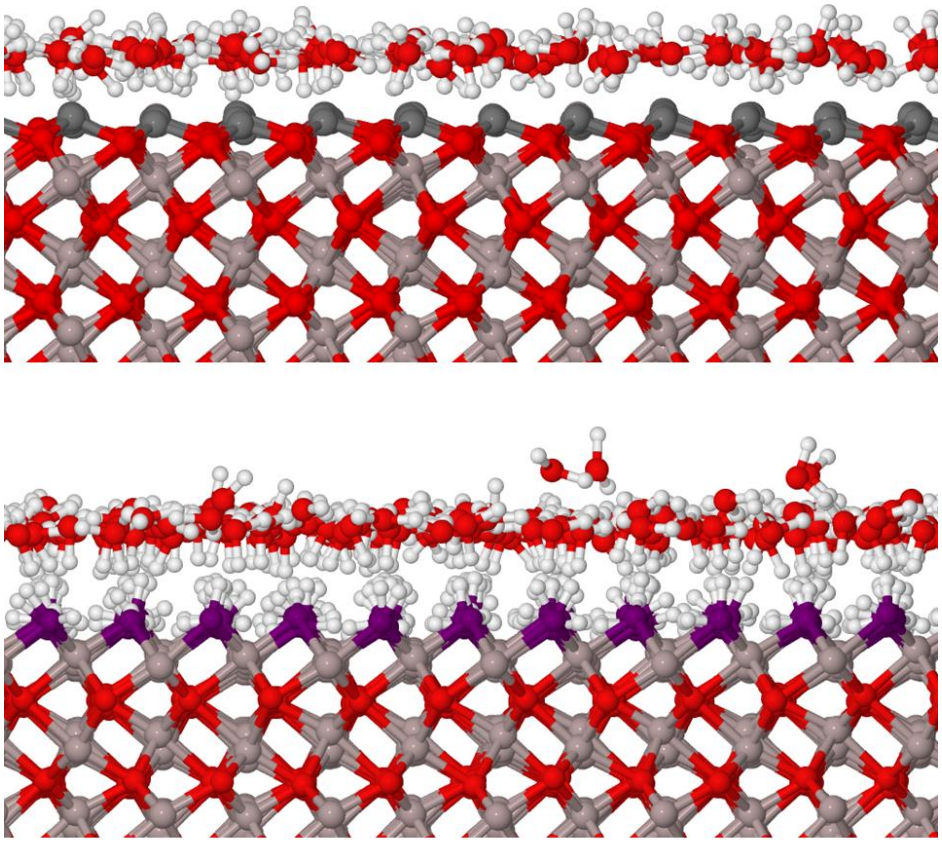

Figure 5.9: Close-up side views of the Al-terminated (top panel) and OH-terminated (bottom panel) alumina surfaces with 1000 water molecules. Red and white spheres represent oxygen and hydrogen atoms of water molecules, respectively. Color scheme for alumina substrates is the same as in Figure 5.1.

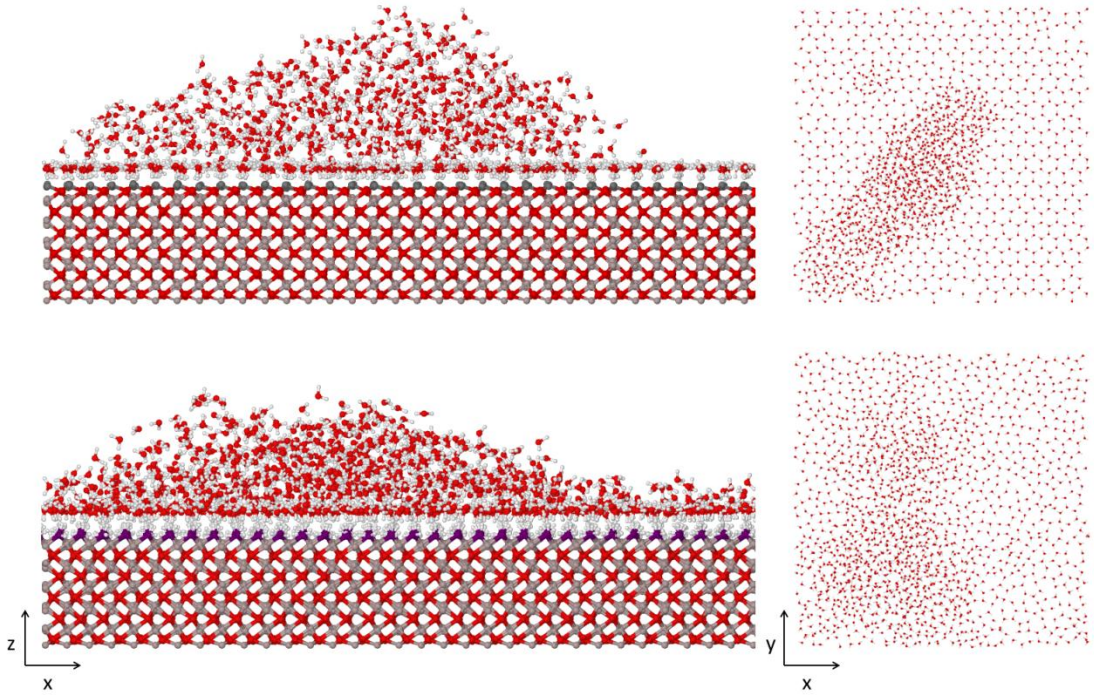


Figure 5.10: Side views of the Al-terminated (top left) and OH-terminated (bottom left) alumina surfaces with 2000 water molecules. Top views of interfacial water are shown in the right and the alumina surfaces are not shown for clarity. Color scheme for alumina substrates is the same as in Figure 5.1.

## 5.5 Conclusions

All-atom equilibrium molecular dynamics simulations were employed to study interfacial water at two alumina surfaces. To assess the effect of surface chemistry on the structural and dynamic behavior of water we used Al-terminated and OH-terminated alumina surfaces. Interfacial water was investigated by means of atomic density profiles, charge density profiles, and planar density distributions. The orientation of water in contact with alumina was evaluated by an order parameter related to the angle formed between the water dipole moment vector and the vector normal to the surface. We provide data for the water hydrogen bond network as a function of the distance from the solid substrates. The surface hydrophilicity was qualitatively assessed by analyzing how nanodroplets of 1000 water molecules spread on the two alumina surfaces. The dynamic behavior of interfacial water was quantified in terms of residence probability of water molecules within selected interfacial layers.

Atomic density profiles indicate the formation of well-defined water layers with preferential orientation at the two surfaces considered. In particular, a dense water layer with two types of preferential orientations forms in contact with the Al-terminated alumina surface. Structuring of water in the first hydration layer is observed also at the OH-terminated alumina surface. The differences between the structures observed on each substrate are discussed.

On both surfaces we find that the nature of the surface termination determines the organization of interfacial water molecules yielding well-defined patterns. The surface perturbation on the water properties diminishes at distances greater than 10 Å from both surfaces. Our data suggest the formation of distinct hydrogen-bond networks

among water molecules within the same layer together with evidence of hydrogen bonding between water molecules of adjacent interfacial layers. These findings suggest that water-water correlations play an important role in determining the length scale at which the properties of interfacial water differ compared to those characteristic of bulk water. We observe higher residence probability for water molecules at the Al-terminated surface suggesting that water molecules reside at these adsorption sites significantly longer than on the corresponding ones at the OH-terminated alumina surface.

# 6 Structure and Orientation of Interfacial Water Determine Atomic Force Microscopy Results: Insights from Molecular Dynamics Simulations

The material presented below was submitted to ACS Nano for publication.

## 6.1 Abstract

Massive all-atom molecular dynamics simulations were employed to study hydration forces near α-$Al_2O_3$ (0001) surfaces as sampled during a hypothetical AFM force spectroscopy experiment conducted using a (28, 0) single-walled carbon nanotube as tip at ambient conditions. The results provide the force acting on the carbon nanotube tip, as well as detailed properties of interfacial water, as a function of the nanotube-surface distance. As the tip approaches the solid substrate interfacial water undergoes conformational and structural changes. These changes are responsible for the features observed in the force profiles, including the range at which forces can be measured (up to two hydration shells), the intensity of the forces experienced by the AFM tip, and their oscillatory character.

Our detailed analysis shows that heterogeneous surface chemical composition results in appreciably different force profiles. This observation may explain the variability of AFM data sampling hydration forces even on atomically smooth substrates. In addition, our results suggest that sufficiently accurate AFM force spectroscopy could be used to study how hydration forces depend on surface heterogeneous properties, which could aid our understanding of interfacial phenomena and lead to significant scientific breakthroughs.

## 6.2 Introduction

Interfacial water plays a key role in a number of important phenomena observable in nature including ion adsorption/desorption processes on solid substrates and ion diffusion in biological membranes and ion channels.[52-54, 112, 146] Several molecular-level aspects of water at interfaces have been explored in numerous experimental[15, 19, 113] and theoretical[30, 98, 100, 114, 115] studies. It has been shown that solid substrates affect structural and dynamical properties of interfacial water, resulting in significantly different behavior compared to that of water in the bulk.[116, 117] Probing the properties of hydration water has been the focus of several experimental studies, conducted using a number of techniques including neutron scattering,[13] sum-frequency vibrational spectroscopy,[147] surface force apparatus (SFA),[48] and atomic force microscopy (AFM).[49-51] SFA and AFM yield force profiles between two surfaces or between one surface and the AFM tip, respectively. These force profiles typically show oscillatory behavior with fixed periodicity of roughly the diameter of a water molecule and of increasing amplitude as the separation decreases. Oscillations in the force profiles are believed to occur as water molecules are displaced from discrete interfacial layers. We demonstrate with all-atom molecular dynamics simulations that the density and orientation of interfacial water molecules may lead to force profiles with complex oscillatory character.

Several attempts have been reported using the AFM to sample the properties of interfacial water. For instance, Jarvis et al. reported hydration forces on a self-assembled monolayer by utilizing an AFM with tips made by multiwall carbon nanotubes.[49] Riedo and coworkers[50] sampled the viscosity of water confined between

the AFM tip and surfaces of various degrees of hydrophilicity. These and other[48, 148, 149] experimental reports consistently show oscillatory force profiles as the AFM tip approaches the surface, suggesting that the technique could be used to obtain details regarding the hydration layers.[51, 150] Simulation studies have been conducted to aid both planning and interpreting such AFM experiments. For example, Patrick and Lynden-Bell provide molecular insights obtained by means of molecular dynamics simulations on the solvation forces acting on an AFM tip and present force-distance curves for a number of tips configurations.[151] Smaller amplitude oscillations are observed in the force profile for sharper tips. Ho et al.[152] employed classical density functional theory to estimate the magnitude and the range of solvation forces as measured by AFM. The results suggest that solvation forces depend on the shape of the AFM tip apex, and that the solvation forces do not extend for distances larger than 2-3 molecular diameters from the substrate. Both experimental and simulation AFM simulation data reported by Riedo and coworkers[50] show oscillatory hydration forces, although with different characteristics depending on the nature of the substrates considered. However, these authors lamented the difficulty of obtaining reproducible experimental results for the force profiles.

The surface employed for the study of hydration forces in this project is alumina. The surface chemistry of crystalline and amorphous $Al_2O_3$ under various conditions has been extensively investigated both experimentally and theoretically.[119-124] It has been observed experimentally that in a dry environment the (0001) $\alpha$-$Al_2O_3$ surface can terminate with an aluminum layer.[119] In agreement, Garofalini and co-workers predicted, using theoretical arguments, that the most energetically stable

termination for aluminum oxide is the aluminum terminated.[125] In humid environments complex surface hydroxylation and dehydroxylation phenomena occur.[41-47] For instance, Eng et al. reported experimental evidence for an oxygen-terminated surface, and also for the formation of an ordered layer of contact water on the hydrated $\alpha$-$Al_2O_3$ (0001) surface.[126] An experimental investigation by Coustet et al. confirms a well-defined surface hydroxylation on $\alpha$-$Al_2O_3$ surfaces, in which the oxygen atoms are strongly coordinated with interfacial water.[127] An ab initio molecular dynamics study by Hass et al. revealed that the first atomic layer on a highly reactive Al-terminated $\alpha$-alumina (0001) surface, at high water coverage, is likely to be etched away, yielding a completely hydroxylated surface.[129] Several AFM studies have been conducted for imaging metal oxide surfaces, including $\alpha$-$Al_2O_3$. These studies provided results consistent with various surface terminations.[128, 153] For example, recent contact-mode AFM results by Gan et al. revealed atomic scale features on the (0001) $\alpha$-$Al_2O_3$ surface in water suggesting O-termination, consistent with a fully hydroxylated surface.[154]

In this study, we employed massive all-atom molecular dynamics simulations to mimic a capped carbon nanotube (CNT) tip that may be used as an AFM probe for the measurement of hydration forces at the alumina-water interface. Two alumina surfaces were considered for this work, both obtained from the (0001) crystallographic face of corundum $\alpha$-$Al_2O_3$. One surface was Al-terminated and the other fully hydroxylated. The AFM tip was simulated as a capped (28, 0) rigid single walled carbon nanotube (CNT). The simulations were conducted in the presence of explicit water at 300K.

## 6.3 Simulation Details

The (0001) crystallographic face of corundum α-$Al_2O_3$ (space group $R\bar{3}c$)[131] was used to model the alumina solid substrate according to the CLAYFF force field.[132] Two fully flexible (0001) α-$Al_2O_3$ surfaces were considered. One Al-terminated and one OH-terminated (fully hydroxylated surface with ~15 OH/nm$^2$) alumina surfaces were employed to assess water properties under different surface chemistry conditions. The $x$ and $y$ dimensions of the solid substrate were both approximately 90.5 Å in length, for a total surface area of ~82 nm$^2$. A rigid (28 0) capped single wall CNT was positioned perpendicular to the solid substrate at a fixed separation. Interactions between the CNT tip and the alumina surface were excluded during our simulations since the CNT was fixed and the changes on the alumina structure due to the CNT were out of the scope of this work. In Figure 6.1 we report a simulation snapshot for the entire simulation system.

The carbon atoms of the CNT were modeled as Lennard-Jones spheres using the parameters proposed by Cheng and Steele,[63] and kept rigid during the simulations. The SPC/E model was used to describe water. This model is known to reproduce well structure and dynamics of bulk water.[79] The bonds and angles of water molecules were kept fixed by employing the SETTLE algorithm.[81] Non-bonded interactions were modeled by means of dispersive and electrostatic forces. The electrostatic interactions were modeled by a Coulombic potential. The dispersive interactions were modeled with a 12-6 Lennard-Jones (LJ) potential. The LJ parameters for unlike interactions were determined by Lorentz-Berthelot mixing rules.[65] The cutoff distance for all interactions

was 9 Å and long range electrostatic interactions were treated using the particle mesh Ewald (PME) method.[134]

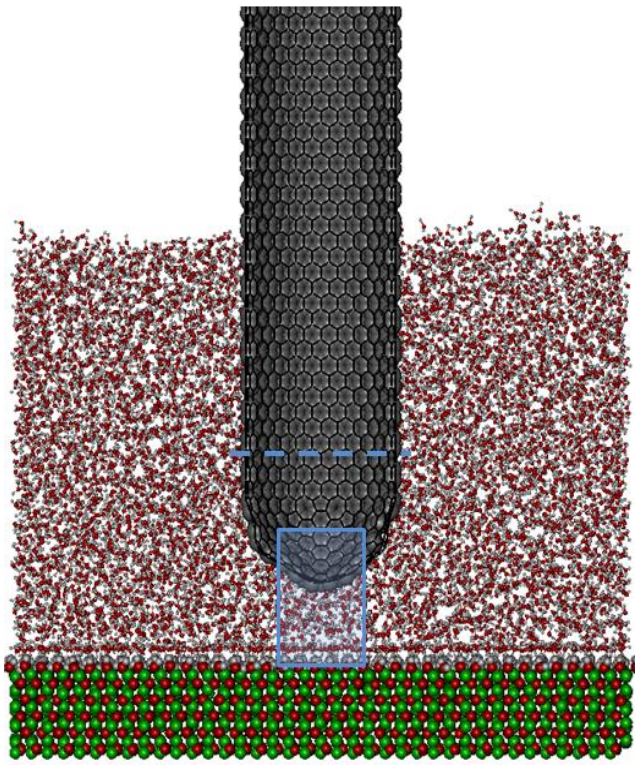

Figure 6.1: Cross-sectional view of one flat alumina substrate, the CNT, and water molecules considered in our simulations. Aluminum, oxygen, hydrogen atoms of the fully hydroxylated alumina surface are shown as green, red, and white spheres, respectively. Carbon atoms are shown in dark grey. Water molecules are represented by red (oxygen) and white (hydrogen) spheres. Carbon atoms considered for the force calculation of Figure 6.2 are those below the blue dashed line. The snapshot also provides a side view of the cylindrical volume considered for the calculation of atomic and charge densities (blue box below the CNT tip).

All simulations were performed in the canonical ensemble where the number of particles ($N$), the simulation volume ($V$), and the temperature ($T$) were kept constant. The system temperature was fixed at 300 K and controlled by a Nosé-Hoover thermostat[135, 136] with a relaxation time of 100 fs. Periodic boundary conditions were applied in the three directions.

We performed 24 independent simulations for each of the two alumina surfaces at decreasing separation, from 15 to 0.5 Å, between the CNT and the solid substrate. At furthest distance, the CNT was located 15 Å away from the substrate. The decrement in the separation distance for the first 7 simulations was 1 Å; 0.5 Å for the remaining ones. The closest tip-surface separation corresponds to contact. In all cases 15,000 water molecules were simulated to create a thin water film in contact with the solid surface. Approximately 50% of the 10 nm long CNT was immersed in water. The equations of motion were integrated with the simulation package GROMACS[83, 85] by using the leapfrog algorithm[137] and a 1.0 fs time step. The data analysis was performed for 1 ns of production phase, conducted after 3 ns of equilibration.

The actual speed at which an AFM tip approaches the solid substrate in an experimental setup cannot be reproduced in our molecular dynamics simulations and thus employed independent simulations for a range of fixes separations. The simulation time is sufficient for water equilibration at the alumina surface and the CNT and analysis can provide equilibrium properties for the calculation of solvation forces.

## 6.4 Results and Discussion

### 6.4.1 Force Profiles

To evaluate the effect of CNT on the structure of interfacial water we calculated the forces acting on the tip as a function of its distance from the alumina surface. For the calculation of the forces acting on the tip we considered the forces on the carbon atoms within the lowest 20% of the CNT length (closest to the alumina surface). In Figure 6.1 we illustrate a schematic showing the carbon atoms considered. In Figure 6.2 we reported the ensemble average sum of the *z*-component forces acting on the various

carbon atoms as a function of the CNT-surface distance. Forces due to surface atoms and water molecules are considered, while those due to the carbon atoms of CNT are not accounted for. The average of the total force obtained from 10 to 15 Å is used to offset the data along the $y$-axis. The separation is defined as distance along the $y$-axis between the terminal carbon atom of the CNT cap and the top aluminum atomic layer and the oxygen of the hydroxyl group of the Al-terminated and OH-terminated surfaces respectively. The force-distance data, which are in qualitative agreement with previous theoretical studies,[50, 151] may be directly compared to results from AFM force spectroscopy experiments. More importantly the detailed analysis of simulation data can provide molecular insights on the features that appear in experimental AFM force-distance data. Specifically, the black solid curves shown in Figure 6.2a and b represent the $z$-component of the total force acting on the CNT at the Al-terminated and OH-terminated alumina surfaces, respectively. In addition, we present the components of the total force due to the solvent (water) and the solid surface (blue dashed and red dash-dotted curves, respectively).

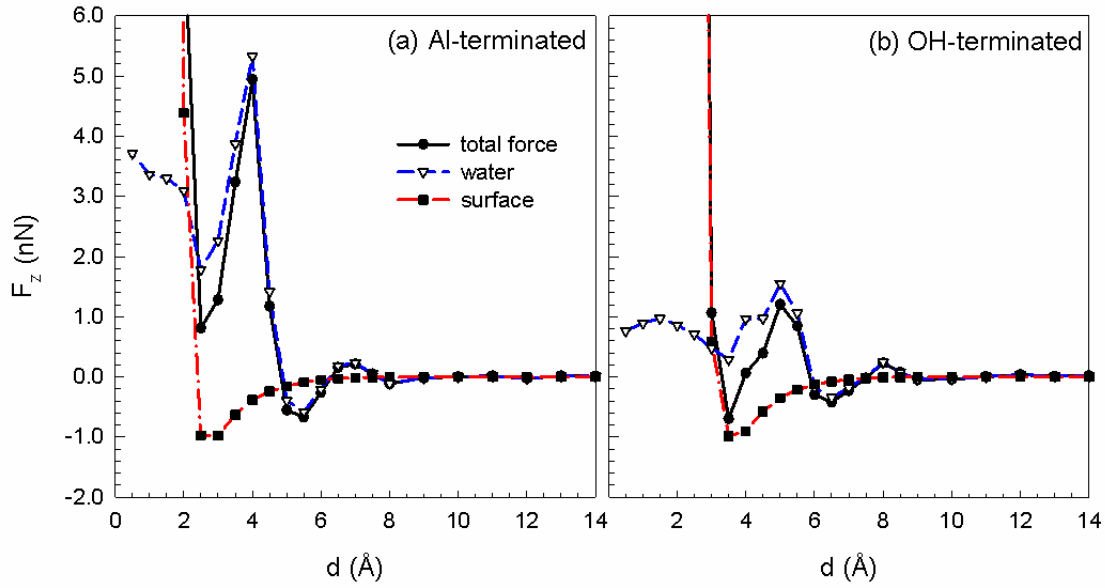


Figure 6.2: The *z*-component of the total force experienced by one (28, 0) CNT, used as AFM tip, as a function of the tip-surface distance in the presence of water is shown as black curve (filled circles). The contributions due to interfacial water molecules and to the alumina surfaces are shown as blue dashed (open triangles) and red dash-dotted (filled squares) curves, respectively.

On both surfaces we found no significant contribution to the total force due to the alumina surface at distances greater than 6.0 Å. At smaller separations we observe attractive alumina-CNT forces, followed by a strong repulsion when the tip comes in contact with the surface. The *z*-component of the force on the CNT due to water molecules (blue dashed curve) shows an oscillatory behavior for tip-sample distances smaller than ~9.0 Å. The width of the force oscillations is ~2.5 Å at the Al-terminated alumina surface and a much stronger repulsive force is observed at 4.0 Å than at 7.0 Å. The different intensity of the two repulsive forces is due primarily to the differences in density observed, which correspond to first and second interfacial layers. The total force profile data obtained on the fully hydroxylated alumina surface, given in Figure 6.2b, shows two repulsive peaks at 5.0 and 8.0 Å. The width of the first peak is ~3.0 Å. It is slightly larger than expected from the diameter of a water molecule because it includes

a shoulder at ~4.0 Å. Comparing simulated force data along the shoulder shows that hydration forces do not change significantly as the separation distance decreases from 4.5 to 4.0 Å, while the tip-surface interactions become notably more attractive. Models of solvent structure which specify a Gaussian diffusion distribution for each solvent layer and reduce the width of the distribution for layers near the surface due to confinement lead to sinusoidal force profiles.[155] Our findings suggest that non-sinusoidal oscillatory forces may appear on AFM force-distance data because of changes in location and orientation experienced by interfacial water when confined between the solid substrate and the AFM tip. This observation cannot be captured by theoretical predictions unless the detailed properties of the solid substrate and the molecular features of water are taken into account, as can be done by atomistic molecular dynamics simulations.

### 6.4.2 Density Profiles

Density changes near the tip due to the structure of the interfacial water lead to the force profiles shown in Figure 6.2. Because understanding how the local water density changes in the region between the approaching CNT and the solid substrate is critical for the characterization of hydration forces, a cylindrical volume with ~11 Å diameter to the CNT parallel and centered on the CNT axis was considered for interfacial water density and orientation calculations. A schematic showing the cylindrical volume used for density and charge density calculations is represented in Figure 6.1. The approach implemented allows us to quantify local changes of water structure around the CNT tip without obscuring results with data from the broader interfacial region. The same cylindrical volume was considered for the data presented in

Figure 6.5, Figure 6.6, and Figure 6.7. The water molecule oxygen atom density as a function of distance from the OH-terminated surface is shown for a few CNT-surface distances in Figure 6.3a. Two well-defined interfacial water layers form at OH-terminated alumina surface. One additional pronounced layer forms around the CNT. When the CNT-surface separation is larger than ~9.0 Å, the two hydration layers on the OH-terminated α-$Al_2O_3$ surface form at $z$ = 2.60 and 5.25 Å. The hydration layer on the CNT forms at approximately 3.0 Å from the carbon atoms. As the apex of the CNT tip approaches the interfacial water non-sinusoidal oscillatory forces are observed (see Figure 6.2b). The intensity and width of these oscillatory forces are directly related to the density and structural properties of the interfacial hydration layers. It is important to point out that the maxima in the force profiles are not strictly associated with the expulsion of water molecules from the region between the AFM tip and the alumina surface, but are rather due to the interactions between merging interfacial water layers from the alumina-water and CNT-water interfaces. These effects are shown explicitly in the density profiles of Figure 6.3a, obtained at four different tip-surface separation distances. Note that as the tip approaches the surface, the peak located closest to the surface shows only changes in intensity that will be discussed later in Figure 6.4. Both peak position and intensity change for the second hydration layer near the OH-terminated surface for different tip-surface separation distances. We focus here on the second layer highlighted by the two vertical black lines in Figure 6.3a. Further detailed analysis concerning interfacial water density changes on both Al-terminated and OH-terminated alumina surfaces as a function of the CNT-surface separation are discussed later in this chapter.

To further investigate the AFM effects on the second hydration layer we computed in-plane density distribution for interfacial water molecules. The results, shown in Figure 6.3b-e, are calculated within $x-y$ planes parallel to the solid substrate, of thickness $dz$ = 1 Å, and centered at 5.25 Å from the OH-terminated surface. This distance corresponds to the position of the second hydration peak on the OH-terminated surface when the AFM tip is far from the surface. The black vertical lines in Figure 6.3a delimit the region used to calculate in-plane density profiles. Data in Figure 6.3b illustrate a uniform distribution of water along the $x-y$ plane when the tip-surface distance is 12.0 Å. The water density distribution changes dramatically when the tip-surface distance is 8.5 Å (Figure 6.3c) due to a significant increase in the local water density due to merging of the second hydration layer on the OH-terminated surface and the hydration shell on the CNT tip. When the tip-surface distance decreases from 8.5 to 8.0 Å a simultaneous decrease in peak density and a displacement of the peak position towards the surface is observed. The in-plane water density distribution (Figure 6.3d) provides evidence of a ring-like structure suggesting that the CNT, external to the hydration layer, significantly perturbs the structure of interfacial water. Because at a tip-surface separation distance of 8.0 Å our force profile (Figure 6.2b) indicates a pronounced repulsive peak, comparing the results in Figure 6.2b to those in Figure 6.3d suggests that the strong repulsive force is related to the interaction between the CNT tip and the hydration layer. When the CNT tip is located at 5.5 Å from the surface, it has completely penetrated the hydration layer originally found at 5.25 Å. The correspondent in-plane density profile (Figure 6.3e) illustrates the exclusion of water

from the central region, where the CNT is, and the formation of a hydration layer around the CNT perimeter.

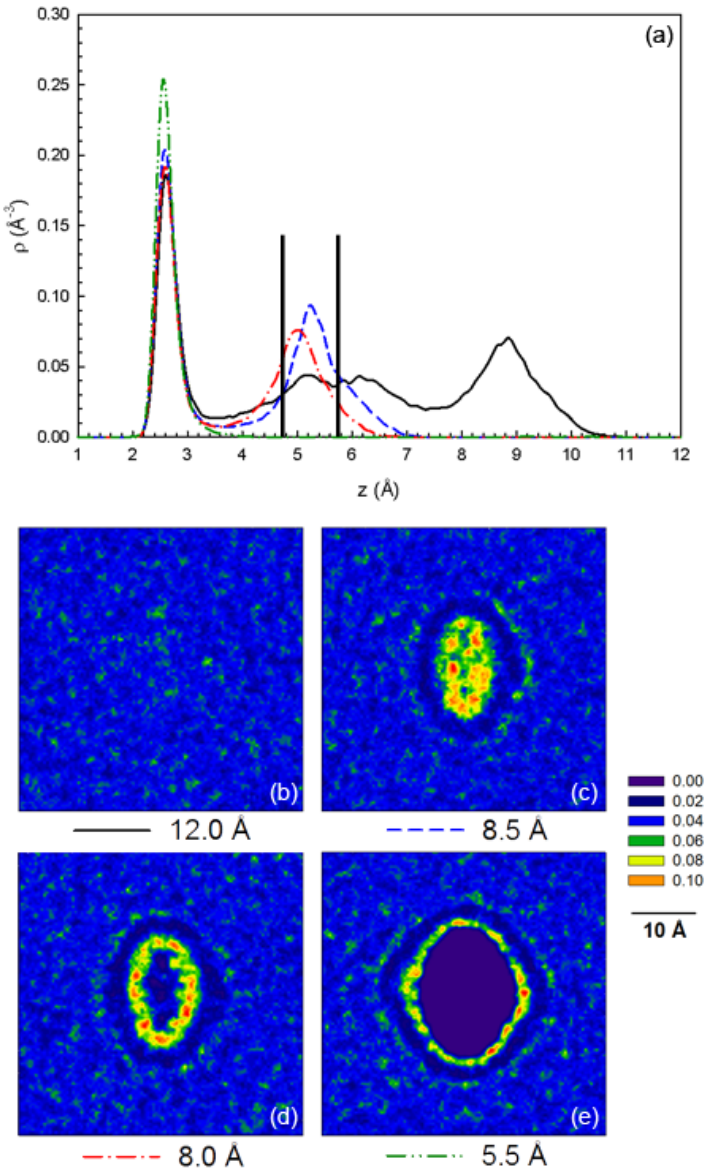


Figure 6.3: (a) Atomic density profiles of water oxygen as a function of the distance $z$ perpendicular to the OH-terminated alumina surface for tip-surface distances at 12.0, 8.5, 8.0 and 5.5 Å are shown in solid black, dashed blue, dash-dotted red, and dash-double-dotted green curves respectively. The two vertical black lines highlight the second hydration layer, whose position changes as the CNT tip approaches the surface. (b-e) The $x - y$ planar density distributions of the second interfacial water layer at 5.25 Å for the four tip-surface distances.

To highlight the effect of the CNT tip on the structural properties of water we calculated the density of two interfacial water layers near the alumina surface as a function of CNT-surface distance. At CNT-alumina separations greater than ~10 Å, we note less pronounced variations on the density of interfacial water layers, suggesting that disruption of the hydration layer structure only happens at close separation from a solid substrate, in agreement with a number of previous reports.[30, 98, 138] The first two density maxima on the Al-terminated and OH-terminated surfaces are located at 5.0 and 7.5 Å and 5.5 and 8.5 Å, respectively (see Figure 6.4). The positions of these peaks change as the CNT approaches the two surfaces, but remain within 0.5 Å of the peak positions observed in absence of the CNT.

In Figure 6.4 we report the intensity of the density peaks (first and second on both surfaces), as a function of the CNT-surface separation distance. The results, shown for the Al-terminated (Figure 6.4a) and OH-terminated surfaces (Figure 6.4b), clearly demonstrate that the local water density strongly depends on the tip position. It is important to point out that the CNT-surface separation distances at which the local density reaches maximum values do not necessarily corresponds to CNT-surface separations at which the force profiles show maxima. For example, the density of the second hydration layer on the OH-terminated surface is maximum at CNT-surface separation distance of 8.5 Å, while the local maximum in the correspondent force profile (Figure 6.2b) is observed at 8.0 Å. The changes in density at the maxima, as well as changes in their position, show that although interfacial water density is responsible for the oscillatory hydration forces shown in Figure 6.2, the details of the measured force profiles are due to merging of hydration layers, as well as to the orientation of

interfacial water (discussed later). Further, our results show that the AFM tip affects the structure of interfacial water as it approaches the surface. Thus we argue that AFM data could be used to assess the properties of hydration water only when coupled to detailed all-atom simulation studies such as those reported herein.

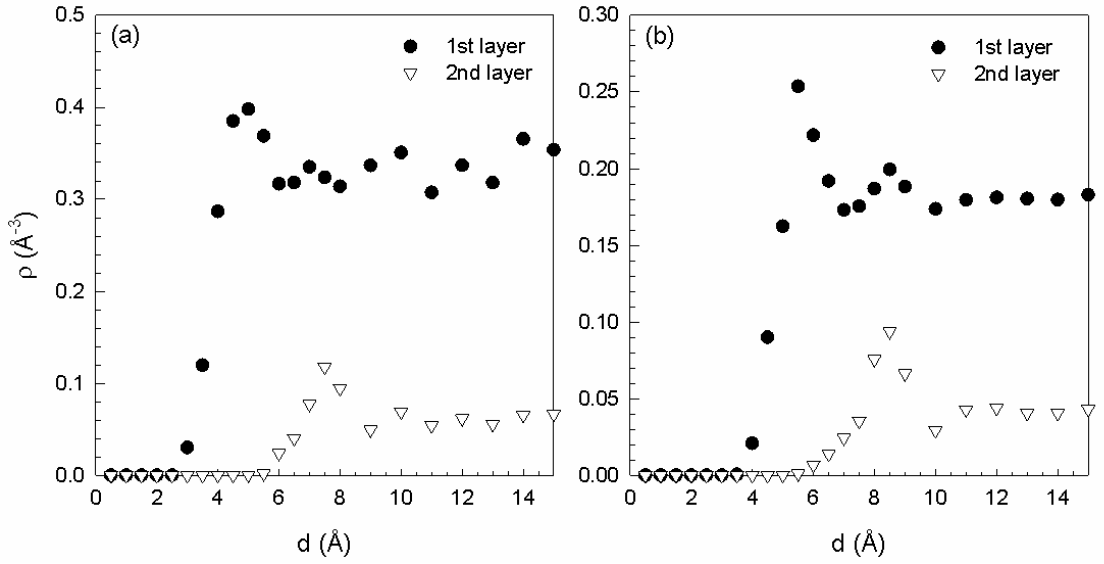


Figure 6.4: (a) Peak density of hydration layers located at 1.90 (solid circles) and 4.55 Å (empty triangles) at the Al-terminated alumina shown as a function of tip-surface distance. (b) Peak density of hydration layers at 2.60 and 5.25 Å at the OH-terminated alumina.

The structure of interfacial water as a function of the separation distance between the CNT and the alumina surface was assessed by atomic density profile calculations. In Figure 6.5 we present multiple atomic density profiles for water oxygen atoms as a function of the distance from the alumina surface. Each curve represents the density profile for a different CNT-alumina separation, varying from 15 to 0.5 Å. The atomic density data shown in Figure 6.5 and Figure 6.6 were calculated for oxygen of water at the Al-terminated and OH-terminated α-$Al_2O_3$ surfaces, respectively. Collectively, our results demonstrate that the increase/decrease in water density within

the hydration layers as the CNT approaches the substrate is responsible for the oscillatory forces shown in Figure 6.2.

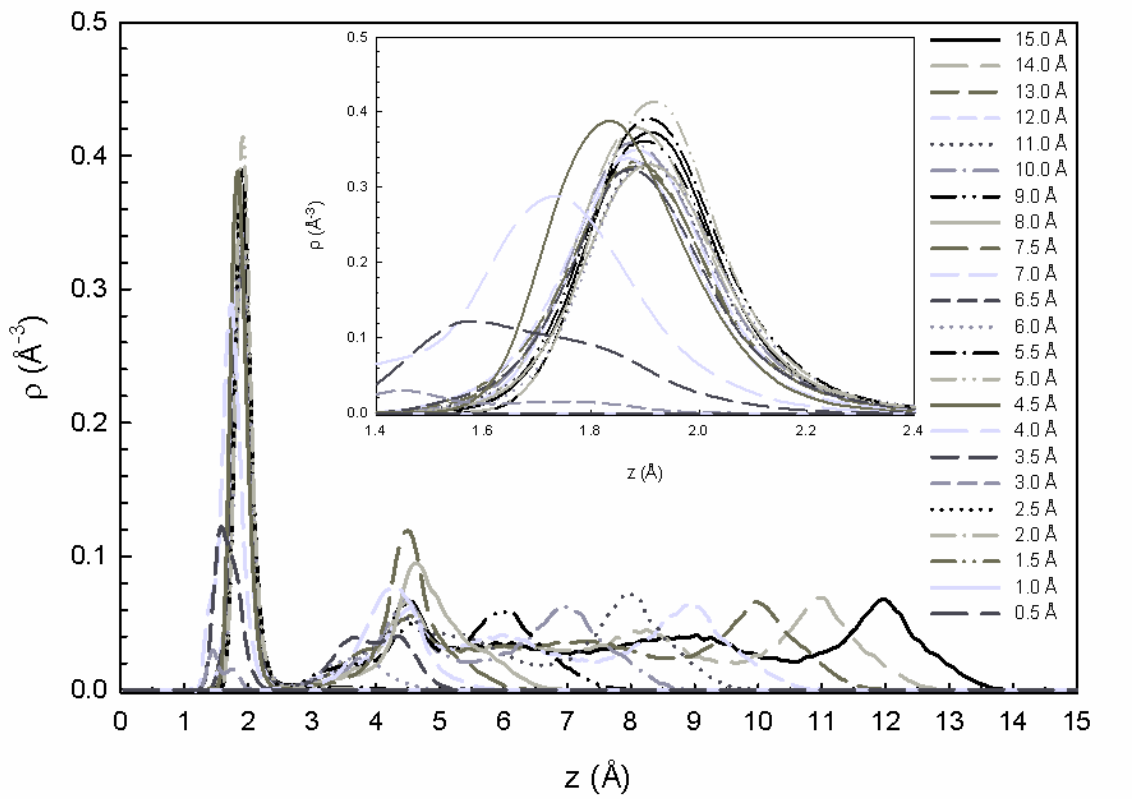


Figure 6.5: Atomic density profiles for water oxygen as a function of the distance *z* perpendicular from the Al-terminated α-$Al_2O_3$ surface. Each curve corresponds to data for a fixed tip-surface separation varying from 15 to 0.5 Å. Data in the inset show an enlargement of the first interfacial water layer. Only water molecules in a cylindrical density volume with diameter ~11 Å centered on the CNT were considered. The reference $z = 0$ is the outermost plane of aluminum atoms.

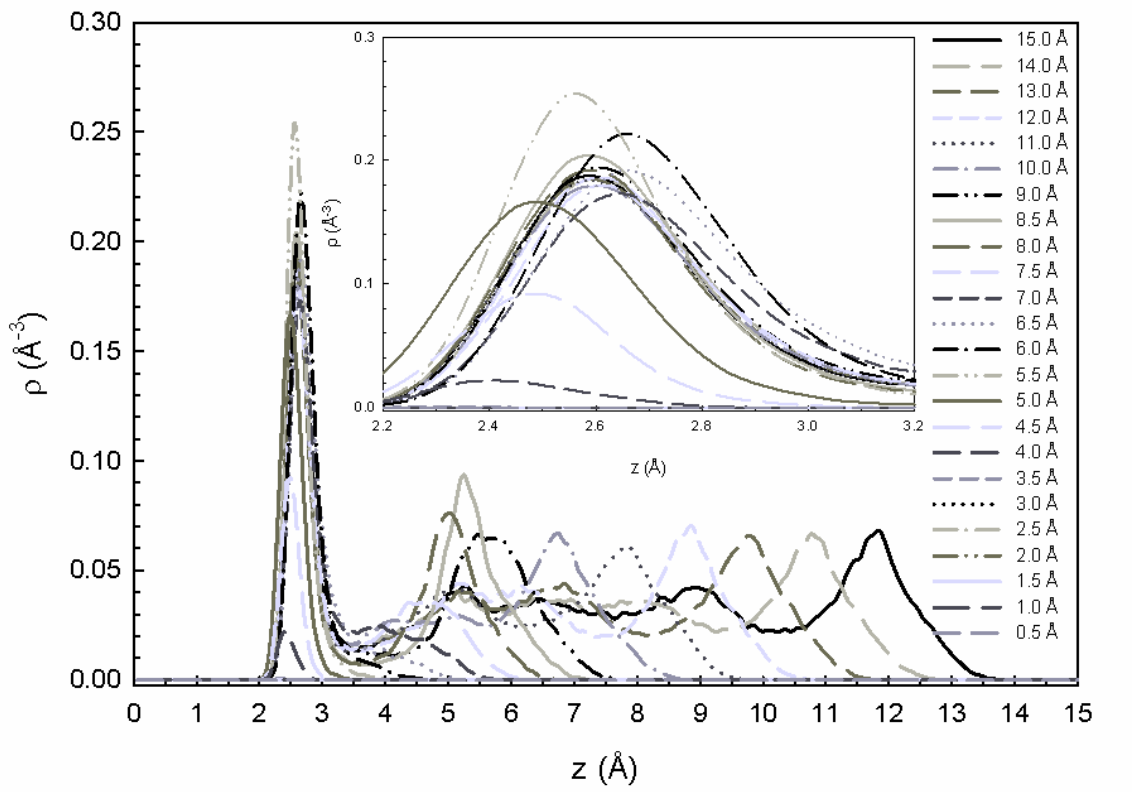


Figure 6.6: Same as Figure 6.5, but for water at the OH-terminated α-$Al_2O_3$ surface. The reference $z$ = 0 is the plane of hydroxyl group oxygen atoms.

### 6.4.3 Charge Density Profiles

As observed on silica surfaces,[98] we expect that changing the degree of hydroxylation in alumina affects not only the density distribution of interfacial water, but also its orientation. It is likely that both water local density and orientation affect CNT-surface interactions. To assess the orientation of interfacial water we calculated charge density profiles at specific CNT-alumina separations. The results are presented in Figure 6.7a and b for Al-terminated and OH-terminated alumina surface, respectively. The data give a qualitative description of the orientation of water molecules as a function of distance from the solid substrate. Positive and negative peaks are due to contributions from water hydrogen and oxygen atoms, respectively, as they

organize in layers. The data indicate a distinct preferential orientation for water molecules at the interface at the two alumina substrates. For instance, water molecules in the first layer have a hydrogen-down orientation on both surfaces. In regions where water has little or no preferential orientation the charge density values are close to zero.

When the CNT is close to the surface, the orientation of the interfacial water becomes important. The data presented in Figure 6.7a for the Al-terminated surface (5.0 Å, red dotted line) indicate that the tip approaching the surface (black line to red dotted line) causes an increase of the charge density consistent with an increasing atomic hydrogen density near 2.3 Å, which means the water molecules present in the first hydration layer at 1.9 Å have a pronounced hydrogen-up orientation. The data presented for the hydroxylated surface, in Figure 6.7b, illustrate a similar behavior for water in the first interfacial layer. For the OH-terminated surface, when the CNT is at 5.5 Å, both positive and negative peaks in the charge density increase. The different response of interfacial water on the Al-terminated and OH-terminated alumina to the approaching CNT tip suggests that force spectroscopy experiments might be very sensitive to local changes in the chemical nature of the solid substrate. The contribution of the molecular orientation, typically overlooked because of secondary importance to the effect of local water density, contributes to explain the effects of heterogeneous surface charge distributions on hydration forces.

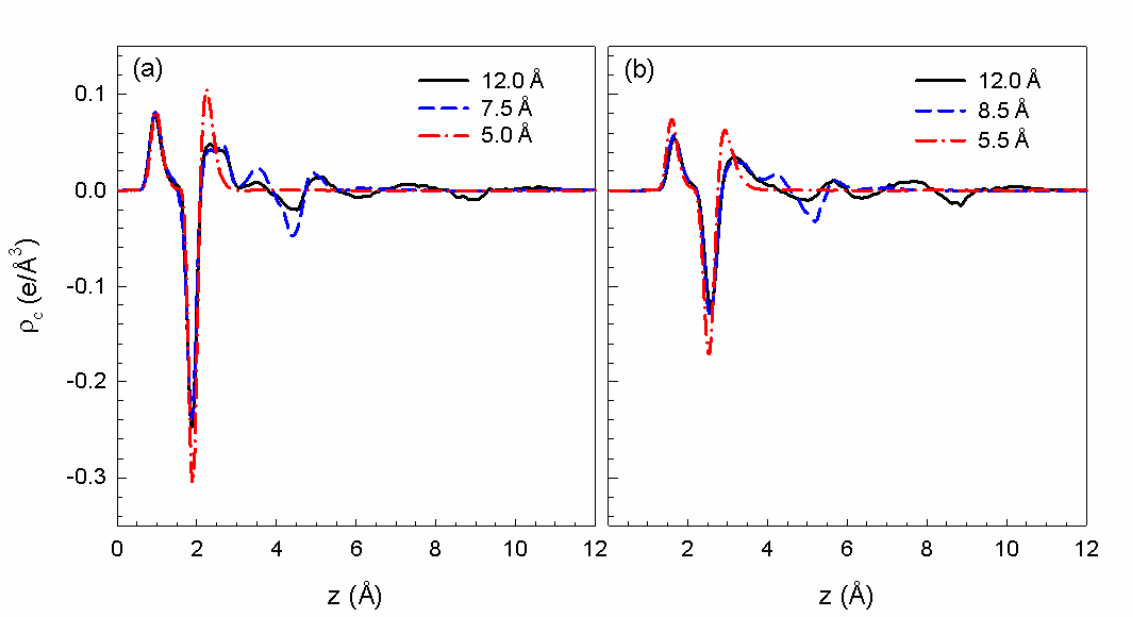


Figure 6.7: Charge density profiles of water as a function of the distance $z$ from Al-terminated (a) and OH-terminated (b) α-$Al_2O_3$ surfaces. The reference $z$ = 0 is the plane of aluminum and hydroxyl group oxygen atoms of the corresponding surface. Continuous, dotted, and dashed lines correspond to different CNT-surface separations.

### 6.4.4 Planar Density Distributions

Representative planar density distribution profiles obtained in planes parallel to the CNT axis are presented in Figure 6.8 at specific CNT-surface distances for both alumina surfaces. The data are calculated along the $x - z$ plane passing through the CNT axis. The plane has thickness $dy$ = 3 Å. A pronounced water layer forms around the CNT, consistent with the formation of dense water layers near hydrophobic solid substrates like graphite, carbon nanotubes, and fullerenes.[69, 117, 156, 157] Two water layers are present at 1.90 and 4.55 Å from the Al-terminated alumina surface (Figure 6.8a). On the OH-terminated alumina (Figure 6.8d) the two water layers form at 2.60 and 5.25 Å. Structural differences are easily noticed between the first layers on the two alumina surfaces. For example, the water molecules on the first layer in Figure 6.8a yield a

highly patterned structure whereas the density distribution data in Figure 6.8d reveal rather a continuous distribution. The second hydration layer appears less dense than the first one on both surfaces.

For large CNT-alumina separations (Figure 6.8a and d) we observe no perturbation of the interfacial water structure at the alumina surface due to the CNT. A significant change in the local water density of the second interfacial layer is observed in Figure 6.8b and e when the CNT-alumina separation is of ~8 Å. At that distance, the water layer at the lower edge of the CNT tip is merging with the second water layer on the alumina surface. This configuration results to an increased density along the $x - y$ plane within the region immediately underneath the CNT. Due to the differences in the structure of the two secondary water layers we obtain different densities at contact with the CNT. For instance, in Figure 6.8b high density areas appear near the apex of the CNT tip. These high density areas are less pronounced in Figure 6.8e. These two planar density profiles were obtained at CNT-surface separation of 7.5 and 8.5 Å for the Al-terminated and OH-terminated surfaces, respectively. They correspond to the local water density maxima shown in Figure 6.4.

In Figure 6.8c and f we present the data obtained at CNT-alumina separation 5.0 and 5.5 Å, respectively. At these separations we observe local density peaks of water in contact with surface (the density of these layers is analyzed as a function of the CNT-surface distance in Figure 6.4). In Figure 6.8c, water molecules between the edge of the CNT and the alumina surface appear to be severely restricted localized along the $x$ and $z$ directions. At smaller separations we observe the breaking of the interfacial water structure due to excluded-volume effects. Simulation snapshots of selected interfacial

water molecules around the CNT tip at the Al-terminated alumina surface are shown in Figure 6.9.

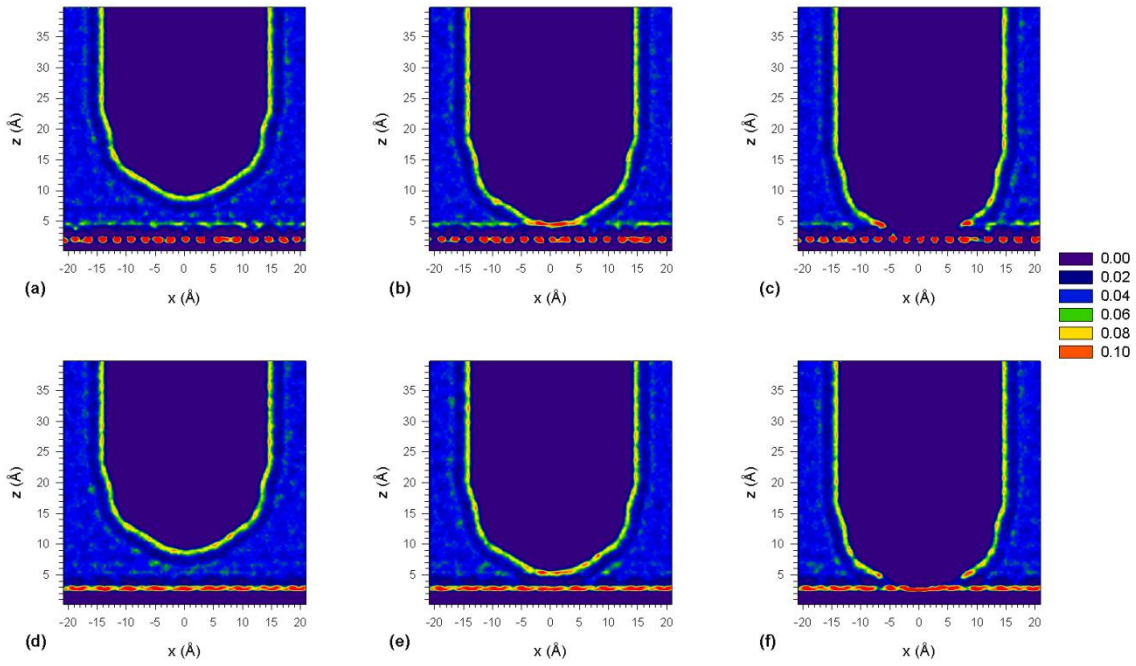


Figure 6.8: Planar density distribution of oxygen water along the $x-z$ plane (parallel to the CNT) with slab thickness $dy$ = 3 Å. The average in-plane density shown in panels (a)-(c) corresponds to tip-surface distances at 12.0, 7.5 and 5.0 at the Al-terminated alumina surface. Data in panels (d)-(e) correspond separation distances 12.0, 8.5, and 5.5Å at the OH-terminated alumina surface.

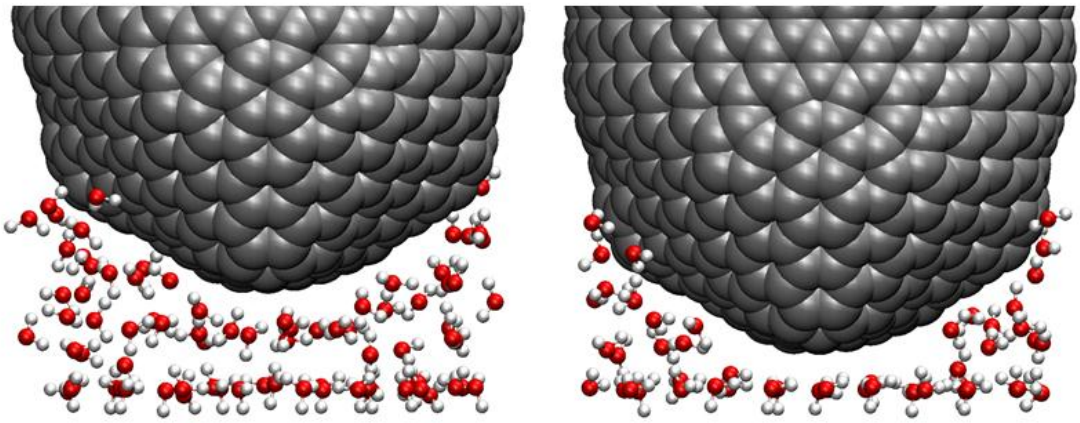

Figure 6.9: Simulation snapshots of interfacial water at the Al-terminated alumina surface. In these simulation snapshots the CNT is located at 7.5 Å (left panel) and 5.5 Å (right panel) from the surface. The alumina surface is not shown for clarity.

## 6.5 Conclusions

In summary, we conducted massive all-atom molecular dynamics simulations to interpret hypothetical experimental data that could be obtained when an AFM with a carbon nanotube tip (CNT) is used to sample the structure of interfacial water on an atomically smooth $\alpha$-$Al_2O_3$ surface. Aluminum and hydroxyl terminations of the alumina surfaces were considered to assess the effect of the surface chemistry on the forces acting on the AFM tip. A capped (28, 0) single walled CNT was considered as the AFM tip. A number of independent simulations were conducted at ambient conditions for various tip-surface separations to reconstruct the force profile. The results suggest that oscillatory forces act on the CNT at small separations (less than 10 Å). Both intensity and width (~2.5-3.0 Å) of the oscillations are primarily due to significant changes on local water density and molecular orientation at the alumina interface due to the CNT. Local density increases yield pronounced repulsive forces, while local density depletions yield less repulsive forces, which in some circumstance may become

attractive, depending on the system considered. However, the maxima and minima in the force profiles do not necessarily correspond to the position of the hydration layers. The orientation of interfacial water, which affects the hydrogen-bonding network between interfacial water molecules, modulates the hydration forces, although to a smaller extent compared to local water density.

Because the features of the force profiles are always related to the behavior of the water molecules confined between the CNT tip and the alumina surface, changes in the surface termination, which affect both structure and orientation of interfacial water, most likely lead to markedly different force profiles in terms of both intensity of repulsive force and periodicity of oscillatory forces. Based on our results, experimental force spectroscopy analysis should be able to sample and differentiate between hydration forces observed on materials characterized by heterogeneous properties. By coupling experimental AFM studies to detailed theoretical insights such as those provided by all-atom simulations, it will be possible to correctly interpret the structure and properties of hydration water, offering the possibility of leaps forward in a number of nanotechnological applications, such as the design of nanofluidic devices.

# 7 Ion-Specific Effects under Confinement: The Role of Interfacial Water

The material presented below was published in 2010 in volume 4, issue 4 of ACS Nano.

## 7.1 Abstract

All-atom molecular dynamics simulations were employed for the study of the structure and dynamics of aqueous electrolyte solutions within slit-shaped silica nanopores of width 10.67 Å at ambient temperature. All simulations were conducted for 250 ns to capture the dynamics of ion adsorption and to obtain the equilibrium distribution of multiple ionic species ($Na^+$, $Cs^+$, and $Cl^-$) within the pores. The results clearly support the existence of ion-specific effects under confinement, which can be explained by the properties of interfacial water. $Cl^-$ strongly adsorbs onto the silica surface. Although neither $Na^+$ nor $Cs^+$ are in contact with the solid surface, they show ion-specific behavior. The differences between the density distributions of cations within the pore are primarily due to size effects through their interaction with confined water molecules. The majority of $Na^+$ ions appear within one water layer in close proximity to the silica surface, whereas $Cs^+$ is excluded from well-defined water layers. As a consequence of this preferential distribution we observe enhanced in-plane mobility for those $Cs^+$ ions found near the center of the pore compared to that for those $Na^+$ ions closer to the solid substrate. These observations illustrate the key role of interfacial water in determining ion-specific effects under confinement and have practical importance in several fields, from geology to biology.

## 7.2 Introduction

The understanding of aqueous electrolyte solutions near charged surfaces continues to attract great attention due to recent advances in nanofabrication[158-160] and a wide range of applications including nanofluidics and "lab-on-chip" processes,[161-164] manipulation of biological membranes and ion-channels,[52, 53] design of ion-exclusion processes and desalination membranes.[54-56] The development of nanoporous materials for any of these applications requires a detailed molecular-level understanding of solvent-electrolyte behavior at interfaces and under confinement. Additionally, a predictive understanding of fluid-matrix interactions in subsurface systems also requires insights into phenomena operating at the atomistic and molecular scales.[165]

Computer simulation studies have been used extensively to describe the structural properties of water near solid surfaces at various temperature and pressure conditions.[25, 31, 69, 114, 139, 166-169] The dynamic behavior of interfacial water has also been investigated for a number of systems.[28, 30, 35, 116] The results of these investigations support the conclusion that interfacial water properties differ significantly from those observed in the bulk. A number of experimental studies confirmed the predicted behavior. Such studies include backscattering spectroscopy,[15] quasi-elastic neutron scattering,[16] attenuated total reflectance infrared spectroscopy,[17] X-ray reflectivity measurements,[18] and ultrafast infrared spectroscopy.[19]

For most of the applications mentioned above the fluid systems contains water with electrolytes. We demonstrate herein that understanding the properties of pure interfacial water is essential for accurately describing ion distributions under confinement.

Our current theoretical understanding of aqueous electrolyte solutions at interfaces is not well developed. The classical Poisson-Boltzmann (PB) approach is hampered by the mean-field approximation and the infinitesimal description of ions it implements, which could lead to an unsatisfactory description of the electric double layer. At short distances from a charged surface the PB prediction for ion distributions cannot be accurate due to the finite size ion effects[170] and also because of the molecular nature of water,[171] as shown by the Monte Carlo simulation results reported by Yang et al.[172] The assumption of uniform surface charge density may also lead to unrealistic predictions of the distributions of ions at interfaces. A promising approach to describe ion distribution at interfaces has recently been used by Lima et al.[91] This mean-field approach requires knowledge of the local value for the dielectric constant, generally not available.

Unlike the theoretical approaches just summarized, molecular simulations can explicitly account for the molecular nature of both ions and water, and they can also treat surfaces with atomically detailed precision, thus yielding heterogeneous distributions of surface charges where appropriate. Although long simulations times are required to achieve properly equilibrated states, the growing interest in ion-exclusion processes, ion selectivity, and ion transport through pores and membranes justifies attempting atomistic simulations for realistic systems.[55, 173-176] Shirono et al.[177] employed Monte Carlo and molecular dynamics simulations to study KCl distribution and transport in silica nanopores that contain both hydrophobic and hydrophilic surface patches. Their results suggest adsorption of $Cl^-$ at the silica walls and diffusion of $K^+$ through the center of the hydrophilic pore region. Similar computational studies

conducted for various electrolyte solutions on a goethite (α-FeOOH) surface have shown the importance of the molecular structure of interfacial water in determining the distribution of ions near the solid substrate.[178] Marry et al.[143] showed that the nature of counterions does not significantly alter the structure and dynamics of water near a clay surface.

A large body of literature exists describing the properties of bulk electrolytes solutions that provide the foundation for comparisons with behavior of confined fluids. For example, Lee et al.[179] used molecular dynamics simulations to study the mobility and hydration numbers of alkali metal ions and halides at ambient temperature. Diffusion coefficients[180] for $Na^+$ and $Cl^-$ and the solubility of NaCl and KF in water have been reported at different temperatures by Sanz and Vega.[181] The effect of salt concentration on ionic structural and transport properties of aqueous CsCl solutions have been described by Du et al.[182]

In this study we report structural and dynamic behavior of aqueous electrolyte solutions under nanoscale confinement. We employed equilibrium all-atom molecular dynamics simulations to study aqueous systems confined within a positively charged silica nanopore of width 10.67 Å. Because simulations conducted on thin water films show that the water-structure perturbation at the interface persists for about 10 Å from the substrate, the pore width considered here ensures that the structure of the confined solution is perturbed simultaneously by both surfaces. After allowing for extensive equilibration times, we calculated density profiles and mobilities for the confined ions. The results clearly demonstrate the existence of ion-specific effects under confinement. More importantly however, we found that by describing the structure and dynamics of

water we could adequately explain all our results, suggesting that water-ion correlations cannot be overlooked when a detailed prediction of ionic behavior is required, especially under nanoscale confinement.

## 7.3 Simulation Details

Slit-shaped nanopore configurations were used in our simulations. Two silica substrates with identical surfaces were placed at a distance of 10.67 Å along the $z$-axis. The (111) crystallographic face of β-cristobalite[61] was used to model the solid substrate. The surface area of each periodic system is 104.8×100.8 Å$^2$ ($x-y$ plane) with plate thickness 10.3 Å; details on the surface preparation can be found elsewhere.[20] To obtain a chemically realistic surface all the non-bridging oxygen atoms are hydroxylated. The resulting surface hydroxyl group density is ~4.5 OH/nm$^2$, which corresponds to experimental densities observed in silica surfaces.[183] The surface charge density of the simulated surface is 0.31 C/m$^2$. The CLAYFF force field[132] was implemented to model the silica surface. The silicon and oxygen atoms were held at fixed positions while the surface hydrogen atoms were allowed to vibrate and thus account for momentum exchange between aqueous solution and surface. We did not account for surface reconstruction or silanol deprotonation. The rigid SPC/E water model was used to describe water. This model is known to adequately reproduce experimentally observed structural and dynamic properties, such as pair correlations and diffusion coefficients at ambient conditions.[79] Bond lengths and angles for water molecules were kept fixed using the SETTLE algorithm.[81] Non-bonded interactions were modeled by means of dispersive and electrostatic forces. Van der Waals interactions were treated according to the 12-6 Lennard-Jones (LJ) potential. The LJ parameters for unlike interactions were

obtained using the Lorentz-Berthelot mixing rules from pure component ones.[65] The electrostatic forces were described by a Coulombic potential with a cutoff set to 9 Å. Long range interactions were calculated by the particle mesh Ewald (PME) method.[134] All simulations were performed in the NVT ensemble.[65]

Three different electrolyte solutions, each including 3,570 water molecules, were confined between the two identical silica substrates. The three electrolyte mixtures consisted of 64 pairs of either NaCl or CsCl, and 32 pairs of both NaCl and CsCl, respectively. The ionic strength in all systems was 1 M. The potential parameters for sodium ($Na^+$), cesium ($Cs^+$), and chloride ($Cl^-$) ions were fitted for the SPC/E water model by Dang and collaborators to reproduce accurately the bulk properties.[184, 185] The parameters have been used previously to study ion mobility in water[179] and ion adsorption at solid-liquid interfaces.[186] The system temperature was maintained at 300 K by using the Nosé-Hoover thermostat[135, 136] with a relaxation time of 100 fs. Periodic boundary conditions were applied in the three directions. The equations of motion were solved using the molecular dynamics package GROMACS,[82, 83, 85] by implementing the leap-frog algorithm[137] with a time step of 1.0 fs. The total simulation time for all cases was 250 ns ($250 \cdot 10^6$ time steps). Only the last 40 ns were used to calculate the properties of interest. We found that long simulations are necessary to obtain reliable results.

## 7.4 Results and Discussion

### 7.4.1 Cation-Anion Distributions

A side view of the slit-shaped silica pore with the 64 pairs of NaCl ions is shown in Figure 7.1a. The pore width of 10.67 Å, is defined by the distance between the two planes of non-bridging oxygen atoms facing across the pore volume. This simulation snapshot is taken after 250 ns of simulation time. Sodium and chloride ions are presented as purple and green spheres, respectively; water molecules are not shown for clarity. In this figure we observe the adsorption of $Cl^-$ on the positively charged silica surface and the distribution of $Na^+$ throughout the pore width. Similar qualitative observations are valid for the CsCl solution. Further, we observe a noticeable reorientation of the surface hydroxyl groups associated with $Cl^-$ ion adsorption, as shown in Figure 7.1b. This reorientation demonstrates that accounting for the heterogeneous distribution of surface charged sites is crucial for obtaining a realistic description of the ionic distribution accurate at the atomic level.

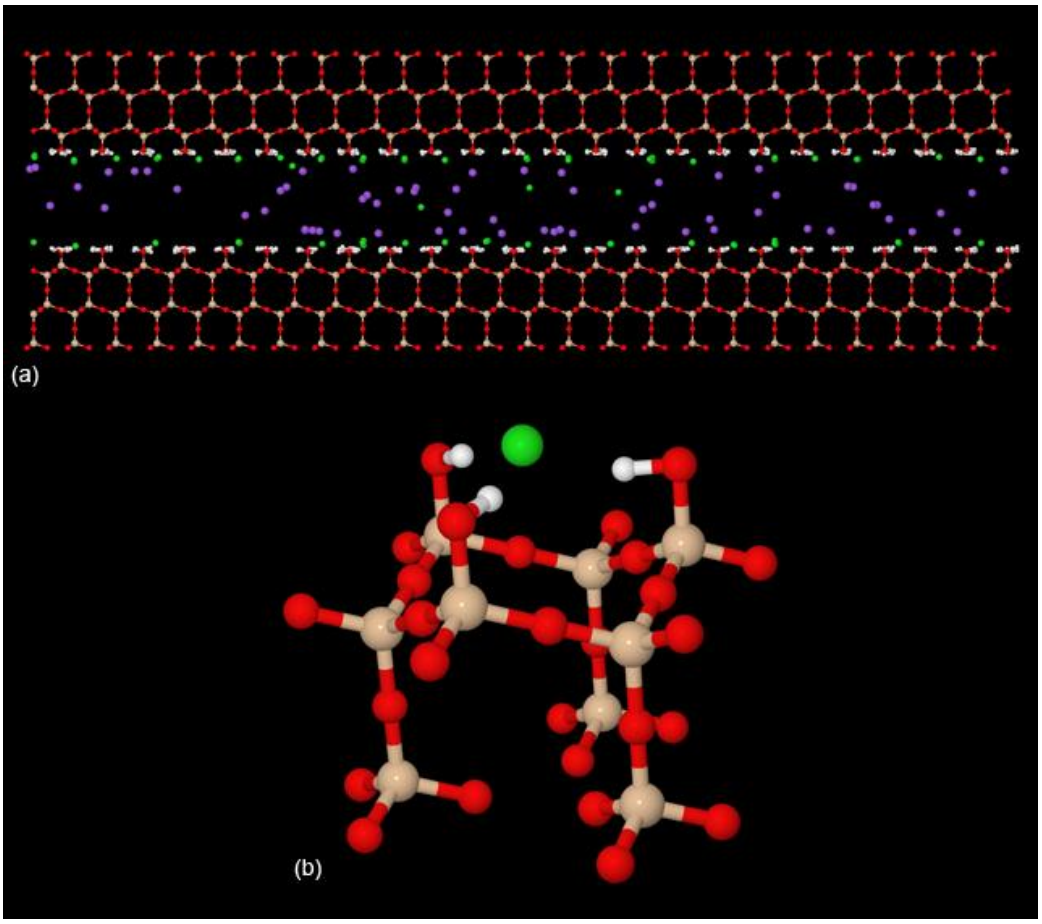


Figure 7.1: (a) Side view of the silica pore of width 10.67 Å. $Na^+$ (purple spheres) and $Cl^-$ (green spheres) ions in the silica pore are shown after 250 ns of simulation at 300 K. White, red, and brown spheres represent hydrogen, oxygen, and silicon atoms of the solid substrate, respectively. Water molecules are not shown for clarity. (b) Enlarged detail of one simulation snapshot illustrating one $Cl^-$ ion in contact with the silica surface. Only selected atoms from the solid substrate are shown to illustrate the reorientation of the surface hydroxyl groups near the $Cl^-$ ion.

The ion density profiles for NaCl and CsCl solutions are presented in Figure 7.2a and in Figure 7.2b, respectively. The reference plane ($z$ = 0) for all calculations is the lower innermost plane of silicon atoms (brown spheres in Figure 7.1a). The results indicate the formation of two chloride layers in contact with the pore surfaces (peaks at 2.45 and 11.30 Å) for both systems considered. As expected, these results confirm that the positively charged surfaces attract the counter ions ($Cl^-$). We point out that the $Cl^-$ layers formed in contact with the $SiO_2$ surface are rather sparse due to the relatively low

$Cl^-$ concentration. No significant changes in the density profiles were observed within the last 40 ns of our simulations, but it should be pointed out that adsorbed $Cl^-$ ions very rarely desorb from the solid substrate.

The difference in the intensity of the $Cl^-$ density peaks near the two solid surfaces exhibited in Figure 7.2a is due to a slightly higher number of chloride ions adsorbed on the upper pore surface. Note that all ions were initially randomly placed near the pore center. Because the asymmetry observed in Figure 7.2a is primarily due to the slow adsorption-desorption process with respect to the length of our simulation, simulations far longer than those conducted here are necessary to obtain symmetric distributions for the $Cl^-$ ions across the pore. In contrast, the results presented in Figure 7.2b for the CsCl solution present two equally dense chloride layers near the solid surfaces. To better understand the kinetic effect responsible for the asymmetric density distribution observed in some cases for $Cl^-$ ions, different simulation time segments are shown in Figure 7.3 demonstrating how the $Cl^-$ density profiles change as the simulation progresses. These results clearly highlight that long simulations are required to obtain reliable data. Although no significant change in the $Cl^-$ density profiles is observed from 100 to 140 ns of simulation (solid black line in Figure 7.3), we continued our simulation for 250 ns, and only $Cl^-$ density data obtained from 210 to 250 ns were used to draw our conclusions. We note that $Na^+$ and $Cs^+$ ions in all cases reached the equilibrium density profile within the first 20 ns and no changes were observed in their density distributions from that point forward. The data in Figure 7.2 also suggest that a limited number of $Cl^-$ ions remain in the center of the pore at specific distances from the two surfaces (~5 Å).

More important for our discussion are the density distributions of cations, for which we report ion-specific behavior. The density data for $Na^+$ in Figure 7.2a suggest the formation of two peaks near each of the pore surfaces. The first pronounced peaks appears at 3.75 Å from the surface whereas the broader second peaks form at 5.90 Å from each surface. Our results suggest that 76% of $Na^+$ ions accumulate at 3.75 Å from the surface and the rest within the central region of the pore. In contrast, the data for $Cs^+$ in Figure 7.2b do not show well defined density peaks, and thus provide no evidence supporting the formation of local structures. We observe only a minimal accumulation occurring at ~4.60 Å, which is in contact with interfacial water layers.

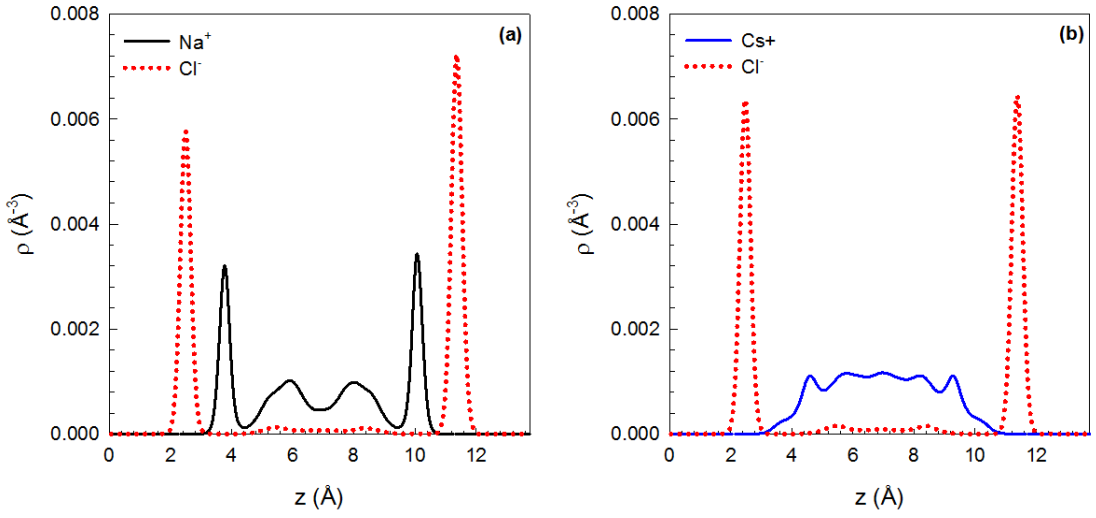


Figure 7.2: Atomic density profiles for $Na^+$, $Cs^+$, and $Cl^-$ ions as a function of the distance $z$ from the fully hydroxylated silica surfaces. Panels a and b show data for NaCl and CsCl aqueous solutions, respectively. The reference ($z$ = 0) for these calculations is the first innermost plane of silicon atoms. All simulations are conducted at $T$ = 300 K, results are obtained as average during the last 40 ns of the 250 ns simulations.

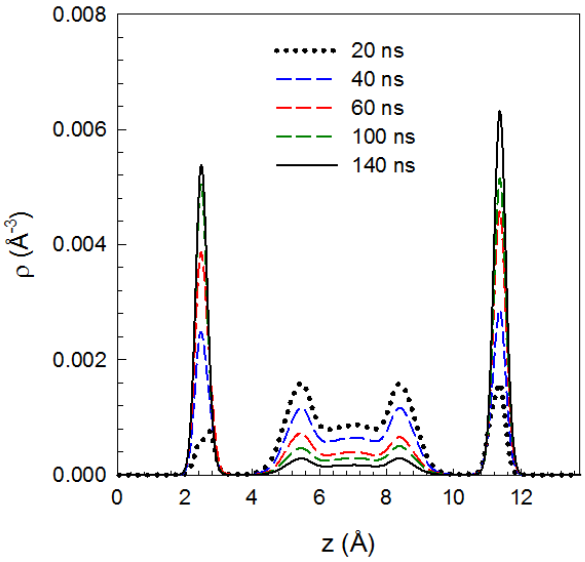


Figure 7.3: Atomic density profiles for $Cl^-$ ions as a function of the distance *z* obtained at different simulation time segments. The data shown are for the system with 64 pairs of NaCl ions. Dotted black, dashes blue, red, and green, and solid black correspond to density profiles at 20 ns, 40 ns, 60 ns, 100 ns and 140 ns, respectively. Each curve is obtained as average of simulations results observed during 40ns of simulation (eg., data obtained from 60 to 100 ns are shown as the green dashed line labeled "100 ns"). The reference ($z$ = 0) for this calculation is the first innermost plane of silicon atoms.

### 7.4.2 Relation between Water Structure and Ion Distributions

The different density distributions of $Na^+$ and $Cs^+$ ions within the pores are related to size effects (the diameters of $Na^+$ and $Cs^+$ are 2.58 Å and 3.88 Å, respectively, while all other parameters used for these ions remain the same for both simulations), but also to the structure of interfacial water. Numerous simulation studies have reported on the structural and dynamic behavior of interfacial water on silica.[25, 98, 99, 168] In general, highly structured water is observed for up to 10 Å from the solid substrate, and slower dynamics is observed in this interfacial region compared to bulk water. The specific details of this behavior, however, depend on the features of the solid substrate. The water density profiles within the fully hydrated silica nanopores considered in this study are given in Figure 7.4. The atomic density profile for oxygen shows the formation of

two hydration layers near each surface, with peaks appearing at 2.35 and 3.90 Å, respectively. Correspondingly, the data for water hydrogen density distribution show the formation of two atomic layers located at 3.05 and 4.65 Å from each surface. The hydrogen density distribution also shows a small shoulder at 2.20 Å, suggesting localized water structuring at the contact with the silica surfaces. Although local perturbations in the water structure near each ion are likely because of ion-hydration phenomena, we note that the differences observed in the averaged water density profiles are negligible when either NaCl or CsCl are in solution and that the density profiles for water are similar to those obtained for pure water as shown in Figure 7.4. This suggests that the ions considered in this study, at 1 M concentration, do not alter the interfacial water structure significantly. Similar results were reported by Marry et al.[143] for aqueous solutions of NaCl and CsCl confined within clay pores. The positions of all atomic layers are reported in Table 7.1. The Lennard-Jones size parameters for $Na^+$, $Cs^+$, and water are 2.58, 3.88 and 3.17 Å, respectively. A comparison of these results suggests that the dense interfacial water layer at 3.90 Å plays a significant role in determining the ionic distribution. This water layer appears permeable to $Na^+$ ions, allowing them to being incorporated within its structure (the first $Na^+$ density peak also appears at 3.90 Å). In contrast, $Cs^+$, due to volume-exclusion effects, cannot fit within the well-defined water layer located at 3.90 Å.

Table 7.1: Positions of the first two atomic layers for the cations, anions and water considered in this study.[a] The data reported is for the mixture with 32 pairs of NaCl and CsCl. The same layer positions are observed for the simulated systems with 64 pairs of NaCl or CsCl.

| Aqueous Electrolyte Mixture | Atomic species | Position of layers (Å) |
|---|---|---|
| NaCl – CsCl | $Na^+$ | 3.75 / 5.90 |
| | $Cs^+$ | 4.60 / 5.75 |
| | $Cl^-$ | 2.45 / ~5.45[b] |
| Water | $O^-$ | 2.35 / 3.90 |
| | $H^+$ | 2.20[c] / 3.05 / 4.65 |

[a] The distances given for the atomic layer positions are the same for both surfaces of the nanopores. All distances are given with respect to the innermost plane of the silicon atoms in the nanopore along the *z*-axis.
[b] This distance from the surface corresponds to denounced layer of $Cl^-$ in which the anions preferentially accumulate when are present in the center of the nanopore.
[c] This feature on the density profiles corresponds to a shoulder.

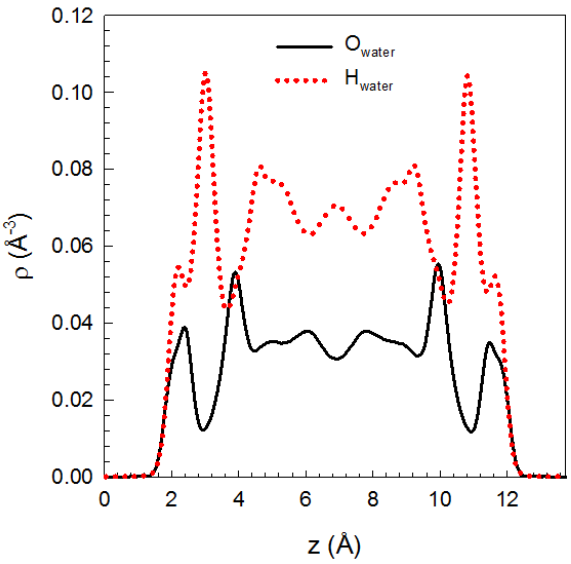


Figure 7.4: Atomic density profiles for water oxygen and hydrogen atoms as a function of the position *z* across the silica pore. The reference ($z$ = 0) is the first innermost plane of silicon atoms. Results are identical in all system considered in this study.

### 7.4.3 Mixed Solute Behavior

In order to evaluate the importance of ion-ion correlations, and the possible competition between $Na^+$ and $Cs^+$ for adsorption sites within the nanopore, a multi-ion mixture was studied by introducing 32 pairs of NaCl and CsCl while keeping the ionic strength at 1 M. Density profiles for solvent-anions and solvent-cations pairs are presented in Figure 7.5a and b, respectively. We note that the formation of $Na^+$ and $Cs^+$ layers (as shown in Figure 7.5a) occurs at the same positions as those given in Figure 7.2a and Figure 7.2b for NaCl and CsCl solutions, respectively. The difference in the peak intensities is due to the reduced number of each cation type used for the simulations of mixtures, compared to those used for the results in Figure 7.2. The incorporation of $Na^+$ and exclusion of $Cs^+$ within the interfacial water layer observed at 3.90 Å becomes more evident in Figure 7.5a. In Figure 7.5b the $Cl^-$ density data are plotted together with those for water oxygen atoms. The formation of one $Cl^-$ layer in contact with the surface is clearly observed, and is analogous with the results displayed in Figure 7.2. At the distance of 2.35 Å we notice evidence of water structuring. These findings suggest a strong $Cl^-$ surface attraction that is not affected by the repulsive forces that might arise because of the negatively-charged water oxygen atomic layer that also forms in contact with the substrate. This is possible because $Cl^-$ ions strongly correlate with the surface hydroxyl groups, as shown in Figure 7.1b. In contrast, evidence for a strong repulsion of $Cl^-$ due to a pronounced water oxygen layer is observed at 3.90 Å, where the $Cl^-$ density is effectively zero. The interfacial water layer acts as a kinetic barrier to $Cl^-$ adsorption. The slow transport of $Cl^-$ from the center of the pore to the solid-liquid interface (documented in Figure 7.3) is related to the slow *z*-directional mobility of that ion, presumably due to the dense, negatively-charged

oxygen water layer formed at 3.90 Å from the surface. The slow mobility of $Cl^-$ ions perpendicular to the interface is coupled with slow mobility in the direction parallel to the interface, as described below. Selected snapshots of $Na^+$ and $Cl^-$ are shown in Figure 7.6, along with the layer of interfacial water formed at 3.90 Å, to schematically illustrate the role of water on the ion distribution at the interface. $Na^+$ ions are easily incorporated within the water layer, and the exchange identified in Figure 7.6a is consequently fast. On the other hand, $Cl^-$ ions are repelled by the dense negatively-charged interfacial water layer. Consequently, the transport event shown in Figure 7.6b is kinetically slow.

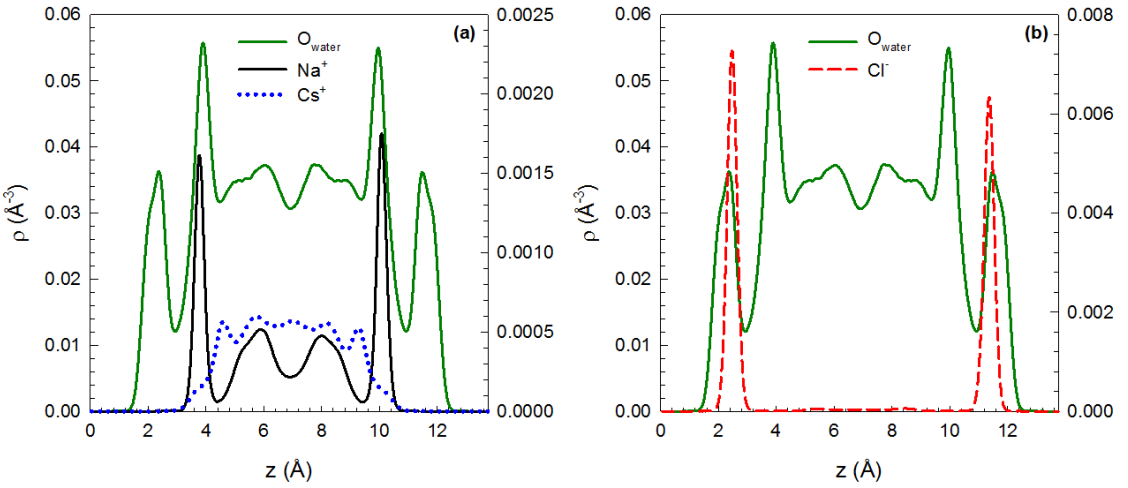


Figure 7.5: (a) Atomic density profiles of oxygen water with cations ($Na^+$, $Cs^+$) and oxygen water with anions ($Cl^-$) as a function of distance $z$ from the solid surface. The data are shown for the aqueous solution containing both NaCl and CsCl. The reference ($z$ = 0) for this calculation is the first innermost plane of silicon atoms.

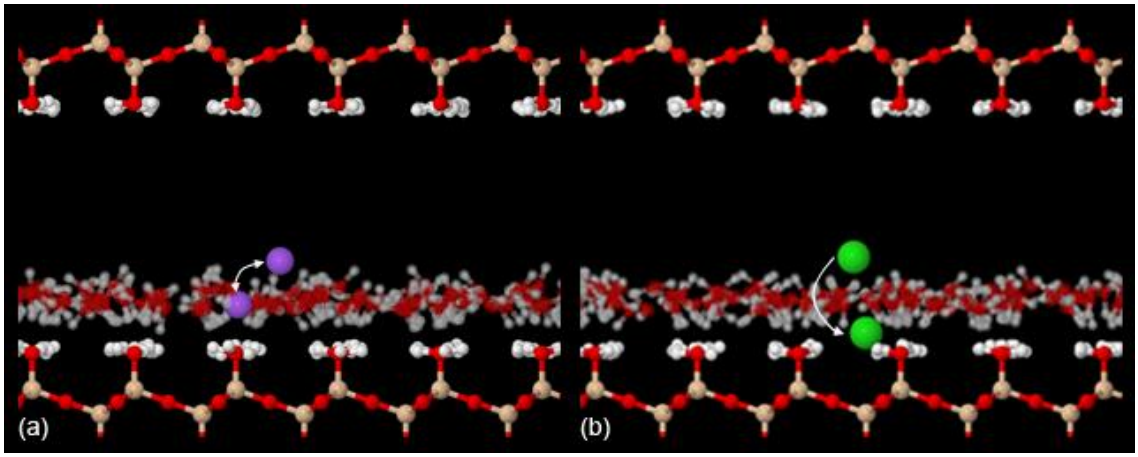


Figure 7.6: Simulation snapshots are illustrating the movement of cations in the silica nanopores. (a) The diffusion of $Na^+$ along its equilibrium positions. (b) The adsorption path for $Cl^-$ on the silica surface. Only the second (at 3.90 Å, see Table 7.1) layer of interfacial water is shown for clarity.

### 7.4.4 Dynamics of Confined Water and Ions

Because the in-plane diffusion of interfacial water strongly depends on the distance from a silica surface,[40, 116] it is likely that the mobility of the ionic species within our system differs depending on the preferential distribution within the pore. Namely, it is expected that ions closer to the surface will exhibit slower diffusion. The dynamic behavior for each ionic species was assessed by means of in-plane mean square displacements, calculated along the direction parallel to the solid surface. The results are shown in Figure 7.7. The data shown were calculated for the systems with 64 pairs of either NaCl or CsCl. No significant difference was observed when the mixed system in which 32 pairs of NaCl and 32 pairs of CsCl were simulated simultaneously.

The results shown in Figure 7.7 confirm that those ions that are further from the surface ($Cs^+$) move faster than the others. The $x - y$ diffusion coefficients can be evaluated from the slope of the curves shown in Figure 7.7. The calculated self-

diffusion coefficients are $1.84 \cdot 10^{-6}$, $4.37 \cdot 10^{-6}$, and $1.98 \cdot 10^{-7}$ $cm^2/s$ for $Na^+$, $Cs^+$, and $Cl^-$, respectively. These data are consistent with limited in-plane mobility for $Cl^-$, which is in contact with the surface. The larger diffusion coefficient for $Cs^+$ is due to the fact that these cations are found primarily at the center of the nanopore. Simulations results indicate that $Na^+$ ions appear to have slower diffusion than $Cs^+$. This behavior is explained by the incorporation of $Na^+$ in the more dynamically hindered hydration layer near the solid surface, where $Na^+$ substitutes for interfacial water molecules.

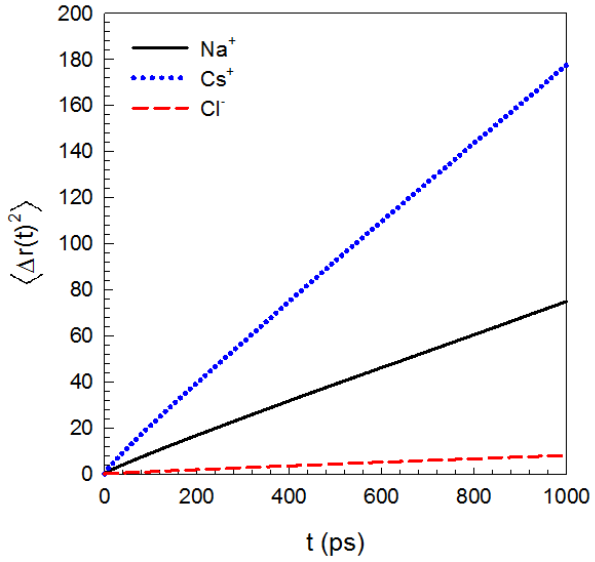


Figure 7.7: In-plane mean square displacement of $Na^+$, $Cs^+$, and $Cl^-$ in the silica pores. The data are shown for NaCl and CsCl aqueous solutions. We note that the in-plane means square displacement curve for $Cl^-$ is identical in both systems.

## 7.5 Conclusions

Aqueous electrolyte solutions confined within silica nanopores were studied by means of all-atom molecular dynamics simulations. Long (250 ns) molecular dynamics simulations were conducted to reach equilibrium and capture the structural and dynamical aspects of the adsorption process. Three different electrolyte solutions (NaCl, CsCl, and NaCl + CsCl) each with an ionic strength of 1 M were simulated at ambient temperature. To access structural and dynamic behavior of electrolytes we calculated density profiles and in-plane diffusion coefficients. Strong ion-specific behavior is reported for both the equilibrium ion distribution and mobility. We provide evidence according to which the observed difference in mobility for each ionic species is determined by the equilibrium distributions within the pores. We observed that $Cl^-$ ions preferentially adsorb onto the positively charged surfaces, where they associate with the surface hydroxyl groups. $Na^+$ ions are incorporated predominantly into the second adsorbed water layer. The larger $Cs^+$ ions are excluded from the interfacial water layers and for the most part accumulate at the pore center. As a consequence of these preferential ionic distributions we found that (1) $Cl^-$ mobility is the slowest of all simulated ions because $Cl^-$ ions bond with hydroxyl groups present at the silica surface; (2) $Na^+$ ions move faster than $Cl^-$ ions, but because they are strongly incorporated within an interfacial water layer characterized by slow diffusion, their diffusivities are hindered; (3) $Cs^+$ ions, which predominately accumulate at the pore center, exhibit a self-diffusion coefficient that is more than twice that obtained for $Na^+$ ions. No significant difference in the structure and dynamics is observed when $Na^+$ and $Cs^+$ coexist compared to when either $Na^+$ or $Cs^+$ are simulated separately. The above observations suggest that water-ion and silica-ion interactions play primary roles in

dictating the ion-specific behavior for the system considered here, while ion-ion correlations have limited influence. Consequently, a deep understanding of the properties of interfacial water appears crucial towards accurately predicting ion-specific effects under confinement.

# 8 Advantages and Limitations of Molecular Dynamics Simulations

Molecular dynamics is a computer simulation technique in which atoms and molecules interact over a period of time following the laws of classical mechanics. The system configuration is produced by the integration of Newton's equation of motion. In our implementation, the integration of the equations of motion is performed by the velocity-Verlet algorithm[65] and the leapfrog algorithm[137] generating the positions and velocities of all particles in the system as a function of time. In this molecular modeling method the forces (derivative of the potential energy) are calculated as a function of atomic positions. The dispersive interactions between the particles considered in this work are modeled with a 12-6 Lennard-Jones potential and the electrostatic interactions are described by a Coulombic potential. The parameters $\varepsilon_{ij}$ and $\sigma_{ij}$ of the Lennard-Jones potential function given below have units of energy and length, respectively.

$$E\left(r_{ij}\right) = 4\varepsilon_{ij}\left[\left(\frac{\sigma_{ij}}{r_{ij}}\right)^{12} - \left(\frac{\sigma_{ij}}{r_{ij}}\right)^{6}\right] \tag{8.1}$$

The use of this empirical potential requires the well depth parameter $\varepsilon_{ij}$, which describes the strength of the attraction between atoms and the collision diameter $\sigma_{ij}$, which is related to the atomic size. The Lennard-Jones parameters for unlike interactions are determined using the Lorentz-Berthelot mixing rules from the parameters of the pure compounds.

A reliable force field to accurately describe the energy of atomic interactions is critical for the study of aqueous systems at the solid-liquid interface using molecular dynamics simulations. The rigid SPC/E model was exclusively used in this work to

describe water. This model is known to adequately reproduce experimentally observed structural and dynamic properties, such as pair correlations and diffusion coefficients at ambient conditions.[79] The CLAYFF force field[132] was implemented to model silica and alumina substrates. CLAYFF is a general force field developed for the study of minerals and their interfaces with water. The development of empirical parameters for the interatomic potential incorporates spectroscopic data of hydrated compounds and structures of simple oxides and hydroxides. Additionally, the atomic partial charges were derived by Mulliken analysis of density functional theory results.

The implementation of reliable and accurate force fields in molecular dynamics simulations allows us to provide a fundamental level interpretation and atomic level-insights of aqueous systems at the solid-liquid interface. The results provided by the simulations can be directly compared to data from various experimental methods including backscattering spectroscopy[15] and ultrafast infrared spectroscopy.[19] Data from molecular simulations can complement experimental results and help the interpretation of findings. Molecular modeling methods may be useful in the study of systems that are difficult to investigate experimentally. These studies include systems at high temperature and high pressure, aqueous systems under extreme confinement, and systems that include hazardous compounds. Molecular simulations studies are also employed for the exploration and prediction of properties of new materials and the study of novel materials that could be used in various applications including hydrogen storage[187, 188] and water desalination.[55]

Despite these advantages, all simulations, including those implemented in this study, have limitations and disadvantages. The calculation of intermolecular forces and

the solution of Newton's equation for long equilibration periods require extensive computing times. Thus the timescale of simulated systems investigated via all-atom molecular dynamics does not typically exceed tens of nanoseconds for million-atom systems.[189] Microsecond timescale simulations for protein folding studies have been recently performed indicating the relentless increase of computing power coupled with new algorithms.[190] Similar restrictions apply to the size of the simulated systems which is typically limited in the sub-micrometer scale with the existing computing capabilities. A critical subject in molecular dynamics simulations is the description of atomic interactions and the accuracy of the calculated forces. Typically, the force fields implemented in molecular simulations are derived from fitting given experimental data and electronic structure calculations. Interatomic interaction potentials are not typically widely adaptable. Their accuracy may be compromised when the complexity of the simulated system increases and when the force fields are employed outside the parameterization range. The simplicity of the force fields used in this study provides a good description of all interatomic interactions but cannot model dissociation reaction dynamics nor account for quantum effects. Such limitations can be resolved by using more computationally demanding methods including ab initio molecular dynamics simulations and density functional theory calculations. These later simulation techniques can provide a more detailed molecular level description of interfacial phenomena such as the dissociative adsorption of water on solid substrates and dissociation of surface sites. The main disadvantage of these simulation techniques is the intensive computational resources that are required compared to the classical molecular dynamics simulations.

# 9 Conclusions and Future Work

The analysis of equilibrated interfacial water properties obtained by conducting massive molecular dynamics simulations provided molecular level insights regarding the first few hydration shells at the silica, alumina, and graphite surfaces. The simulation data were used to assess the effects of surface chemistry on the structural and dynamic behavior of interfacial water. Atomic and charge density profiles suggest that the perturbation of water structure due to the surface decreases as the distance from the solid substrate increases, becoming a nonfactor for distances greater ~14 Å. In-plane density distribution data also suggest that water molecules in the contact hydration layer are organized in well-defined patterns associated with the atomic arrangement of the solid surface. We found strong evidence that the properties of the second water layer are determined by an enhanced hydrogen bond network formed between water molecules in the first and second layer. This behavior is particularly evident in the case of the silica surface with high density of hydroxyl groups where highly ordered structures of water are observed. Our results show that the degree of hydroxylation on the silica substrate also affects the in-plane mobility of water molecules in the first few hydration layers. The data suggest that interfacial water molecules at the fully hydroxylated silica surface remain longer in the interfacial region than water molecules at the partially and non-hydroxylated surfaces do. We provide evidence of slower rotational dynamics for water at the interfacial region compared to bulk water. We report anisotropic behavior of interfacial water based on the calculations of reorientation correlation functions of the water dipole moment and hydrogen-hydrogen vector. An isotropic dynamic behavior

was obtained at 14 Å away from any surface considered, further suggesting no impact by the substrate on water properties at that distance or above.

Properties of interfacial water were also studied at the alumina surface. In addition, we assessed the effects of surface chemistry of alumina on the forces acting on an atomic force microscopy (AFM) experiment. A capped (28, 0) single walled carbon nanotube (CNT) was considered as the AFM tip. We conducted a number of independent simulations at various tip-surface separations to reconstruct the force profiles. The results suggest that oscillatory hydration forces act on the CNT at small separations (less than 10 Å). The significant changes on the local water density and molecular orientation at the alumina interface due to the CNT approaching the alumina surface are responsible for the non-sinusoidal oscillations on the force profiles. The width of the all pronounced oscillations is approximately the size of a water molecule (~2.5-3.0 Å). Local density increases yield pronounced repulsive forces, while local density depletions yield less repulsive forces, which in some circumstances may become attractive. These simulation results provide useful molecular insights and help the interpretation of AFM experimental data. It is also of great interest to further analyze experimental force-distance data we obtained using a high-deflection sensitivity AFM to study hydration force on sapphire. Our experimental results supported by our simulation findings could greatly improve the current picture of solvation forces at interfaces. Our future work will contribute to the better understanding of the conformational changes of water that occur under confinement and their relationship with the oscillatory nature of hydration forces.

Molecular dynamics simulations were finally conducted to study aqueous electrolyte solutions within slip-shaped silica nanopores. Long equilibration times were required to capture structural and dynamic aspects of electrolyte adsorption processes. Pronounced ion-specific behavior is reported for both the equilibrium ion distribution and mobility. Data suggest that the observed difference in mobility for each ionic species is determined by the equilibrium distributions within the pores. $Cl^-$ ions preferentially adsorb onto the positively charged surfaces while the $Na^+$ ions are incorporated predominantly into the second adsorbed water layer. The larger $Cs^+$ ions are excluded from the interfacial water layers and for the most part accumulate at the pore center. Most importantly, our results suggest that the observed difference in mobility for each of the ionic species is determined by the equilibrium distributions within the silica pores. These observations suggest that water-ion and silica-ion interactions play primary roles in dictating the ion-specific behavior for the silica pores considered, while ion-ion correlations have limited influence. The results of this project could provide the fundamental framework for the design of separation membranes and will allow the deep understanding of the key role interfacial water appears to play in determining ion-specific effects near charged surfaces. This work can expand in many directions and can be complimented by studying the effects of pore size, ionic strength, and surface charge on the distribution and mobility of confined electrolytes.

# 10 References


1. Bhushan, B.; Israelachvili, J. N.; Landman, U., Nanotribology: friction, wear and lubrication at the atomic scale. *Nature* **1995,** *374* (6523), 607-616.

2. Leng, Y.; Cummings, P. T., Fluidity of hydration layers nanoconfined between mica surfaces. *Physical Review Letters* **2005,** *94* (2), 026101-4.

3. Binggeli, M.; Mate, C. M., Influence of capillary condensation of water on nanotribology studied by force microscopy. *Applied Physics Letters* **1994,** *65* (4), 415-417.

4. Darhuber, A. A.; Troian, S. M., Principles of microfluidic actuation by modulation of surface stresses. *Annual Review of Fluid Mechanics* **2005,** *37* (1), 425-455.

5. Craighead, H., Future lab-on-a-chip technologies for interrogating individual molecules. *Nature* **2006,** *442* (7101), 387-393.

6. Srinivasan, V.; Pamula, V. K.; Fair, R. B., An integrated digital microfluidic lab-on-a-chip for clinical diagnostics on human physiological fluids. *Lab on a Chip* **2004,** *4* (4), 310-315.

7. Pal, S. K.; Zewail, A. H., Dynamics of water in biological recognition. *Chemical Reviews* **2004,** *104* (4), 2099-2124.

8. Tajkhorshid, E.; Nollert, P.; Jensen, M. O.; Miercke, L. J. W.; O'Connell, J.; Stroud, R. M.; Schulten, K., Control of the selectivity of the aquaporin water channel family by global orientational tuning. *Science* **2002,** *296* (5567), 525-530.

9. Hille, B., *Ionic channels of excitable membranes*. Sinauer Associates: Sunderland, Massachusetts, 1992.

10. Cox, J. J.; Reimann, F.; Nicholas, A. K.; Thornton, G.; Roberts, E.; Springell, K.; Karbani, G.; Jafri, H.; Mannan, J.; Raashid, Y.; Al-Gazali, L.; Hamamy, H.; Valente, E. M.; Gorman, S.; Williams, R.; McHale, D. P.; Wood, J. N.; Gribble, F. M.; Woods, C. G., An SCN9A channelopathy causes congenital inability to experience pain. *Nature* **2006,** *444* (7121), 894-898.

11. Fitter, J.; Lechner, R. E.; Dencher, N. A., Interactions of hydration water and biological membranes studied by neutron scattering. *The Journal of Physical Chemistry B* **1999,** *103* (38), 8036-8050.

12. Kim, J.; Lu, W.; Qiu, W.; Wang, L.; Caffrey, M.; Zhong, D., Ultrafast hydration dynamics in the lipidic cubic phase: Discrete water structures in nanochannels. *The Journal of Physical Chemistry B* **2006,** *110* (43), 21994-22000.

13. Mamontov, E.; Vlcek, L.; Wesolowski, D. J.; Cummings, P. T.; Wang, W.; Anovitz, L. M.; Rosenqvist, J.; Brown, C. M.; Garcia Sakai, V., Dynamics and structure of hydration water on rutile and cassiterite nanopowders studied by quasielastic neutron scattering and molecular dynamics simulations. *The Journal of Physical Chemistry C* **2007,** *111* (11), 4328-4341.

14. Bruni, F.; Ricci, M. A.; Soper, A. K., Water confined in Vycor glass. I. A neutron diffraction study. *The Journal of Chemical Physics* **1998,** *109* (4), 1478-1485.

15. Mamontov, E.; Wesolowski, D. J.; Vlcek, L.; Cummings, P. T.; Rosenqvist, J.; Wang, W.; Cole, D. R., Dynamics of hydration water on rutile studied by backscattering neutron spectroscopy and molecular dynamics simulation. *The Journal of Physical Chemistry C* **2008,** *112* (32), 12334-12341.

16. Malikova, N.; Cadene, A.; Marry, V.; Dubois, E.; Turq, P., Diffusion of water in clays on the microscopic scale: Modeling and experiment. *The Journal of Physical Chemistry B* **2006,** *110* (7), 3206-3214.

17. Barnette, A. L.; Asay, D. B.; Kim, S. H., Average molecular orientations in the adsorbed water layers on silicon oxide in ambient conditions. *Phys Chem Chem Phys* **2008,** *10* (32), 4981-4986.

18. Zhang, Z.; Fenter, P.; Cheng, L.; Sturchio, N. C.; Bedzyk, M. J.; Predota, M.; Bandura, A.; Kubicki, J. D.; Lvov, S. N.; Cummings, P. T.; Chialvo, A. A.; Ridley, M. K.; Benezeth, P.; Anovitz, L.; Palmer, D. A.; Machesky, M. L.; Wesolowski, D. J., Ion adsorption at the rutile-water interface: Linking molecular and macroscopic properties. *Langmuir* **2004,** *20* (12), 4954-4969.

19. Fenn, E. E.; Wong, D. B.; Fayer, M. D., Water dynamics at neutral and ionic interfaces. *Proceedings of the National Academy of Sciences* **2009,** *106* (36), 15243-15248.

20. Puibasset, J.; Pellenq, R. J. M., Grand canonical Monte Carlo simulation study of water structure on hydrophilic mesoporous and plane silica substrates. *The Journal of Chemical Physics* **2003,** *119* (17), 9226-9232.

21. Lee, S. H.; Rossky, P. J., A comparison of the structure and dynamics of liquid water at hydrophobic and hydrophilic surfaces - A molecular dynamics simulation study. *The Journal of Chemical Physics* **1994,** *100* (4), 3334-3345.

22. Gallo, P.; Ricci, M. A.; Rovere, M., Layer analysis of the structure of water confined in vycor glass. *The Journal of Chemical Physics* **2002,** *116* (1), 342-346.

23. Gordillo, M. C.; Nagy, G.; Martí, J., Structure of water nanoconfined between hydrophobic surfaces. *The Journal of Chemical Physics* **2005,** *123* (5), 054707-9.

24. Leng, Y.; Cummings, P. T., Hydration structure of water confined between mica surfaces. *The Journal of Chemical Physics* **2006,** *124* (7), 074711-4.

25. Giovambattista, N.; Debenedetti, P. G.; Rossky, P. J., Hydration behavior under confinement by nanoscale surfaces with patterned hydrophobicity and hydrophilicity. *The Journal of Physical Chemistry C* **2007,** *111* (3), 1323-1332.

26. Nangia, S.; Washton, N. M.; Mueller, K. T.; Kubicki, J. D.; Garrison, B. J., Study of a family of 40 hydroxylated β-cristobalite surfaces using empirical potential energy functions. *The Journal of Physical Chemistry C* **2007,** *111* (13), 5169-5177.

27. Janecek, J.; Netz, R. R., Interfacial water at hydrophobic and hydrophilic surfaces: Depletion versus adsorption. *Langmuir* **2007,** *23* (16), 8417-8429.

28. Gordillo, M. C.; Martí, J., Molecular dynamics description of a layer of water molecules on a hydrophobic surface. *The Journal of Chemical Physics* **2002,** *117* (7), 3425-3430.

29. Spohr, E., Molecular dynamics simulation studies of the density profiles of water between (9-3) Lennard-Jones walls. *The Journal of Chemical Physics* **1997,** *106* (1), 388-391.

30. Argyris, D.; Tummala, N. R.; Striolo, A.; Cole, D. R., Molecular structure and dynamics in thin water films at the silica and graphite surfaces. *The Journal of Physical Chemistry C* **2008,** *112* (35), 13587-13599.

31. Striolo, A.; Gubbins, K. E.; Gruszkiewicz, M. S.; Cole, D. R.; Simonson, J. M.; Chialvo, A. A.; Cummings, P. T.; Burchell, T. D.; More, K. L., Effect of temperature on the adsorption of water in porous carbons. *Langmuir* **2005,** *21* (21), 9457-9467.

32. Weiss, D. R.; Raschke, T. M.; Levitt, M., How hydrophobic buckminsterfullerene affects surrounding water structure. *The Journal of Physical Chemistry B* **2008**.

33. Gordillo, M. C.; Martí, J., Hydrogen bond structure of liquid water confined in nanotubes. *Chem Phys Lett* **2000,** *329* (5-6), 341-345.

34. Gordillo, M. C.; Martí, J., Water on the outside of carbon nanotube bundles. *Physical Review B* **2003,** *67* (20), 205425.

35. Striolo, A., The mechanism of water diffusion in narrow carbon nanotubes. *Nano Letters* **2006,** *6* (4), 633-639.

36. Striolo, A.; Chialvo, A. A.; Gubbins, K. E.; Cummings, P. T., Water in carbon nanotubes: Adsorption isotherms and thermodynamic properties from molecular simulation. *The Journal of Chemical Physics* **2005,** *122* (23), 234712-14.

37. Tikhonov, A. M.; Patel, H.; Garde, S.; Schlossman, M. L., Tail ordering due to headgroup hydrogen bonding interactions in surfactant monolayers at the water-oil Interface. *The Journal of Physical Chemistry B* **2006,** *110* (39), 19093-19096.

38. Romero-Vargas Castrillón, S.; Giovambattista, N.; Aksay, I. A.; Debenedetti, P. G., Evolution from surface-influenced to bulk-like dynamics in nanoscopically confined water. *The Journal of Physical Chemistry B* **2009,** *113* (23), 7973-7976.

39. Martí, J.; Sala, J.; Guardia, E.; Gordillo, M. C., Molecular dynamics simulations of supercritical water confined within a carbon-slit pore. *Physical Review E* **2009,** *79* (3), 031606-10.

40. Romero-Vargas Castrillón, S.; Giovambattista, N.; Aksay, I. A.; Debenedetti, P. G., Effect of surface polarity on the structure and dynamics of water in nanoscale confinement. *The Journal of Physical Chemistry B* **2009,** *113* (5), 1438-1446.

41. Catalano, J. G.; Park, C.; Zhang, Z.; Fenter, P., Termination and water adsorption at the α-$Al_2O_3$ (012) - Aqueous solution interface. *Langmuir* **2006,** *22* (10), 4668-4673.

42. Catalano, J. G., Relaxations and interfacial water ordering at the corundum (110) Surface. *The Journal of Physical Chemistry C* **2010,** *114* (14), 6624-6630.

43. Wittbrodt, J. M.; Hase, W. L.; Schlegel, H. B., Ab initio study of the interaction of water with cluster models of the aluminum terminated (0001) α-aluminum oxide surface. *The Journal of Physical Chemistry B* **1998,** *102* (34), 6539-6548.

44. Hass, K. C.; Schneider, W. F.; Curioni, A.; Andreoni, W., The chemistry of water on alumina surfaces: Reaction dynamics from first principles. *Science* **1998,** *282* (5387), 265-268.

45. Shapovalov, V.; Truong, T. N., Ab initio study of water adsorption on α-$Al_2O_3$ (0001) crystal surface. *The Journal of Physical Chemistry B* **2000,** *104* (42), 9859-9863.

46. Wang, X. G.; Chaka, A.; Scheffler, M., Effect of the environment on α-$Al_2O_3$ (0001) surface structures. *Physical Review Letters* **2000,** *84* (16), 3650-3653.

47. Lodziana, Z.; Norskov, J. K.; Stoltze, P., The stability of the hydroxylated (0001) surface of α-$Al_2O_3$. *The Journal of Chemical Physics* **2003,** *118* (24), 11179-11188.

48. Israelachvili, J., Solvation forces and liquid structure, as probed by direct force measurements. *Accounts Chem Res* **1987,** *20* (11), 415-421.

49. Jarvis, S. P.; Uchihashi, T.; Ishida, T.; Tokumoto, H.; Nakayama, Y., Local solvation shell measurement in water using a carbon nanotube probe. *The Journal of Physical Chemistry B* **2000,** *104* (26), 6091-6094.

50. Li, T. D.; Gao, J. P.; Szoszkiewicz, R.; Landman, U.; Riedo, E., Structured and viscous water in subnanometer gaps. *Physical Review B* **2007,** *75* (11), 115415.

51. Kimura, K.; Ido, S.; Oyabu, N.; Kobayashi, K.; Hirata, Y.; Imai, T.; Yamada, H., Visualizing water molecule distribution by atomic force microscopy. *The Journal of Chemical Physics* **2010,** *132* (19), 194705.

52. Hille, B., *Ion channels of excitable membranes*. Sinauer Associates Inc: Sunderland, Massachusetts, 2001

53. Jiang, Y.; Lee, A.; Chen, J.; Cadene, M.; Chait, B. T.; MacKinnon, R., Crystal structure and mechanism of a calcium-gated potassium channel. *Nature* **2002,** *417* (6888), 515-522.

54. Fornasiero, F.; Park, H. G.; Holt, J. K.; Stadermann, M.; Grigoropoulos, C. P.; Noy, A.; Bakajin, O., Ion exclusion by sub-2-nm carbon nanotube pores. *Proceedings of the National Academy of Sciences* **2008,** *105* (45), 17250-17255.

55. Corry, B., Designing carbon nanotube membranes for efficient water desalination. *The Journal of Physical Chemistry B* **2008,** *112* (5), 1427-1434.

56. Leung, K.; Rempe, S. B.; Lorenz, C. D., Salt permeation and exclusion in hydroxylated and functionalized silica pores. *Physical Review Letters* **2006,** *96* (9), 095504-4.

57. Barrer, R. M., *Zeolites and clay minerals as sorbents and molecular sieves*. Academic Press: London, 1978.

58. Hensen, E. J. M.; Smit, B., Why clays swell. *The Journal of Physical Chemistry B* **2002,** *106* (49), 12664-12667.

59. Israelachvili, J.; Pashley, R., The hydrophobic interaction is long range, decaying exponentially with distance. *Nature* **1982,** *300* (5890), 341-342.

60. Verdaguer, A.; Sacha, G. M.; Bluhm, H.; Salmeron, M., Molecular structure of water at interfaces: Wetting at the nanometer scale. *Chemical Reviews* **2006,** *106* (4), 1478-1510.

61. Schmahl, W. W.; Swainson, I. P.; Dove, M. T.; Graeme-Barber, A., Landau free energy and order parameter behaviour of the ab phase transition in cristobalite. *Zeitschrift für Kristallographie* **1992,** *201*, 125-145.

62. Berendsen, H. J. C.; Grigera, J. R.; Straatsma, T. P., The missing term in effective pair potentials. *The Journal of Physical Chemistry* **1987,** *91* (24), 6269-6271.

63. Cheng, A.; Steele, W. A., Computer simulation of ammonia on graphite. 1. Low temperature structure of monolayer and bilayer films. *The Journal of Chemical Physics* **1990,** *92* (6), 3858-3866.

64. Brodka, A.; Zerda, T. W., Properties of liquid acetone in silica pores: Molecular dynamics simulation. *The Journal of Chemical Physics* **1996,** *104* (16), 6319-6326.

65. Allen, M. P.; Tildesley, D. J., *Computer simulation of liquids*. Oxford University Press: Oxford, 2004.

66. Ryckaert, J.-P.; Ciccotti, G.; Berendsen, H. J. C., Numerical integration of the cartesian equations of motion of a system with constraints: molecular dynamics of n-alkanes. *Journal of Computational Physics* **1977,** *23* (3), 327-341.

67. Plimpton, S., Fast parallel algorithms for short-range molecular dynamics. *Journal of Computational Physics* **1995,** *117* (1), 1-19.

68. Martí, J.; Nagy, G.; Gordillo, M. C.; Guardia, E., Molecular simulation of liquid water confined inside graphite channels: Thermodynamics and structural properties. *The Journal of Chemical Physics* **2006,** *124* (9), 094703-7.

69. Striolo, A.; Chialvo, A. A.; Cummings, P. T.; Gubbins, K. E., Water adsorption in carbon-slit nanopores. *Langmuir* **2003,** *19* (20), 8583-8591.

70. Thomas, J. L.; Roeselova, M.; Dang, L. X.; Tobias, D. J., Molecular dynamics simulations of the solution-air interface of aqueous sodium nitrate. *The Journal of Physical Chemistry A* **2007,** *111* (16), 3091-3098.

71. Pertsin, A.; Grunze, M., Water-graphite interaction and behavior of water near the graphite surface. *The Journal of Physical Chemistry B* **2004,** *108* (4), 1357-1364.

72. Martí, J., Analysis of the hydrogen bonding and vibrational spectra of supercritical model water by molecular dynamics simulations. *The Journal of Chemical Physics* **1999,** *110* (14), 6876-6886.

73. Landman, U.; Luedtke, W. D.; Burnham, N. A.; Colton, R. J., Atomistic mechanisms and dynamics of adhesion, nanoindentation, and fracture. *Science* **1990,** *248* (4954), 454-461.

74. Wensink, E. J. W.; Hoffmann, A. C.; Apol, M. E. F.; Berendsen, H. J. C., Properties of adsorbed water layers and the effect of adsorbed layers on interparticle forces by liquid bridging. *Langmuir* **2000,** *16* (19), 7392-7400.

75. van der Spoel, D.; Wensink, E. J. W.; Hoffmann, A. C., Lifting a wet glass from a table: A microscopic picture. *Langmuir* **2006,** *22* (13), 5666-5672.

76. Tummala, N. R.; Striolo, A., SDS surfactants on carbon nanotubes: Aggregate morphology. *ACS Nano* **2009,** *3* (3), 595-602.

77. Notman, R.; Walsh, T. R., Molecular dynamics studies of the interactions of water and amino acid analogues with quartz surfaces. *Langmuir* **2009,** *25* (3), 1638-1644.

78. Garofalini, S. H., Molecular dynamics computer simulations of silica surface structure and adsorption of water molecules. *Journal of Non-Crystalline Solids* **1990,** *120* (1-3), 1-12.

79. Berendsen, H. J. C.; Grigera, J. R.; Straatsma, T. P., The missing term in effective pair potentials. *J. Phys. Chem.* **1987,** *91* (24), 6269-6271.

80. Essmann, U.; Perera, L.; Berkowitz, M. L.; Darden, T.; Lee, H.; Pedersen, L. G., A smooth particle mesh Ewald method. *The Journal of Chemical Physics* **1995,** *103* (19), 8577.

81. Miyamoto, S.; Kollman, P. A., Settle: An analytical version of the SHAKE and RATTLE algorithm for rigid water models. *Journal of Computational Chemistry* **1992,** *13* (8), 952-962.

82. Lindahl, E.; Hess, B.; van der Spoel, D., GROMACS 3.0: a package for molecular simulation and trajectory analysis. *Journal of Molecular Modeling* **2001,** *7* (8), 306-317.

83. Hess, B.; Kutzner, C.; vanderSpoel, D.; Lindahl, E., GROMACS 4: Algorithms for highly efficient, load-balanced, and scalable molecular simulation. *Journal of Chemical Theory and Computation* **2008,** *4* (3), 435-447.

84. Berendsen, H. J. C.; van der Spoel, D.; van Drunen, R., GROMACS: A message-passing parallel molecular dynamics implementation. *Computer Physics Communications* **1995,** *91* (1-3), 43-56.

85. van der Spoel, D.; Lindahl, E.; Hess, B.; Groenhof, G.; Mark, A. E.; Berendsen, H. J. C., GROMACS: Fast, flexible, and free. *Journal of Computational Chemistry* **2005,** *26* (16), 1701-1718.

86. Lu, L.; Berkowitz, M. L., Hydration force between model hydrophilic surfaces: Computer simulations. *The Journal of Chemical Physics* **2006,** *124* (10), 101101-4.

87. Tanford, C., *The hydrophobic effect: Formation of micelles and biological membranes*. 2nd ed.; Wiley: New York, 1980.

88. Giovambattista, N.; Rossky, P. J.; Debenedetti, P. G., Phase transitions induced by nanoconfinement in liquid water. *Physical Review Letters* **2009,** *102* (5), 050603-4.

89. Chandler, D., Interfaces and the driving force of hydrophobic assembly. *Nature* **2005,** *437* (7059), 640-647.

90. Tanford, C., The hydrophobic effect and the organization of living matter. *Science* **1978,** *200* (4345), 1012-1018.

91. Lima, E. R. A.; Bostrom, M.; Horinek, D.; Biscaia, E. C.; Kunz, W.; Tavares, F. W., Co-ion and ion competition effects: Ion distributions close to a hydrophobic solid surface in mixed electrolyte solutions. *Langmuir* **2008,** *24* (8), 3944-3948.

92. Bostrom, M.; Kunz, W.; Ninham, B. W., Hofmeister effects in surface tension of aqueous electrolyte solution. *Langmuir* **2005,** *21* (6), 2619-2623.

93. Rafferty, J. L.; Siepmann, J. I.; Schure, M. R., The effects of chain length, embedded polar groups, pressure, and pore shape on structure and retention in reversed-phase liquid chromatography: Molecular-level insights from Monte Carlo simulations. *Journal of Chromatography A* **2009,** *1216* (12), 2320-2331.

94. Rafferty, J. L.; Siepmann, J. I.; Schure, M. R., Influence of bonded-phase coverage in reversed-phase liquid chromatography via molecular simulation: I. Effects on chain conformation and interfacial properties. *Journal of Chromatography A* **2008,** *1204* (1), 11-19.

95. Zhang, Y.; Liu, K.-H.; Lagi, M.; Liu, D.; Littrell, K. C.; Mou, C.-Y.; Chen, S.-H., Absence of the density minimum of supercooled water in hydrophobic confinement. *The Journal of Physical Chemistry B* **2009,** *113* (15), 5007-5010.

96. Bryk, T.; Haymet, A. D. J., Ice 1h/water interface of the SPC/E model: Molecular dynamics simulations of the equilibrium basal and prism interfaces. *The Journal of Chemical Physics* **2002,** *117* (22), 10258-10268.

97. Martí, J.; Nagy, G.; Guardia, E.; Gordillo, M. C., Molecular dynamics simulation of liquid water confined inside graphite channels: Dielectric and dynamical properties. *The Journal of Physical Chemistry B* **2006,** *110* (47), 23987-23994.

98. Argyris, D.; Cole, D. R.; Striolo, A., Hydration structure on crystalline silica substrates. *Langmuir* **2009,** *25* (14), 8025-8035.

99. Puibasset, J.; Pellenq, R. J. M., Water adsorption on hydrophilic mesoporous and plane silica substrates: A grand canonical Monte Carlo simulation study. *The Journal of Chemical Physics* **2003,** *118* (12), 5613-5622.

100. Wang, J. W.; Kalinichev, A. G.; Kirkpatrick, R. J., Asymmetric hydrogen bonding and orientational ordering of water at hydrophobic and hydrophilic surfaces: A comparison of water/vapor, water/talc, and water/mica interfaces. *The Journal of Physical Chemistry C* **2009,** *113* (25), 11077-11085.

101. Djikaev, Y. S.; Ruckenstein, E., The effect of hydrogen bonding on the solvent-mediated interaction of composite plates. *Journal of Colloid and Interface Science* **2009,** *336* (2), 575-583.

102. Djikaev, Y. S.; Ruckenstein, E., A probabilistic approach to the effect of hydrogen bonding on the hydrophobic attraction. *The Journal of Chemical Physics* **2009,** *130* (12), 124713-10.

103. Kim, J. H.; Garofalini, S. H., Modeling microstructural evolution using atomic density function and effective pair potentials. *Physical Review B* **2008,** *78* (14), 144109-7.

104. Mahadevan, T.; Garofalini, S., Dissociative chemisorption of water onto silica surfaces and formation of hydronium ions. *The Journal of Physical Chemistry C* **2009,** *113* (25), 11177-11177.

105. Nangia, S.; Garrison, B. J., Reaction rates and dissolution mechanisms of quartz as a function of pH. *The Journal of Physical Chemistry A* **2008,** *112* (10), 2027-2033.

106. Leetmaa, M.; Wikfeldt, K. T.; Ljungberg, M. P.; Odelius, M.; Swenson, J.; Nilsson, A.; Pettersson, L. G. M., Diffraction and IR/Raman data do not prove tetrahedral water. *The Journal of Chemical Physics* **2008,** *129* (8), 084502-13.

107. Ha, J.; Hyun Yoon, T.; Wang, Y.; Musgrave, C. B.; Brown, J. G. E., Adsorption of organic matter at mineral/water interfaces: 7. ATR-FTIR and quantum chemical study of lactate interactions with hematite nanoparticles. *Langmuir* **2008,** *24* (13), 6683-6692.

108. Anderson, J.; Ullo, J. J.; Yip, S., Molecular dynamics simulation of dielectric properties of water. *The Journal of Chemical Physics* **1987,** *87* (3), 1726-1732.

109. Yoshii, N.; Miura, S.; Okazaki, S., A molecular dynamics study of dielectric constant of water from ambient to sub- and supercritical conditions using a fluctuating-charge potential model. *Chem Phys Lett* **2001,** *345* (1-2), 195-200.

110. Sverjensky, D. A., Standard states for the activities of mineral surface sites and species. *Geochimica et Cosmochimica Acta* **2003,** *67* (1), 17-28.

111. Martí, J.; Padro, J. A.; Guardia, E., Molecular dynamics simulation of liquid water along the coexistence curve: Hydrogen bonds and vibrational spectra. *The Journal of Chemical Physics* **1996,** *105* (2), 639-649.

112. Argyris, D.; Cole, D. R.; Striolo, A., Ion-specific effects under confinement: The role of interfacial water. *ACS Nano* **2010,** *4* (4), 2035-2042.

113. Malikova, N.; Cadene, A.; Marry, V.; Dubois, E.; Turq, P., Diffusion of water in clays on the microscopic scale: Modeling and experiment. *J Phys Chem B* **2006,** *110* (7), 3206-3214.

114. Kerisit, S.; Liu, C. X.; Ilton, E. S., Molecular dynamics simulations of the orthoclase (001)- and (010)-water interfaces. *Geochimica Et Cosmochimica Acta* **2008,** *72* (6), 1481-1497.

115. Giovambattista, N.; Rossky, P. J.; Debenedetti, P. G., Effect of temperature on the structure and phase behavior of water confined by hydrophobic, hydrophilic, and heterogeneous surfaces. *The Journal of Physical Chemistry B* **2009,** *113* (42), 13723-13734.

116. Argyris, D.; Cole, D. R.; Striolo, A., Dynamic behavior of interfacial water at the silica surfaces. *The Journal of Physical Chemistry C* **2009,** *113* (45), 19591-19600.

117. Gordillo, M. C.; Martí, J., Effect of surface roughness on the static and dynamic properties of water adsorbed on graphene. *The Journal of Physical Chemistry B* **2010,** *114* (13), 4583-4589.

118. Godawat, R.; Jamadagni, S. N.; Garde, S., Characterizing hydrophobicity of interfaces by using cavity formation, solute binding, and water correlations. *Proceedings of the National Academy of Sciences* **2009,** *106* (36), 15119-15124.

119. Ahn, J.; Rabalais, J. W., Composition and structure of the $Al_2O_3$ {0001}-(1x1) surface. *Surf Sci* **1997,** *388* (1-3), 121-131.

120. Nygren, M. A.; Gay, D. H.; Catlow, C. R. A., Hydroxylation of the surface of the corundum basal plane. *Surf Sci* **1997,** *380* (1), 113-123.

121. Blonski, S.; Garofalini, S. H., Molecular dynamics study of silica-alumina interfaces. *The Journal of Physical Chemistry* **1996,** *100* (6), 2201-2205.

122. Adiga, S. P.; Zapol, P.; Curtiss, L. A., Atomistic simulations of amorphous alumina surfaces. *Physical Review B* **2006,** *74* (6), 064204.

123. Hinnemann, B.; Carter, E. A., Adsorption of Al, O, Hf, Y, Pt, and S atoms on α-$Al_2O_3$ (0001). *The Journal of Physical Chemistry C* **2007,** *111* (19), 7105-7126.

124. Adiga, S. P.; Zapol, P.; Curtiss, L. A., Structure and morphology of hydroxylated amorphous alumina surfaces. *The Journal of Physical Chemistry C* **2007,** *111* (20), 7422-7429.

125. Blonski, S.; Garofalini, S. H., Molecular dynamics simulations of α-alumina and γ-alumina Surfaces. *Surf Sci* **1993,** *295* (1-2), 263-274.

126. Eng, P. J.; Trainor, T. P.; Brown, G. E.; Waychunas, G. A.; Newville, M.; Sutton, S. R.; Rivers, M. L., Structure of the hydrated α-$Al_2O_3$ (0001) surface. *Science* **2000,** *288* (5468), 1029-1033.

127. Coustet, V.; Jupille, J., High-resolution electron-energy-loss spectroscopy of isolated hydroxyl-groups on α-$Al_2O_3$ (0001). *Surf Sci* **1994,** *309*, 1161-1165.

128. Barth, C.; Reichling, M., Imaging the atomic arrangements on the high-temperature reconstructed α-$Al_2O_3$ (0001) surface. *Nature* **2001,** *414* (6859), 54-57.

129. Hass, K. C.; Schneider, W. F.; Curioni, A.; Andreoni, W., First-principles molecular dynamics simulations of $H_2O$ on α-$Al_2O_3$ (0001). *The Journal of Physical Chemistry B* **2000,** *104* (23), 5527-5540.

130. de Leeuw, N. H.; Parker, S. C., Effect of chemisorption and physisorption of water on the surface structure and stability of α-alumina. *J Am Ceram Soc* **1999,** *82* (11), 3209-3216.

131. Többens, D. M.; Stüßer, N.; Knorr, K.; Mayer, H. M.; Lampert, G., E9: The new high-resolution neutron powder diffractometer at the Berlin neutron scattering center. *Mater Sci Forum* **2001,** *378-3,* 288-293.

132. Cygan, R. T.; Liang, J.-J.; Kalinichev, A. G., Molecular models of hydroxide, oxyhydroxide, and clay phases and the development of a general force field. *The Journal of Physical Chemistry B* **2004,** *108* (4), 1255-1266.

133. Ho, T. A.; Argyris, D.; Papavassiliou, D.; Striolo, A.; Lee, L. L.; Cole, D. R., Interfacial water on crystalline silica: A comparative molecular dynamics simulation study. *Molecular Simulation* **2010,** *In Press*.

134. Essmann, U.; Perera, L.; Berkowitz, M. L.; Darden, T.; Lee, H.; Pedersen, L. G., A smooth particle mesh Ewald method. *Journal of Chemical Physics* **1995,** *103* (19), 8577.

135. Nose, S., A molecular-dynamics method for simulations in the canonical ensemble. *Mol Phys* **1984,** *52* (2), 255-268.

136. Hoover, W. G., Canonical dynamics: Equilibrium phase-space distributions. *Phys Rev A* **1985,** *31* (3), 1695-1697.

137. Hockney, R. W.; Goel, S. P.; Eastwood, J. W., Quiet high-resolution computer models of a plasma. *Journal of Computational Physics* **1974,** *14* (2), 148-158.

138. Martí, J.; Sala, J.; Guardia, E., Molecular dynamics simulations of water confined in graphene nanochannels: From ambient to supercritical environments. *J Mol Liq* **2010,** *153* (1), 72-78.

139. Wang, J. W.; Kalinichev, A. G.; Kirkpatrick, R. J., Effects of substrate structure and composition on the structure, dynamics, and energetics of water at mineral surfaces: A molecular dynamics modeling study. *Geochimica et Cosmochimica Acta* **2006,** *70* (3), 562-582.

140. Wang, J. W.; Kalinichev, A. G.; Kirkpatrick, R. J.; Cygan, R. T., Structure, energetics, and dynamics of water adsorbed on the muscovite (001) surface: A molecular dynamics simulation. *The Journal of Physical Chemistry B* **2005,** *109* (33), 15893-15905.

141. Kerisit, S.; Cooke, D. J.; Marmier, A.; Parker, S. C., Atomistic simulation of charged iron oxyhydroxide surfaces in contact with aqueous solution. *Chem Commun* **2005,** (24), 3027-3029.

142. Hu, Z. H.; Weeks, J. D., Acetonitrile on silica surfaces and at its liquid-vapor interface: Structural correlations and collective dynamics. *The Journal of Physical Chemistry C* **2010,** *114* (22), 10202-10211.

143. Marry, V.; Rotenberg, B.; Turq, P., Structure and dynamics of water at a clay surface from molecular dynamics simulation. *Phys Chem Chem Phys* **2008,** *10* (32), 4802-4813.

144. Porcheron, F.; Monson, P. A., Mean-field theory of liquid droplets on roughened solid surfaces: Application to superhydrophobicity. *Langmuir* **2006,** *22* (4), 1595-1601.

145. Grzelak, E. M.; Errington, J. R., Computation of interfacial properties via grand canonical transition matrix Monte Carlo simulation. *The Journal of Chemical Physics* **2008,** *128* (1), 014710.

146. Kerisit, S.; Liu, C. X., Molecular simulations of water and ion diffusion in nanosized mineral fractures. *Environ Sci Technol* **2009,** *43* (3), 777-782.

147. Shen, Y. R.; Ostroverkhov, V., Sum-frequency vibrational spectroscopy on water interfaces: Polar orientation of water molecules at interfaces. *Chemical Reviews* **2006,** *106* (4), 1140-1154.

148. O'Shea, S. J., Oscillatory forces in liquid atomic force microscopy. *Jpn J Appl Phys 1* **2001,** *40* (6B), 4309-4313.

149. Hayes, R.; Warr, G. G.; Atkin, R., At the interface: solvation and designing ionic liquids. *Phys Chem Chem Phys* **2010,** *12* (8), 1709-1723.

150. Fukuma, T.; Kobayashi, K.; Matsushige, K.; Yamada, H., True molecular resolution in liquid by frequency-modulation atomic force microscopy. *Applied Physics Letters* **2005,** *86* (19), 193108-3.

151. Patrick, D. L.; Lynden-Bell, R. M., Atomistic simulations of fluid structure and solvation forces in atomic force microscopy. *Surf Sci* **1997,** *380* (2-3), 224-244.

152. Ho, R. Y.; Yuan, J. Y.; Shao, Z. F., Hydration force in the atomic force microscope: A computational study. *Biophys J* **1998,** *75* (2), 1076-1083.

153. Lauritsen, J. V.; Reichling, M., Atomic resolution non-contact atomic force microscopy of clean metal oxide surfaces. *J Phys-Condens Mat* **2010,** *22* (26), 263001.

154. Gan, Y.; Franks, G. V., High resolution AFM images of the single-crystal α-$Al_2O_3$ (0001) surface in water. *The Journal of Physical Chemistry B* **2005,** *109* (25), 12474-12479.

155. Ashby, P. D.; Lieber, C. M., Brownian force profile reconstruction of interfacial 1-nonanol solvent structure. *J Am Chem Soc* **2004,** *126* (51), 16973-16980.

156. Striolo, A., Water self-diffusion through narrow oxygenated carbon nanotubes. *Nanotechnology* **2007,** *18* (47), 475704.

157. Walther, J. H.; Jaffe, R. L.; Kotsalis, E. M.; Werder, T.; Halicioglu, T.; Koumoutsakos, P., Hydrophobic hydration of C-60 and carbon nanotubes in water. *Carbon* **2004,** *42* (5-6), 1185-1194.

158. Mailly, D., Nanofabrication techniques. *The European Physical Journal - Special Topics* **2009,** *172* (1), 333-342.

159. Wu, M.-Y.; Smeets, R. M. M.; Zandbergen, M.; Ziese, U.; Krapf, D.; Batson, P. E.; Dekker, N. H.; Dekker, C.; Zandbergen, H. W., Control of shape and material composition of solid-state nanopores. *Nano Letters* **2008,** *9* (1), 479-484.

160. Quake, S. R.; Scherer, A., From micro- to nanofabrication with soft materials. *Science* **2000,** *290* (5496), 1536-1540.

161. Plecis, A.; Schoch, R. B.; Renaud, P., Ionic transport phenomena in nanofluidics: Experimental and theoretical study of the exclusion-enrichment effect on a chip. *Nano Letters* **2005,** *5* (6), 1147-1155.

162. Noy, A.; Park, H. G.; Fornasiero, F.; Holt, J. K.; Grigoropoulos, C. P.; Bakajin, O., Nanofluidics in carbon nanotubes. *Nano Today* **2007,** *2* (6), 22-29.

163. Schoch, R. B.; Han, J. Y.; Renaud, P., Transport phenomena in nanofluidics. *Rev Mod Phys* **2008,** *80* (3), 839-883.

164. Mortensen, N. A.; Xiao, S. S.; Pedersen, J., Liquid-infiltrated photonic crystals: enhanced light-matter interactions for lab-on-a-chip applications. *Microfluid Nanofluid* **2008,** *4* (1-2), 117-127.

165. Cole, D. R.; Mamontov, E.; Rother, G., Structure and dynamics of fluids in microporous and mesoporous earth and engineered materials. In *Neutron Applications in Earth, Energy and Environmental Sciences*, 2009; pp 547-570.

166. Lopes, P. E. M.; Murashov, V.; Tazi, M.; Demchuk, E.; MacKerell, A. D., Development of an empirical force field for silica. Application to the quartz-water interface. *The Journal of Physical Chemistry B* **2006,** *110* (6), 2782-2792.

167. Nagy, G.; Gordillo, M. C.; Guardia, E.; Martí, J., Liquid water confined in carbon nanochannels at high temperatures. *The Journal of Physical Chemistry B* **2007,** *111* (43), 12524-12530.

168. Shirono, K.; Daiguji, H., Molecular simulation of the phase behavior of water confined in silica nanopores. *The Journal of Physical Chemistry C* **2007,** *111* (22), 7938-7946.

169. Wander, M. C. F.; Clark, A. E., Structural and dielectric properties of quartz-water interfaces. *The Journal of Physical Chemistry C* **2008,** *112* (50), 19986-19994.

170. Freund, J. B., Electro-osmosis in a nanometer-scale channel studied by atomistic simulation. *The Journal of Chemical Physics* **2002,** *116* (5), 2194-2200.

171. Qiao, R.; Aluru, N. R., Ion concentrations and velocity profiles in nanochannel electroosmotic flows. *The Journal of Chemical Physics* **2003,** *118* (10), 4692-4701.

172. Yang, K.-L.; Yiacoumi, S.; Tsouris, C., Monte Carlo simulations of electrical double-layer formation in nanopores. *The Journal of Chemical Physics* **2002,** *117* (18), 8499-8507.

173. Sint, K.; Wang, B.; Kral, P., Selective ion passage through functionalized graphene nanopores. *J Am Chem Soc* **2008,** *130* (49), 16448-16449.

174. Kalra, A.; Garde, S.; Hummer, G., Osmotic water transport through carbon nanotube membranes. *Proceedings of the National Academy of Sciences* **2003,** *100* (18), 10175-10180.

175. Peter, C.; Hummer, G., Ion transport through membrane-spanning nanopores studied by molecular dynamics simulations and continuum electrostatics calculations. *Biophys J* **2005,** *89* (4), 2222-2234.

176. Lorenz, C. D.; Crozier, P. S.; Anderson, J. A.; Travesset, A., Molecular dynamics of ionic transport and electrokinetic effects in realistic silica channels. *The Journal of Physical Chemistry C* **2008,** *112* (27), 10222-10232.

177. Shirono, K.; Tatsumi, N.; Daiguji, H., Molecular simulation of ion transport in silica nanopores. *The Journal of Physical Chemistry B* **2009,** *113* (4), 1041-1047.

178. Kerisit, S.; Ilton, E. S.; Parker, S. C., Molecular dynamics simulations of electrolyte solutions at the (100) goethite surface. *The Journal of Physical Chemistry B* **2006,** *110* (41), 20491-20501.

179. Lee, S. H.; Rasaiah, J. C., Molecular dynamics simulation of ion mobility. 2. Alkali metal and halide ions using the SPC/E model for water at 25 $^{o}$C. *The Journal of Physical Chemistry* **1996,** *100* (4), 1420-1425.

180. Koneshan, S.; Rasaiah, J. C., Computer simulation studies of aqueous sodium chloride solutions at 298 K and 683 K. *The Journal of Chemical Physics* **2000,** *113* (18), 8125-8137.

181. Sanz, E.; Vega, C., Solubility of KF and NaCl in water by molecular simulation. *The Journal of Chemical Physics* **2007,** *126* (1), 014507-13.

182. Du, H.; Rasaiah, J. C.; Miller, J. D., Structural and dynamic properties of concentrated alkali halide solutions: A molecular dynamics simulation study. *The Journal of Physical Chemistry B* **2007,** *111* (1), 209-217.

183. Zhuravlev, L. T., The surface chemistry of amorphous silica. Zhuravlev model. *Colloid Surface A* **2000,** *173* (1-3), 1-38.

184. Smith, D. E.; Dang, L. X., Computer simulations of NaCl association in polarizable water. *The Journal of Chemical Physics* **1994,** *100* (5), 3757-3766.

185. Dang, L. X., Free energies for association of $Cs^{+}$ to 18-crown-6 in water. A molecular dynamics study including counter ions. *Chem Phys Lett* **1994,** *227* (1-2), 211-214.

186. Predota, M.; Zhang, Z.; Fenter, P.; Wesolowski, D. J.; Cummings, P. T., Electric double layer at the rutile (110) surface. 2. Adsorption of ions from molecular dynamics and X-ray experiments. *The Journal of Physical Chemistry B* **2004,** *108* (32), 12061-12072.

187. Mpourmpakis, G.; Froudakis, G. E.; Lithoxoos, G. P.; Samios, J., SiC Nanotubes: A novel material for hydrogen storage. *Nano Letters* **2006,** *6* (8), 1581-1583.

188. Mpourmpakis, G.; Froudakis, G. E., Why boron nitride nanotubes are preferable to carbon nanotubes for hydrogen storage? An ab initio theoretical study. *Catal Today* **2007,** *120* (3-4), 341-345.

189. Klein, M. L.; Shinoda, W., Large-scale molecular dynamics simulations of self-assembling systems. *Science* **2008,** *321* (5890), 798-800.

190. Freddolino, P. L.; Liu, F.; Gruebele, M.; Schulten, K., Ten-microsecond molecular dynamics simulation of a fast-folding WW domain. *Biophys J* **2008,** *94* (10), L75-L77.